(2)

NAVAL POSTGRADUATE SCHOOL

Monterey, California

THESIS

Natural Convection Liquid Immersion Cooling of High Density Columns of Discrete Heat Sources in a Vertical Channel

by

Alfred C. Gaiser
June 1989

Thesis Advisor: Yogendra Joshi

UNCLASSIFIED
SECURITY CLASSIFICATION OF THIS PAGE

REPORT DOCUMENTATION PAGE

1a REPORT SECURITY CLASSIFICATION UNCLASSIFIED	1b RESTRICTIVE MARKINGS
2a SECURITY CLASSIFICATION AUTHORITY	3 DISTRIBUTION/AVAILABILITY OF REPORT Approved for public release; distribution is unlimited
2b DECLASSIFICATION/DOWNGRADING SCHEDULE	
4 PERFORMING ORGANIZATION REPORT NUMBER(S)	5 MONITORING ORGANIZATION REPORT NUMBER(S)
6a NAME OF PERFORMING ORGANIZATION Naval Postgraduate School 6b OFFICE SYMBOL (If applicable) 69	7a NAME OF MONITORING ORGANIZATION Naval Postgraduate School
6c ADDRESS (City, State, and ZIP Code) Monterey, CA 93943-5000	7b ADDRESS (City, State, and ZIP Code) Monterey, CA 93943-5000
8a NAME OF FUNDING/SPONSORING ORGANIZATION 8b OFFICE SYMBOL (If applicable)	9 PROCUREMENT INSTRUMENT IDENTIFICATION NUMBER
8c ADDRESS (City, State, and ZIP Code)	10 SOURCE OF FUNDING NUMBERS PROGRAM ELEMENT NO / PROJECT NO / TASK NO / WORK UNIT ACCESSION NO

11 TITLE (Include Security Classification)
NATURAL CONVECTION LIQUID IMMERSION COOLING OF HIGH DENSITY COLUMNS OF DISCRETE HEAT SOURCES IN A VERTICAL CHANNEL

12 PERSONAL AUTHOR(S)
GAISER, Alfred C.

13a TYPE OF REPORT	13b TIME COVERED	14 DATE OF REPORT (Year, Month, Day)	15 PAGE COUNT
Master's Thesis	FROM ____ TO ____	1989 June	130

16 SUPPLEMENTARY NOTATION
The view expressed in this thesis are those of the author and do not reflect the offical policy or position of the Department of Defense or the U.S. Government

17 COSATI CODES			18 SUBJECT TERMS (Continue on reverse if necessary and identify by block number)
FIELD	GROUP	SUB GROUP	Convective Flow, Thermal Transport, Flow Visualization

19 ABSTRACT (Continue on reverse if necessary and identify by block number)

Natural convection liquid cooling of simulated electronic components in a vertical channel was investigated. The test surface consisted of three columns of fifteen flush mounted foil heaters. The channel was formed by placing a smooth movable shrouding wall parallel to the test surface. The experimental procedure called for temperature measurements and flow visualization at various power levels and channel spacings. Surface temperatures of each heat source were measured using a centrally located embedded thermocouple. Temperature measurement within the flow was conducted using a thermocouple probe. Flow visualization was conducted with the use of a laser generated plane of light. A visual temperature profile of the board was developed through the use of liquid crystals. From the data obtained, experimental correlations relating the local heat transfer properties with shroud wall spacing and strip heater power levels were developed.

20 DISTRIBUTION/AVAILABILITY OF ABSTRACT	21 ABSTRACT SECURITY CLASSIFICATION
☒ UNCLASSIFIED/UNLIMITED ☐ SAME AS RPT ☐ DTIC USERS	UNCLASSIFIED
22a NAME OF RESPONSIBLE INDIVIDUAL Prof. Gerald	22b TELEPHONE (Include Area Code) [illegible]
	22c OFFICE SYMBOL [illegible]

DD FORM 1473, 84 MAR 83 APR edition may be used until exhausted
All other editions are obsolete

SECURITY CLASSIFICATION OF THIS PAGE
UNCLASSIFIED

Approved for public release; distribution is unlimited

Natural Convection Liquid Immersion Cooling of High Density Columns ofDiscrete Heat Sources in a Vertical Channel

by

Alfred O. Gaiser
Lieutenant, United States Navy
B.E., Stevens Institute of Technology, 1983

Submitted in partial fulfillment of the
requirements for the degree of

MECHANICAL ENGINEER

from the

NAVAL POSTGRADUATE SCHOOL

June 1989

Author:

Alfred O. Gaiser

Approved by:

Yogendra Joshi, Thesis Advisor

Anthony J. Healey, Chairman
Department of Mechanical Engineering

Gordon I. Schacher
Dean of Science and Engineering

ABSTRACT

Natural convection liquid cooling of simulated electronic components in a vertical channel was investigated. The test surface consisted of three columns of fifteen flush mounted foil heaters. The channel was formed by placing a smooth movable shrouding wall parallel to the test surface . The experimental procedure called for temperature measurements and flow visualization at various power levels and channel spacings. Surface temperatures of each heat source were measured using a centrally located embedded thermocouple. Temperature measurement within the flow was conducted using a thermocouple probe. Flow visualization was conducted with the use of a laser generated plane of light. A visual temperature profile of the board was developed through the use of liquid crystals. From the data obtained, experimental correlations relating the local heat transfer properties with shroud wall spacing and strip heater power levels were developed.

TABLE OF CONTENTS

LIST OF SYMBOLS

Symbol	Description	Units
A	Area	m^2
As	Heater Surface Area	m^2
g	Acceleration due to Gravity	m / s^2
Gr*	Flux-based Grashof Number	Dimensionless
h	Heat Transfer Coefficient	$W / m^2 K$
K_f	Fluid Thermal Conductivity	W / m K
K_{pg}	Plexiglass Thermal Conductivity	W / m K
L	Characteristic Length	m
Pr	Prandtl Number	Dimensionless
Nu	Nusselt Number	Dimensionless
Nu*	Modified Nusselt Number	Dimensionless
NDT	Non-dimensional Temperature Excess	Dimensionless
P	Perimeter	m
q''	Convective Heat Flux	W / m^2
Q_{cond}	Conductive Heat Transfer	W
Q_{conv}	Convective Heat Transfer	W
Q_{in}	Input Energy	W
S_n	Heater Number in Relation to the Leading Component	Dimensioless
T	Local Surface Temperature	°C

T_{amb}	Ambient Temperature	°C
T_{film}	Film Temperature	°C
T_s	Surface Temperature	℃
v	Specific Volume	m^3 / kg
X	Vertical Distance from Bottom Edge of Test Surface	m
ß	Expansion Coefficient	1 / K
Ç	Kinematic Viscosity	m^2 / s
Ø	Temperature Difference Between Local Temperature and Ambient	K
$Ø_0$	Temperature Scaling Factor	K

ACKNOWLEDGMENT

I would like to express my thanks to Professor Joshi for his guidance and technical assistance in putting together this research project. I also wish to thank Professor Neta for his assistance in the use of ELLPACK and the development of a three dimensional conduction loss model. Finally, I wish to thank my wife Debbie whose understanding and encouragement helped me through the long hours required to produce this thesis.

I. INTRODUCTION

A. STATEMENT OF PROBLEM

With the continuing development of today's new generation of high speed computers, a continuing trend is seen toward the miniaturization of the electronic components which make up the heart of these machines. As the size of these components decreases, the problem of required cooling becomes increasingly difficult. It is a known fact that the failure rate of IC chips increases exponentially as the junction temperature increases. For every ten degree celsius decrease in device operating temperature, the long term reliability can be improved 50% [Ref. 1].

A demonstration showing the nature of the cooling problem can be provided with the following example. A typical IC chip of 3x3x.5 cm^3 is capable of generating from 1-25 watts of thermal energy resulting in a surface heat flux of 0.1-17 watts/cm^2. Current heat transfer technology can efficiently remove this heat flux while maintaining the junction temperatures well below 100 degrees celsius. However, supposing this IC chip were reduced in size to 1x1x.5 cm^3, the surface heat flux now would range from 2 to 51 watts/cm^2. At the upper limit of this range, the current techniques of high velocity air convection, chilled water heat exchangers or alternating the system design to reduce the thermal resistance may become incapable of dissipating the generated heat causing the component to fail.

Currently chip heat fluxes are approaching 50 w/cm^2 and projected heat fluxes of future components will reach 200 w/cm^2 [Ref 2] . In order to meet the cooling demands of future components, alternative methods of heat transfer must be developed.

Before any heat transfer analysis can begin on a new concept, the overall geometry of the problem must be defined. In most electronic assemblies, small components are often first mounted on cards and the cards then mounted vertically in cabinets. This configuration will produce a geometry similar to a channel for a coolant to pass through, either by natural or forced methods, as it impinges upon the vertical array of components.

The heat transfer analysis of a new electronic cooling technique, begins by evaluating the effects of all three modes of heat transfer. For many electronic cooling configurations, the prevalent mode of heat transfer is direct convection to the ambient environment.

The convection heat transfer rate from a surface at temperature T_s, with exposed surface area, A, to a surrounding fluid at temperature T_{amb}, is given by Newton's law of cooling:

$$Q = h A (T_s - T_{amb})$$

It is important to remember that the above expression is the definition of **h**, the convective heat transfer coefficient, and not a pheomenological law.

Convection heat transfer can be forced, natural or mixed. Forced convection requires the use of a prime mover to impart a flow velocity to the cooling fluid. Natural convection occurs when density gradients within the fluid are acted upon by a body force. Eventhough the heat transfer coefficients for natural convection will be smaller than those for forced convection, a simpler and more reliable design can be employed. Mixed convection occurs when both natural and forced convection are present.

Radiation heat transfer can be significant in air cooled systems and must be accounted for when evaluating the total heat transferred from an individual component to the coolant. This of course will greatly complicate any energy balance analysis needed for design considerations. For liquid cooled systems, radiation is virtually insignificant with respect to both conduction and convection due to the small absorption distances.

The effects of conduction heat transfer will depend upon a particular cooling system's design and must be evaluated in each cooling application. Conduction will always be present, however, in some cases conduction heat transfer is considerably smaller than convection and can be neglected on the basis of shear magnitude.

One possible option to solving the cooling problem which takes advantage of the simplistic design of natural convection cooling systems and the large heat transfer coefficients of high Prandtl number fluids is direct liquid immersion. Previous studies have shown that this method can handle very large component heat fluxes hence the need to analyze this method further [Ref. 3].

B. OBJECTIVES

The following study was performed to evaluate the hydrodynamic and thermal characteristics of buoyancy induced flow resulting from a high density grouping of discrete flush mounted heat sources in a vertical channel. The high density grouping consisting of three columns of fifteen flush mounted heat sources was chosen since it provided a simple geometric representation of modern high density component cards found in many of today's high speed computers.

The study consists of two main sections. The first section analyzes a single column of flush mounted heat sources. The second section continues the study by analyzing the effects of having two flanking columns placed next to the center column. The two sections will be compared in order to understand the effect of component density on heat transfer. For both sections, the study will analyze the heat transfer from the heaters to the fluid with steady state conditions only.

The results of this study will be compared to those obtained in a previous study, [Ref. 3], where a single column of a low density grouping of flush mounted heat sources was used.

Specific objectives of this study were:

- To experimentally and numerically evaluate the effects of conduction losses into the test board.

- For both a single column and all three columns, experimentally determine component temperatures at various power settings and channel widths and develop corresponding heat transfer correlations .

- To visually observe natural convection flow for steady state conditions.

- To explore the thermal boundary layer at various locations on the test surface at various power settings .

- To implement liquid crystal technology in order to visually evaluate temperature profiles along the test surface.

II. EXPERIMENT

A. Experimental Apparatus

As seen in Figure 1, the experimental apparatus consisted of three main assemblies; a Channel Assembly, a Power Assembly, and a Data Acquisition/Reduction Assembly. Each assembly was inter-related by three distinct variables; the input power to the heater strips, the heater strip surface temperatures, and the bath temperature of the water in which the channel assembly was submerged. In very basic terms, these three variables when inserted into Newton's Law of Cooling, provide the first step in evaluating the heat transfer characteristics of the apparatus . Before any conclusions could be reached with respect to natural convection liquid cooling, the experimental apparatus design had to be capable of accurately measuring all three variables throughout the entire range of interest during this study.

1. Channel Assembly Design

The channel assembly consisted of a vertical test surface with 45 flush mounted heater strips placed in three columns of 15, all of which were imbedded within the surface. A parallel shrouding plate was placed in front of the test surface in order to simulate a typical circuit board with the back of another circuit board directly in front of it. With the shrouding plate in place, a channel is formed with the test surface.

The test surface was constructed using a 31.75 cm x 31.75 cm x 1.11 cm plexiglass board with 3.58 cm x .79 cm slots milled out to a depth of .19 cm at each location where a heater strip is to be embedded. A front view of the test surface showing the location of each slot is shown in Figure 2. Within each slot, a .79 cm diameter hole was drilled through the board in order to allow the heater strip power leads and thermocouple wires to pass through. Side and top views of a slot are shown in Figure 3.

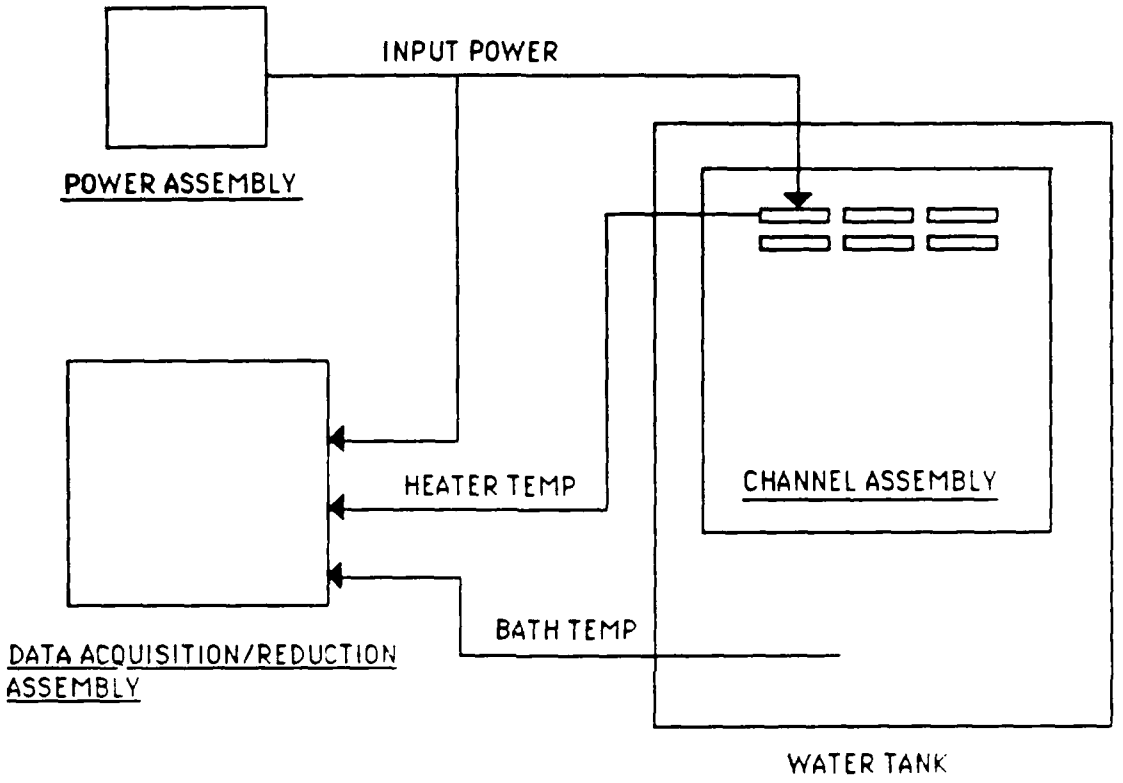

Figure 1. Experimental Apparatus

Before mounting the heater strips to the board, two power leads and a .003 inch copper-constantan thermocouple was attached to the back of each strip. The power leads were simply soldered onto the heater strip however, before the thermocouple could be attached, the back of the strip needed to be coated with a thin layer of Omega 101 high conductivity adhesive. This layer electrically isolates each thermocouple from the heater strip while allowing for accurate temperature measurements. Once the strip was coated, an additional small drop of the adhesive was used to connect the thermocouple onto the center of the heater strip. A picture displaying the front of a heater strip is shown in Figure 4.

In order to construct a flush test surface, great care had to be used in mounting the heater strips. The procedure used consisted of taping each strip into their respective slots with the strip's connected thermocouple and power wires placed through the drilled hole. A fast curing, low thermal conductivity epoxy (Omega bond 100) was then injected back through the hole thus creating a flat surface on the front of the test surface and at the same time sealed up the slots and electrically isolated the heaters from possible short circuit conditions once the assembly was submerged in the tank.

Additional thermocouples were attached both to the back face of the test board and imbedded within the board for use in evaluating the conduction losses out through the back surface. A total of twenty thermocouples were used for this purpose.

The method of attaching the thermocouples on the back face was to simply apply a small coating of the Omega 101 adhesive onto the surface and lay the thermocouple bead directly on the coating. For the embedded thermocouples, a small hole was drilled in from the backface to a depth equal to one half the board width. The hole was then filled with this same adhesive and the thermocouple bead placed within the adhesive pool.

These simple attaching schemes provided for an effective means of evaluating both back surface and interior temperature profiles, hence providing the means for determining conduction losses with minimal construction complexity. The actual location of each of

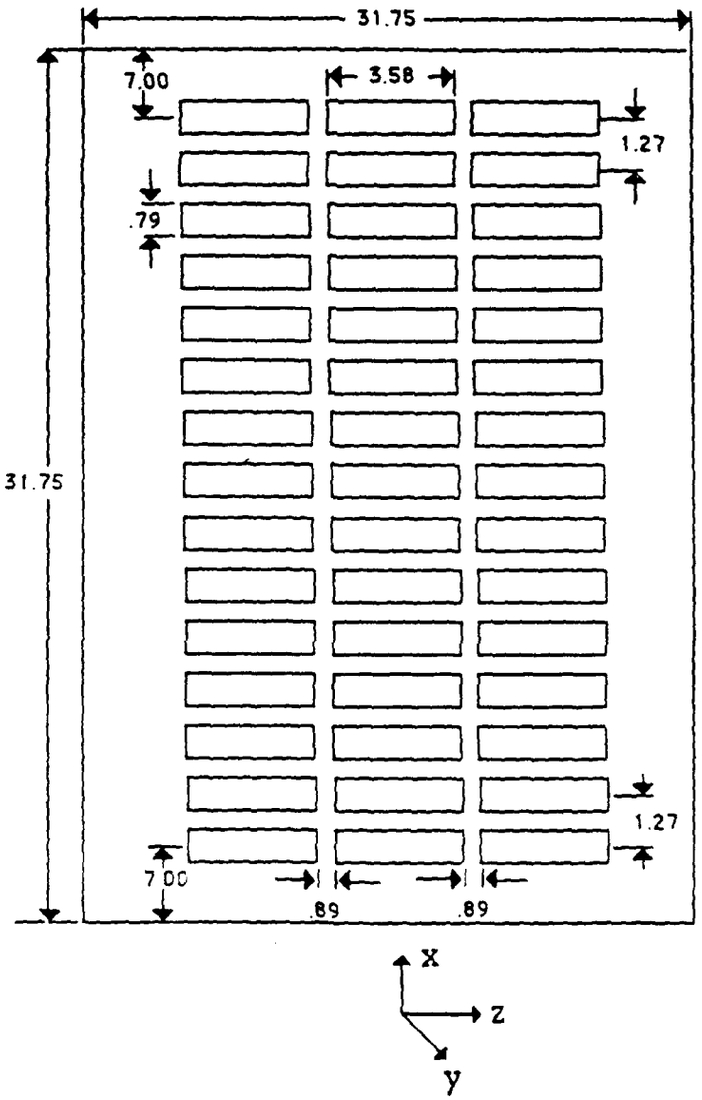

Figure 2. Front View of Test Surface. All Units in cm.

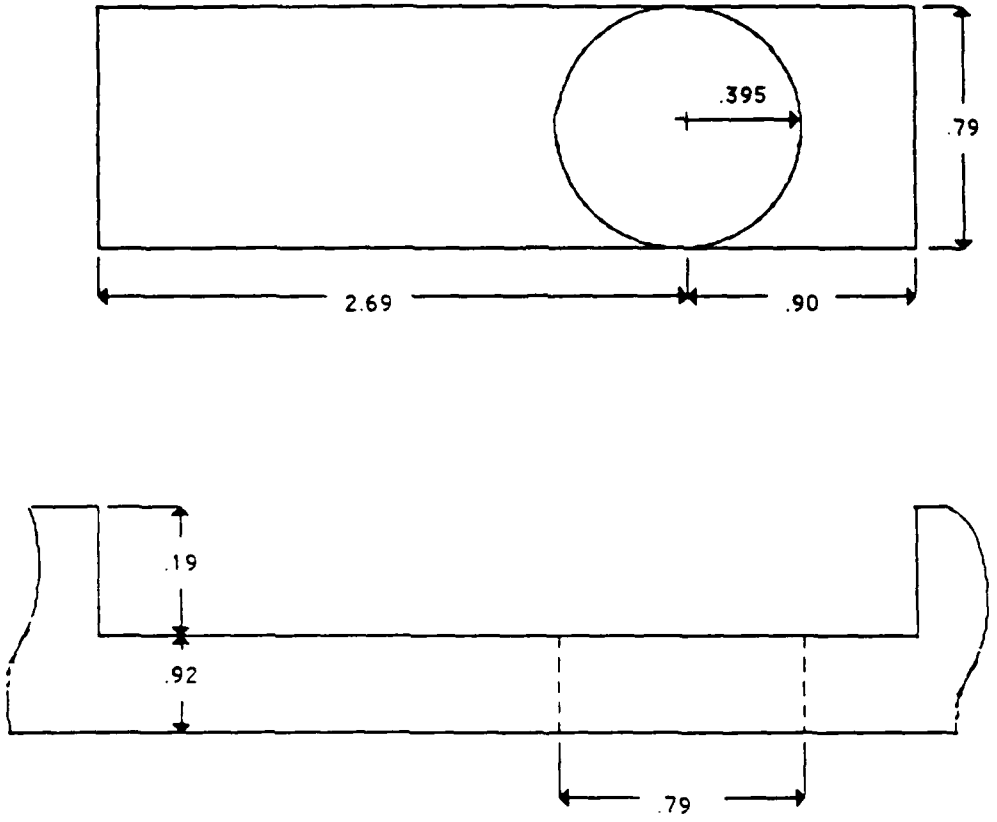

Figure 3. Front and Side Views of the Test Surface Heater Slots. All Units in cm.

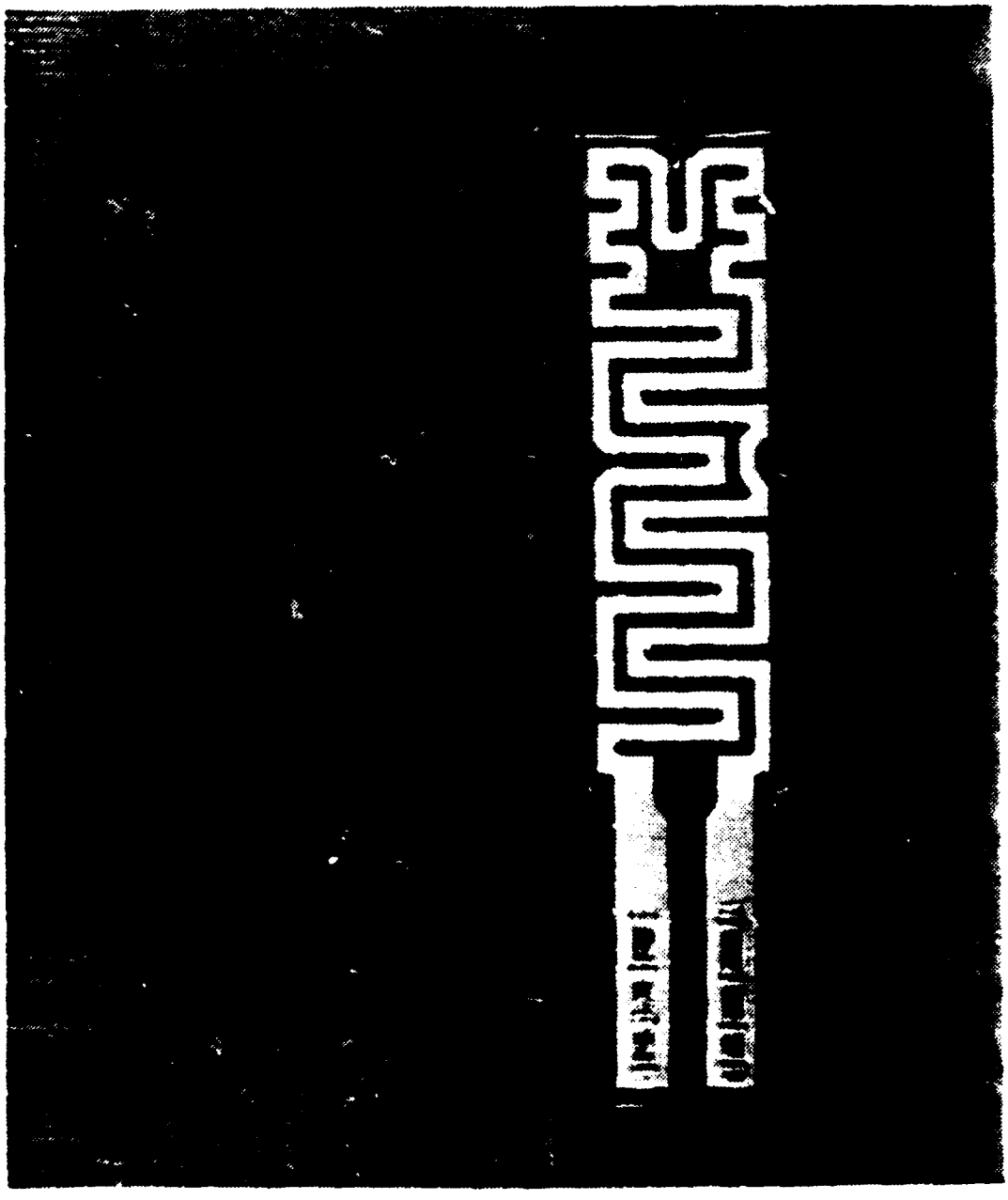

Figure 4. Foil Heater

the conduction loss thermocouples is discussed further in the subsequent chapter entitled Conduction Losses.

2. Power Assembly Design

This was the portion of the experimental apparatus which provided power to the individual heater strips. The power assembly consisted of a HP 6269B power supply unit connected to six distribution panels to which the heater power leads are connected. In simple terms, each distribution panel acts as an individual power supply for a specified number of heaters. A panel is capable of distributing power to 10 heaters. In the case of this experiment, a panel would have connected to it either eight or seven heaters depending on heater grouping. If only seven heaters were connected to a particular panel, a ten ohm resister is used to equilibrate the total power requirement of the panel as compared with an eight heater panel.

Figure 5 shows how a power distribution panel is constructed. Referring to this figure, it is seen that each heater on a panel was connected in series with a precision resister (R=2.01 ohm). This resister pair is connected in parallel to two copper wire bus bars which in turn are connected to the power supply unit. It must be pointed out that for some heaters, additional resisters needed to be connected in parallel in order to maintain a constant value of input power for all heaters. The amount of resistance used for most power equalizing applications was 1.5 kilo-ohms.

The data acquisition system obtains voltage readings across the bus bar (V_{total}) and each heater (V_{heater}). From these two measured values, the input power to an individual heater was easily computed with the following relation:

$$Power = \left(\frac{V_{total} - V_{heater}}{R} \right) V_{heater}$$

The value of R in the above relation represents the 2.01 ohm resister mentioned above.

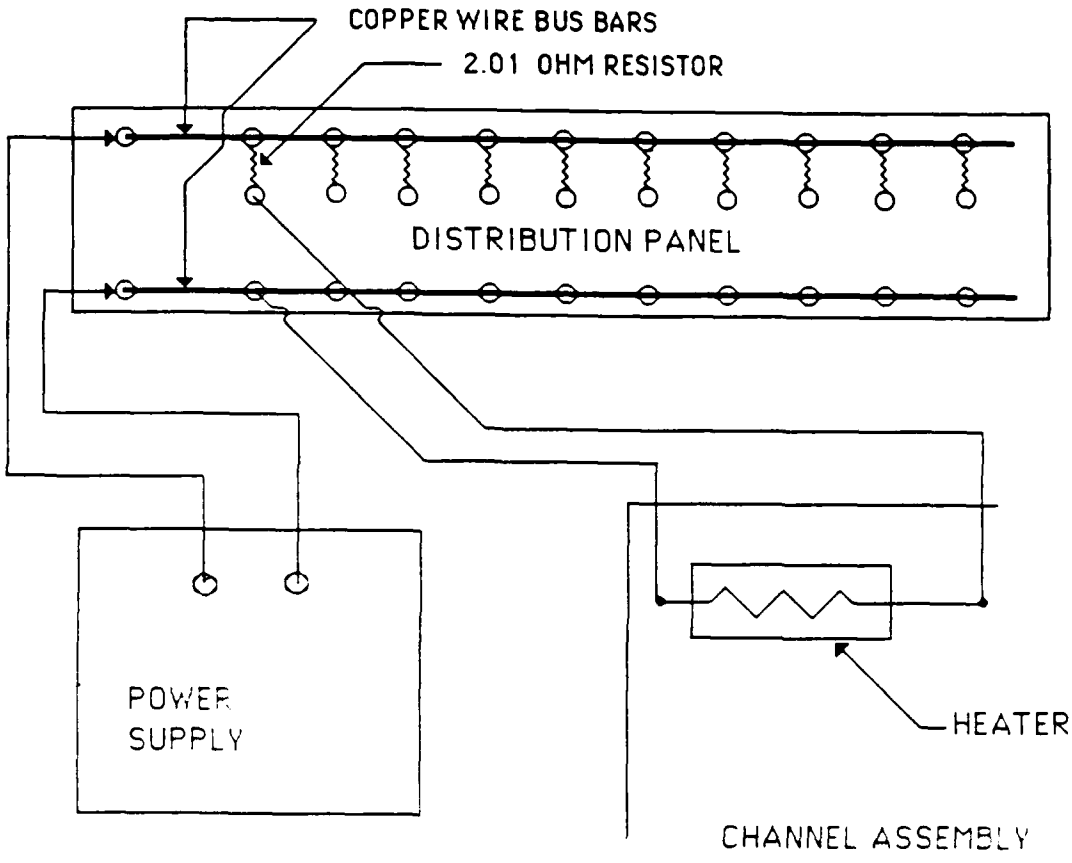

Figure 5. Power Distribution Panel

3. Acquisition/Reduction Assembly Design

The Acquisition/Reduction assembly was made up of two major pieces of equipment; a HP 3852A Data Acquisition Box and a HP 9153 Computer system. This assembly records and processes all data output from the other two assemblies. The channel assembly delivers temperature output from both the thermocouples attached to each heater and those used for evaluating the conduction losses. This output is received by the acquisition box and sent to the computer where the temperatures are computed for each thermocouple analyzed. Prior to being received by the acquisition box, the thermocouple output passes through an ice bath reference junction. This junction is nothing more than additional thermocouples used for providing a reference voltage to be received by the acquisition box and the computer for evaluating the temperature accurately. In a similar manner, the output from the thermocouples used to monitor bath temperature is also sent to an ice bath reference and then to the assembly for analysis.

The power assembly sends to the acquisition box the voltage drops across each heater and the voltage drop across each distribution panel. Once this data is received by the computer, the power for each heater is computed as per the discussion above.

As was seen in figure 1, this last assembly receives as input the three main variables of the experiment. Once these three variables are received by this assembly, further data reduction can begin from which the heat transfer characteristics of the experimental system can be deduced.

B. Experimental Procedure

The entire experimental program consisted of two parts. The first part of the study required temperature measurements from each thermocouple. The first part also called for probe measurements of the thermal boundary layer. This experimental procedure was performed twice: once with only the central column of heaters energized, and once with all

three columns in operation. The second part of the study pertained solely to visualization of both the flow and the surface temperature as seen from liquid crystals. For each of the two parts, both the input power level and the shroud spacing were varied.

For the first part of the program, input powers of .5, 1.0, 1.5, 2.0, 2.5, and 3.0 watts were used. The shroud spacings used were; no shroud, 15, 12, 9, 6, 3, and 1.5 mm. At each of the power levels and shroud spacings, the surface temperatures at the center of each heater were recorded. Also, the bath temperature and the temperatures needed for conduction loss calculations were also recorded.

Once all required temperatures had been recorded, a thermocouple probe was used to collect temperature data within the thermal boundary layer adjacent to the front face of the test surface.

Figure 6 shows a picture of this probe. As seen in this figure, the probe was constructed by stretching a .003 copper constantan thermocouple between two pieces of thin bent glass tubing. The thermocouple bead was protected from touching the surface by two pieces of thin stainless steel tubing. The probe was moved in the fluid with 3 degee of freedom traverse slide. This probe was used only for the unshrouded cases and at power levels of both 1 and 3 watts.

Referring back to Figure 2, the probe was trasversed both horizontally along the z axis and vertically along the y axis with respect to six positions on the board face. The first three positions included the center of the bottom row of heater strips, the center of the central row of strips and the center of the top row of strips. The last three positions all were referenced to the centerline in between heaters. The positions included; the space between the first and second row of heaters, the space between the eighth and ninth row of heaters, and the space .63 cm above the fifteenth row of heaters.

The horizontal trasverse of the probe was accomplished to measure the spanwise temperature variation of the fluid located .5 mm above the heater surface. For the case

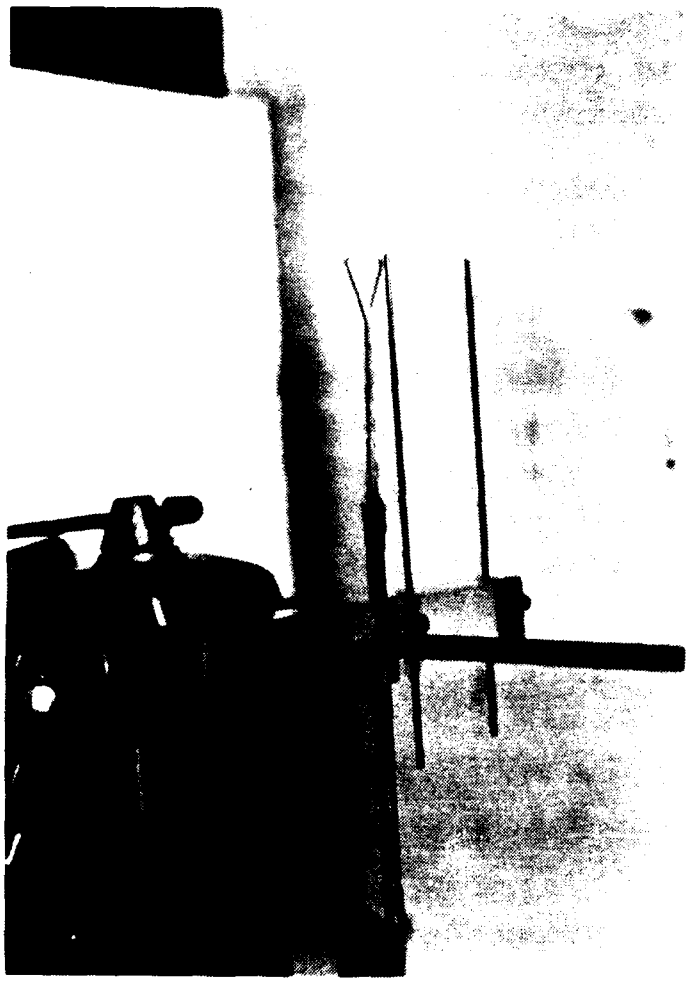

Figure 6. Thermocouple Probe

when only one column of heaters as energized, the probe was moved from one end of the heater to the other. Temperatures were recorded for every 2 mm change in probe displacement. For the case where three columns were energized, the probe was moved from the left most corner of the left column to the right most corner of the right column. Again, temperatures were recorded for every 2 mm change in probe displacement.

The trasverse of the probe in the y direction was used to measure the normal temperature distribution of the fluid starting from the point located .5 mm from the heater surface out to the point where the fluid temperature is ambient. The fluid temperature was recorded for every .1 mm change in normal distance.

The flow and temperature visualization portion of the program was conducted next. The flow visualization was accomplish by suspending finely ground particles of pliolite into the bath water and shining a plane of laser generated light into the bath (refer to figure 7). The scattered laser light from the particles enabled the flow visualization. The plane of laser light was generated using a helium neon laser shining into a cylindrical lens. The light leaving the lens formed a thin vertical sheet of light. By strategically aligning the plane of light onto the test surface at points of interest, a camera can be used to photograph the motion of the particles as they move with the warmer water rising up the test surface as it heats.

By taking extended time exposure photographs, the particle paths of motion were recorded on film. For the best pictures, an exposure time of 20 seconds and a focal length of 2.8 was used. Since these pictures recorded the particle traces as they moved up the test surface, they also provided information about the momentum boundary layer thickness. By blowing up the exposure, the thickness can actually be determined.

The surface temperature patterns were obtained with the use of thermochromic liquid crystals (TLC). These crystals react to fluctuations in temperature by changing color; they are optically active mixtures of organic chemicals. The liquid crystal is

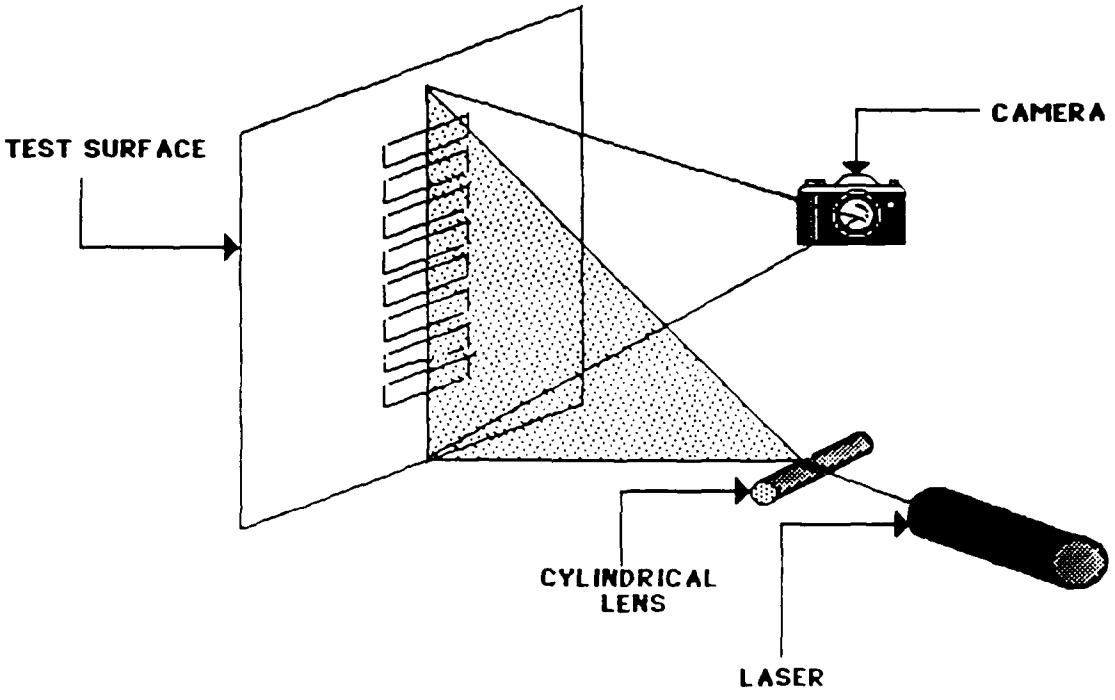

Figure 7. Laser and Camera Arrangement for Photography

liquid crystal is in the form of an aqueous slurry of discrete TLC-containing microcapsules. In this form, the liquid crystals are essentially ready to use temperature sensitive pigments which can be incorporated into water based coating formulations. As an aqueous slurry, a thin coating of the liquid crystals can be applied to a surface with an air brush. Once the surface is heated, the liquid crystals change to specific colors depending upon the temperature profile of the surface. Each color observed represents a specific temperature mean with variation color play bandwidths of between one and five degree celsius. Hence, when a specific color is observed to exist at a particular point, the mean temperature at that location on the surface is known.

To use the liquid crystals for this research a thin coating had to be applied onto the entire front of the test surface. Before applying the liquid crystals, a thin coat of black paint was placed onto the surface first in order to aid in observing the color changes. Once the black coat was dry, the liquid crystal could be applied. For both the coatings of black paint and liquid crystals, an air paint brush was used in order to obtain the thinnest possible continuous coatings. With the liquid crystal on the test surface, the temperature profile of the surface was easily determined by observing the various color regions displayed by the crystal.

C. Data Analysis

The starting point for data analysis was to perform a simple energy balance around each heater. From this energy balance, the energy removed from convective heat transfer is:

$$Q_{CONV} = Q_{IN} - Q_{COND}$$

Referring back to the experimental apparatus design, the input energy, Q_{in}, is a known value given in watts and is based upon the electrical power each heater receives.

The energy each heater gives up due to conduction, Q_{cond}, was determined through analysis of the data received from the special conduction loss thermocouples. This data provided the basis for a formulation of a three dimensional finite difference conduction loss model which gave a numerical value of Q_{cond} in watts for each power level analyzed. Since the values of Q_{in} and Q_{cond} are known, Q_{conv} is also a known quantity. With the value of Q_{conv}, the convective heat flux, **q"**, leaving the heater surface was calculated through the relation:

$$q'' = Q_{conv} / A_s$$

where A_s is the surface area of the heater.

The next logical step followed in reducing the output data was to calculate the value of the local convective heat transfer coefficient **h**. This value is found through application of Newton's law of cooling: This law relates the local value of **h** at a specific point with the heat flux and a temperature difference. The value of **delta T** is the difference between the heater surface temperature and the bath temperature.

$$h = q'' / delta\ T$$

For evaluating the heat transfer characteristics of the experimental system, two additional parameters were calculated. These parameters are: the flux based Grashof number, and the Nusselt number. In order to numerically evaluate each of the above parameters, a length scaling factor had to first be defined, For the purposes of this study, the factor used was the characteristic length of the heater which is defined as:

$$L = A_s / P$$

where **P** is the perimeter of the heater.

With the characteristic length defined, the fluxed based Grashof number was calculated using the following expression:

$$Gr^* = g \beta q'' L^4 / (K_f \zeta^2)$$

In this expression, the values of ß, K_f, and Ç were obtained by applying a third order polynomial curve fit to values obtained from tables of tabulated data on the thermophysical properties of water [Ref. 4]. The polynomial curve fits for the thermophysical properties utilized the local film temperature as a basis for all values. The local film temperature was defined as the difference between a particular heater temperature and the ambient bath temperature divided by two.

$$T_{film} = (T_{heater} - T_{bath}) / 2$$

The local Nusselt number was calculated using the expression:

$$Nu = h L / k_f$$

Once again the value of K_f was obtained in the same manner as mentioned above.

Another important value calculated was a non-dimensional temperature term. This term was defined as the temperature difference between the heater surface and water bath divided by a temperature scaling factor. The scaling factor used for this experiment was:

$$\phi_o = q'' L / k_f$$

Since **delta T** = ø, the non-dimensional temperature factor is simply:

$$NDT = \phi / \phi_o$$

The value of **NDT** has no real significant relation to the heat transfer characteristics of the system however, it was a useful value for presenting temperature data.

An additional term was calculated in order to aid in the presentation of data. This term is a non-dimensional length term defined as **X / L**. The value of **X** is the distance from the bottom edge of the test surface to the local point of interest, while **L** is the overall length of the test surface. This term was used for all plots representing position as an axis.

For the task of reducing the data down into the required forms listed above, a data reducing program was written and is presented in Appendix B. Sample calculations demonstrating the reduction process are shown in Appendix C.

An uncertainty analysis for all measurements and calculations performed for this study is presented in Appendix A.

Quantitative developments were expressed as plots of :

- Nu vs. Gr* for both shrouded and unshrouded conditions
- NDT vs. local thermocouple location
- Temperature distribution within thermal boundary layer along a test surface at various heater locations

III. CONDUCTION LOSSES

As was mentioned previously, a liquid immersion cooling system has two modes of heat transfer present; convection and conduction. Radiation is usually negligible due to the small absorption length in liquids. In the present study, convection is the prevalent mechanism of energy transfer and accounts for most of the desired cooling of the components.

Conduction accounts for only a very small portion of the total energy being transferred, but yet must be taken into account when analyzing the overall effectiveness of a liquid immersion scheme for electronic cooling. The purpose of this chapter is to estimate the conduction losses through the back of the plexiglass substrate on which the heated elements are mounted.

The previous study performed by Knight [Ref. 3] estimated the conducted energy with a one dimensional model. To improve results, the current study analyzed the conduction problem with a more accurate three dimensional model. The results obtained from the three dimensional model were compared with results previously obtained [Ref. 3].

In order to keep the three dimensional model as simple as possible, it was decided to compute the conductive losses for the central heater with only the center column energized. The three dimensional flow of conducted heat within the plexiglass is described by Laplace's equation:

$$\partial^2 T/\partial x^2 + \partial^2 T/\partial y^2 + \partial^2 T/\partial z^2 = 0$$

By prescribing the geometry and boundary conditions of the problem at hand, an accurate three dimensional temperature profile can be created. With temperatures known at all locations, the heat flux leaving a desired surface is easily evaluated. Once the heat flux

is known, the net conducted energy leaving the surface per unit time can be obtained by multiplying the flux term by the area which bounds the surface.

The geometry chosen to describe the model was to take a small region of the test surface surrounding the central heater. Due to symmetry, only a quarter of this region was analyzed producing the geometric boundaries as seen in Figure 8.

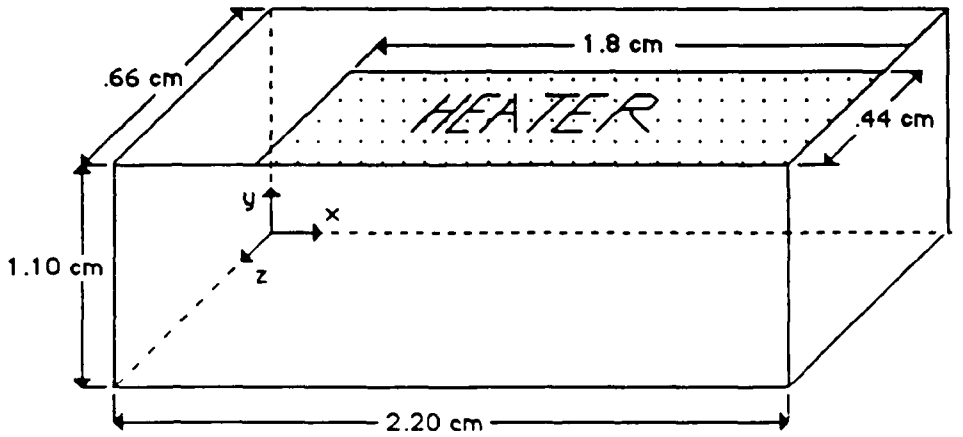

Figure 8. **Conduction Loss Model Geometric Boundaries**

As seen from this figure, the geometry chosen is a rectangular box. The length of this box was 2.20 cm which is the distance measured horizontally from the vertical center line of a heater to a point which is midway between two separate columns of strips. The height of this box was 1.1 cm and represented the thickness of the test surface. The depth of the box was .66 cm and represented the vertical distance on the test surface measured from the horizontal heater center line to the point midway between the heater and the heater directly above in the same column.

Since the geometry of the model is a rectangular box, sufficient boundary conditions are the temperature profiles on each of the six faces. These six boundary conditions needed to solve the elliptic differential equation which governs the model above were

obtained from the conduction loss thermocouples mentioned previously. The data for the boundary conditions was obtained from seven strategically placed thermocouples. Five of the seven were attached to the back surface of the test board and two were imbedded within the test board to a depth equal to one-half the thickness. Figure 9 displays where each thermocouple was placed for producing the desired output.

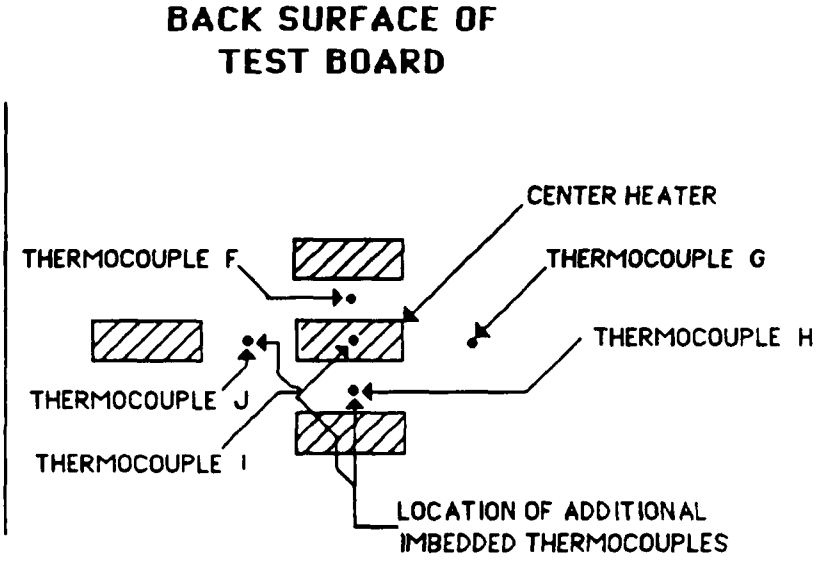

Figure 9. **Conduction Loss Thermocouple Locations**

Referring to this figure, the following procedure was used to convert the thermocouple output into the boundary conditions needed. Thermocouples F, G, H, I, & J were averaged together to provide a constant temperature boundary for the y = 0 plane on the model. For the y = 1.10 cm plane three distinct constant temperature regions were used. The thermocouple which was mounted directly to the heater provided the temperature boundary for the heater region. The other two regions had temperature boundaries determined from the visual observation of the temperature sensitive liquid crystal which was sprayed over the front of the test surface.

Since the model only includes one quarter of a heater region, two surfaces were adiabatic from symmetry considerations. From Figure 8, these surfaces were the x = 2.20 cm plane and the z = .66 cm plane.

The last two boundary conditions were obtained from the output of the two imbedded thermocouples. On the x = 0 plane, a linear regression fit was used to match the temperature data received at points on this plane at y = 0, .55 and at 1.10 cm. On the z = 0 plane a similar technique was used. However, two separate regions are needed for a temperature profile for this boundary. This is due to the two temperatures seen on the intersection of the plane with the line y = 1.10 cm. Without using two temperature regions, matching of the boundary conditions is impossible.

To aid in the understanding of how thermocouple output was used to construct boundary conditions, the following two tables for the case of three watt input power are presented. Table 1 lists the temperature output received from each conduction loss thermocouple. Table 2 lists the boundary conditions on each of the six boundary planes resulting from the input data.

With the boundary conditions defined on all six planes, the mathematical model is ready to be solved. Two approaches are available for solving elliptic differential equations; numerical and analytical.

Due to the rectangular geometry and unusual boundary conditions which define the problem, it was decided to use a finite difference numerical approach to solve the mathematical model described above. The numerical scheme employed was part of a software package entitled ELLPACK [Ref. 5]. The ELLPACK package is a set of numerical schemes each of which is capable of solving an elliptic boundary value problem. The scheme used to solve the conduction loss problem was an over-relaxation technique matched with a 7 point star discretization. A grid was formed for the model by dividing up the x axis length into 21 points, the y axis length into 11 points and the z axis length into 7

points. The output produced from the ELLPACK program consisted of a listing of all temperatures and the values of the first derivative of the temperature with respect to the y coordinate at each node. A copy of the ELLPACK input program used for the three watt input power case is presented in Appendix D.

To find the value of conducted energy leaving the y = 0 plane, the values of $\partial T/\partial y$ for each node on this plane need to be computed. From Fourier's law of conduction, the first derivative of the temperature with respect to a coordinate direction at a location when multiplied by the thermal conductivity, will result in the heat flux at the point of interest.

$$q'' = -K\, \partial T/\partial y$$

TABLE 1 CONDUCTION LOSS THERMOCOUPLE OUTPUT

Thermocouple	Temperature °C
F	18.6321
G	18.6232
H	18.6258
I	18.6325
J	18.6254
imbedded #1	19.3842
imbedded #2	20.4931

TABLE 2 MODEL BOUNDARY CONDITIONS

Plane	Boundary Condition
x = 0	T = 18.6278 + 1.3752 y
x = 2.20	$\partial T/\partial x = 0$
y = 0	T = 18.6278
y = 1.10	If x < .40 T = 20.1405
	If x > .40 & z < .22 T = 22.3584
	If x > .40 & z > .22 T = 30.1998
z = 0	If x < .40 T = 18.6278 + 1.3752 y
	If x > .40 T = 18.6278 + 3.3915y
z = .66	$\partial T/\partial z = 0$

The conducted energy rate at a particular location is then easily evaluated by multiplying the heat flux at this location by the incremental area of the control volume surrounding the node of interest normal to the direction of heat flow.

$$Q_{cond} = q'' A_{surface}$$

The conducted energy leaving the y = 0 plane for the model used was determined by taking $\partial T/\partial y$ at each node on this plane and multiplying the value by the thermal conductivity of the plexiglass, K_{pg}. The result was the heat flux leaving each node, q":

$$q'' = -K_{pg}\, \partial T/\partial y$$

The resulting values when summed together produce the net conducted energy, Q_{cond}, leaving the back surface of the test board.

The above procedure was followed for data obtained from experimental runs having input heater powers of one, two, three and four watts. The values of Q_{cond} vs. **input power** are presented in figure 10 for input power values ranging from 0 to 6 watts. The values from 0 watt to 1 watt input power along with the values above 4 watts are all obtained by extrapolating the known data.

Also shown on figure 10 are the estimated values based upon a one dimensional steady state model. Comparing the two curves for the range between one and six watts, the values for the 3-D model are lower than for the 1-D. This is expected due to the fact that the 3-D model will take into account the energy being transferred in all three coordinate directions, while the 1-D model assumes that all the conducted energy is being transferred in one coordinate direction.

In general, it is seen that the two curves tend to diverge at the high end of the range of interest. At six watts input power, the 1-D model is approximately 10% higher than the 3-D model. However, throughout the entire range of input power analyzed for this research; which was from .2 to 3 watts, the 1-D model gave on the average 3% higher values than

the 3-D model. This means that for this particular range of input power, a 1-D model gives acceptable results and can be utilized with minimal error.

The minor difference of Q_{cond} as seen between the 1-D and 3-D models leads to the conclusion that even though the transfer of energy through the substrate holding each strip is three dimensional, the majority of conducted energy flows perpendicular to the heater back surface. The smaller portion of energy that flows in the other two coordinate directions only accounts for approximately 3% of the total rate of input energy and may be neglected in most applications of interest.

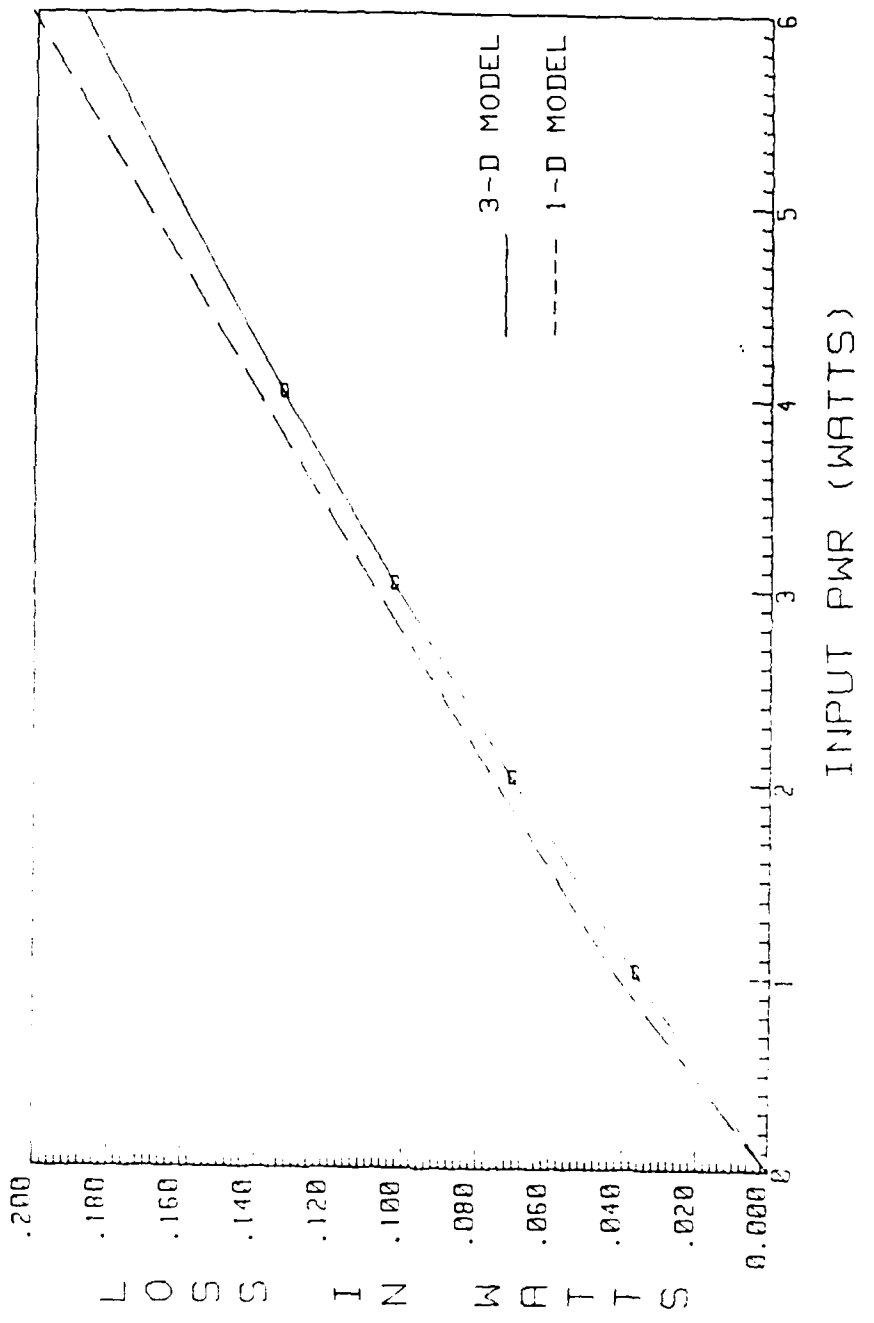

Figure 10. Conduction Losses vs. Input Power

IV. SINGLE COLUMN ANALYSIS

The presentation and analysis of the single column data obtained during this study is divided into two major categories. The first category refers exclusively to the case where the test surface was heated in the absence of the shroud plate. Within this category, heater temperature data, thermal boundary layer profiles obtained from thermocouple probe output and momentum boundary layer thickness at various locations determined from flow visualization pictures, are all discussed. The second category analyzes data and flow visualizations obtained with the shroud placed directly in front of the test surface creating a channel flow. The shroud distance from the test surface was varied in order to evaluate the effects of channel spacing on the heat transfer performance.

A. Single Column Transport without Shroud

The main thrust behind the analysis of a single high density array of distinct heat sources is to determine how the heat transfer characteristics are influenced by the small separation distance between heaters. In the limiting case, the separation distance is zero hence the analysis would then be of a vertical flat plate with a uniform heat flux boundary condition at the fluid interface.

For this special case, the local surface temperature as a function of downstream location is governed by the relation [Ref. 6]:

$$T_s(x) - T_\infty = \left(\frac{5\zeta^2 q_w'' x}{K_f g \beta} \right)^{1/5} f(0)$$

Hence the surface temperature, $T_s(x)$, varies with downstream location to the 1/5 power.

In order to compare measured local surface temperatures with values predicted from 2-Dimensional boundary layer theory, the above equation had to be modified slightly. The temperature variation along the test surface at the heater centers was calculated as a non-dimensional temperature excess, NDT. The equation for the non-dimensional temperature excess was presented in the data analysis section discussed previously. This equation was shown to be:

$$NDT = (T_s(x) - T_\infty) / (q'' L / K_f)$$

By dividing both sides of the temperature difference equation for a uniformly heated flat plate by $(q''L/K_f)$, NDT values are obtained for comparison with experimental data . This comparison will be presented in the quantitative analysis section of this chapter.

1. Quantitative Analysis

The Non-dimensional temperature variation for various power levels along the test surface is displayed in figure 11. In this figure, NDT values are plotted against the non-dimensional location, X/L. Also plotted are the predicted values from two-dimensional boundary layer theory obtained for a uniformly heated flat plate. The flat plate values were obtained via the equations listed above at the same power levels as the test surface.

From this plot of the data, the trend of increasing NDT values along the test surface with increasing X/L location is readily apparent. However, comparing these values with the NDT values representing the flat plate, it is seen that the experimental values do not vary with distance to the 1/5 power as is the case with the flat plate. In general, the experimental values approximately vary with distance to the 1/8 power, hence the correlations developed for a uniformly heated flat plate do not apply for the experimental case of study.

Utilizing the equations presented in chapter two, the temperature data was reduced to form local heat transfer coefficients, Nusselt numbers, and Grashof numbers for locations along the test surface which were at the center of each heater. From the computed values of

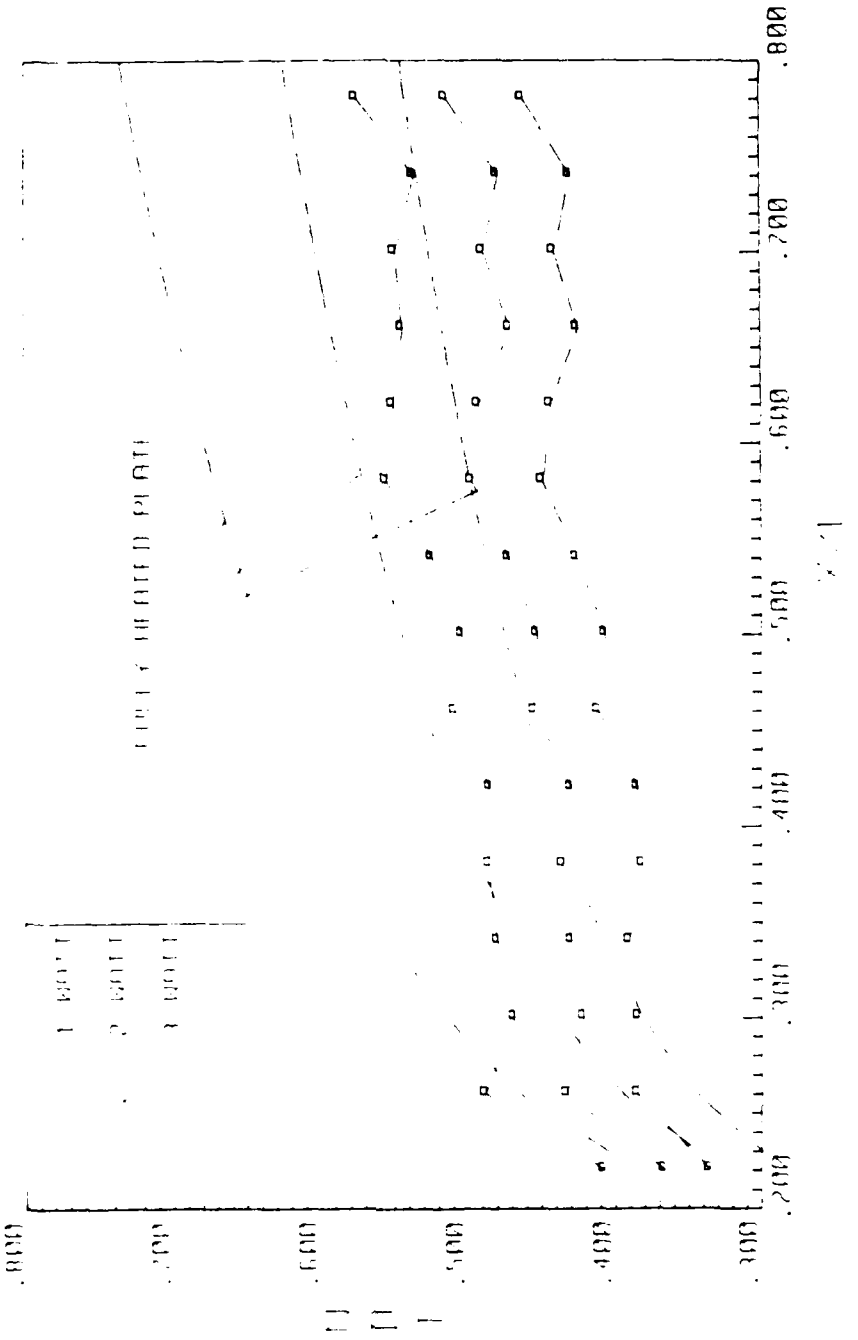

Figure 11. Non-Dimensional Temperature Excess vs. X/L

h, another trend seen, which is related to the variation in **NDT** values, was that the values of **h** indicate a decreasing trend as the flow proceeds from the bottom heater to the top. Since the **NDT** values increase with downstream location, the heat transfer coefficient must decrease due to the fact that the **NDT** values are inversely proportional to **h**. It was also seen that the computed **h** values increased with rising power level. The explanation being that as the component heat flux is increased, the buoyant flow becomes more vigorous. The higher values of **h** at higher power levels cause a corresponding decrease in the non-dimensional temperature excess. This explains the trend of decreasing **NDT** values with rising power at a given **X/L**.

As was mentioned previously, the Nusselt and Grashof numbers were calculated at the geometric center of each heater location. The value of the Nusselt number at each location gives first hand knowledge of the amount of convective energy dissipation from a heater to the fluid, while the value of the Grashof number provides information on the strength of the buoyancy induced flow. With these two non-dimensional parameters known, the heat transfer characteristics needed for evaluation of system performance and design are available, hence the need for determining a correlation which relates the two values.

Figure 12 is a logarithmic scatter plot of all Nusselt and Grashof number data points obtained from the individual heater strip temperatures for power input values of 1, 2, and 3 watts. From the plot it is seen that the Nusselt numbers decrease downstream. This is due to the increasing component temperatures. It is also seen from this plot that the Grashof numbers increase slightly with downstream components. This effect is also related to the rising component temperatures which result in a variation in the fluid thermophysical properties.

From this plot it is obvious that the plots of **Nu** vs. **Gr** data on a logarithmic scale are linear for a given downstream location over the range of power levels analyzed. In order

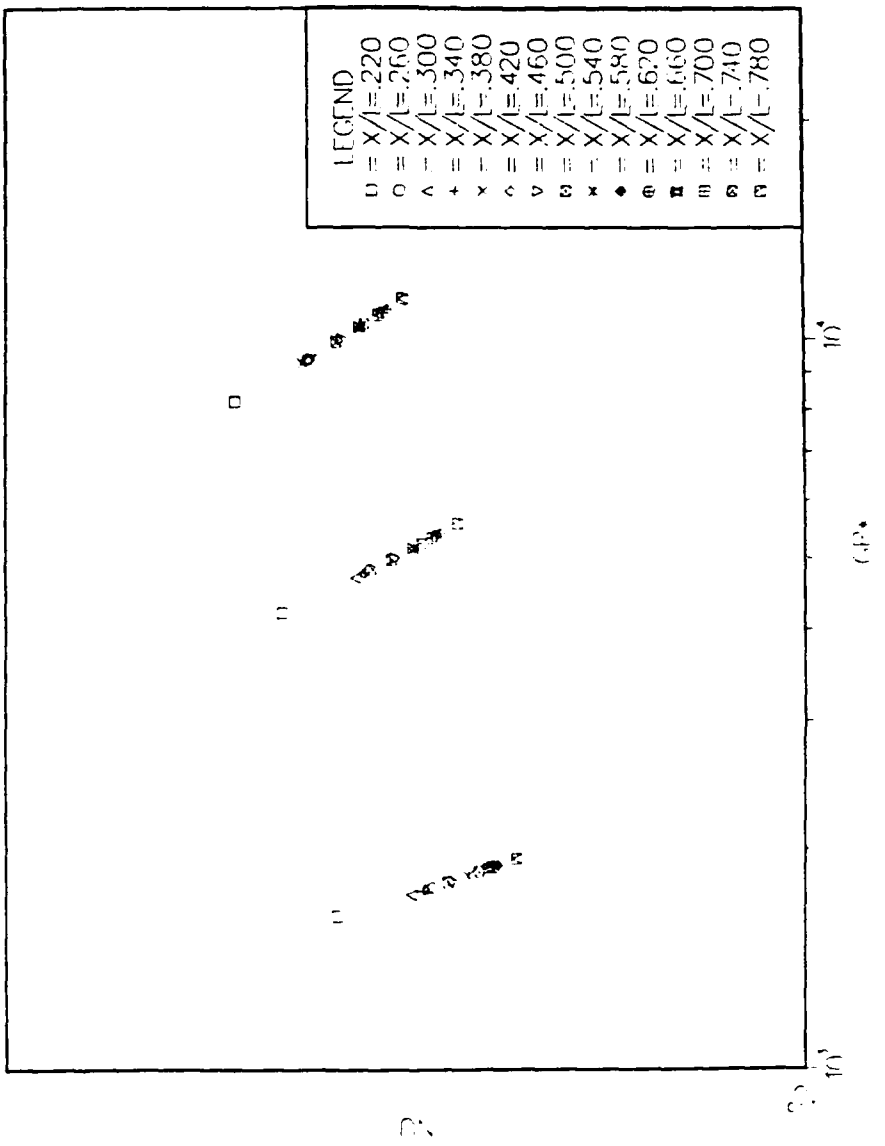

Figure 12. Logarithmic Scatter Plot of Nu vs. Gr*

to have a single correlation for all downstream locations, the increase in the net convected energy downstream needs to be accounted for. This was accomplished by utilizing a modified Nusselt number, **Nu***. In a manner similar to the analysis performed by Knight [Ref. 3], the modified Nusselt number is defined:

$$Nu^* = Nu_n \; S_n^{1/13}$$

The value of $S_n^{1/13}$ in the above expression is a scaling factor and the value of **Sn** refers to the respective heater strip number in the column with one being the bottom heater.

The Nu* vs. Gr* variation is plotted in figure 13. From this plot it is seen that the use of modified Nusselt numbers effectively compresses the data from which the following correlation relating Nu* and Gr* is developed:

$$Nu^* = .910 \; Gr^{*.122}$$

In order to see how well this correlation fits the experimental data, this equation is plotted on figure 13 along with ± 5% deviation lines. The majority of data fall within the ± 5% boundaries thus justifying its use for describing the thermal transport. The correlation is applicable for a Grashof number range of $1600 < Gr^* < 21000$ for fluids having a Prandtl number approximately equal to 7.

2. Probe Measurements

With a thermocouple probe, the temperature of the fluid adjacent to the test surface was measured at precise locations in order to evaluate how the thermal boundary layer developed as the flow proceeded downstream. The probe was moved both in the normal and spanwise directions in the vicinity of the test surface.

During spanwise movement, the probe provided information on the shape of the thermal boundary layer along the length of a particular heater. Figures 14 and 15 are the spanwise fluid temperature variations at y = 9 mm along the first, eighth and fifteenth heater at one and three watts respectively. The probe was traversed 18 mm in both the

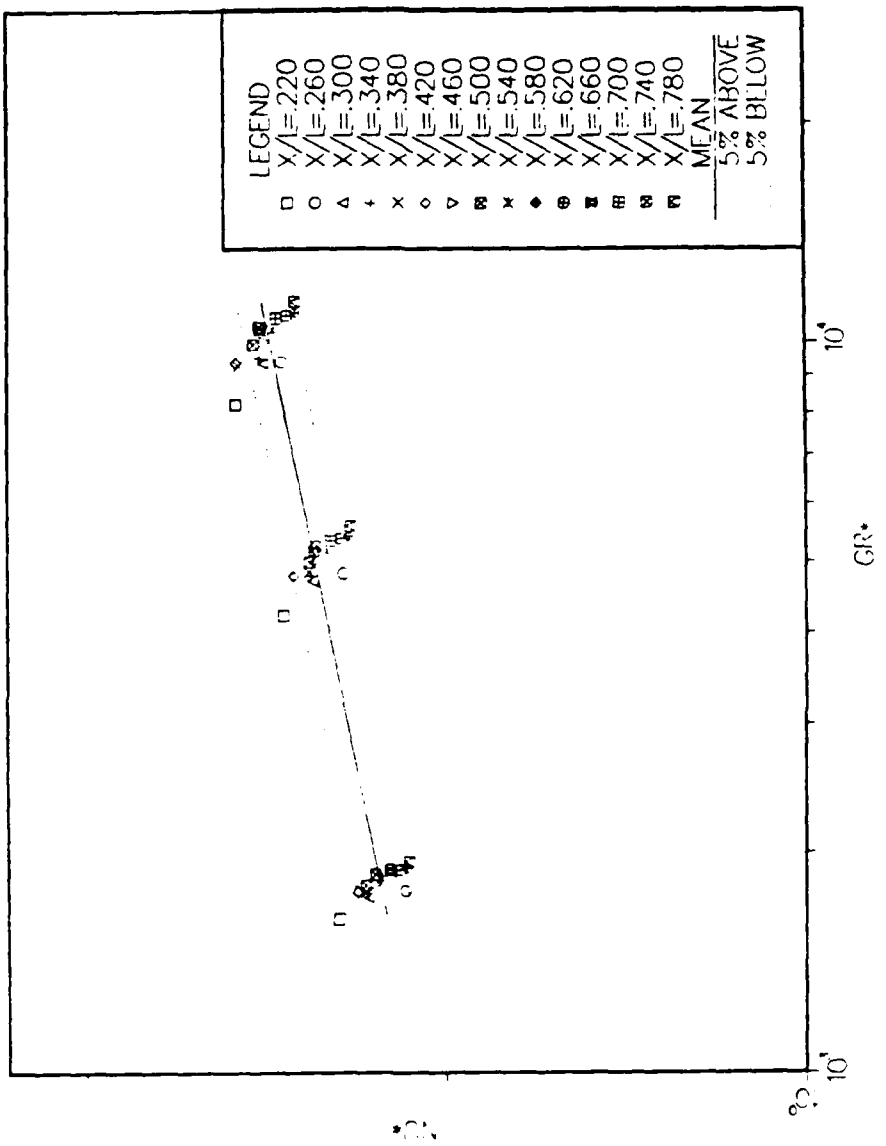

Figure 13. Nu* vs. Gr* on a Logarithmic Scale

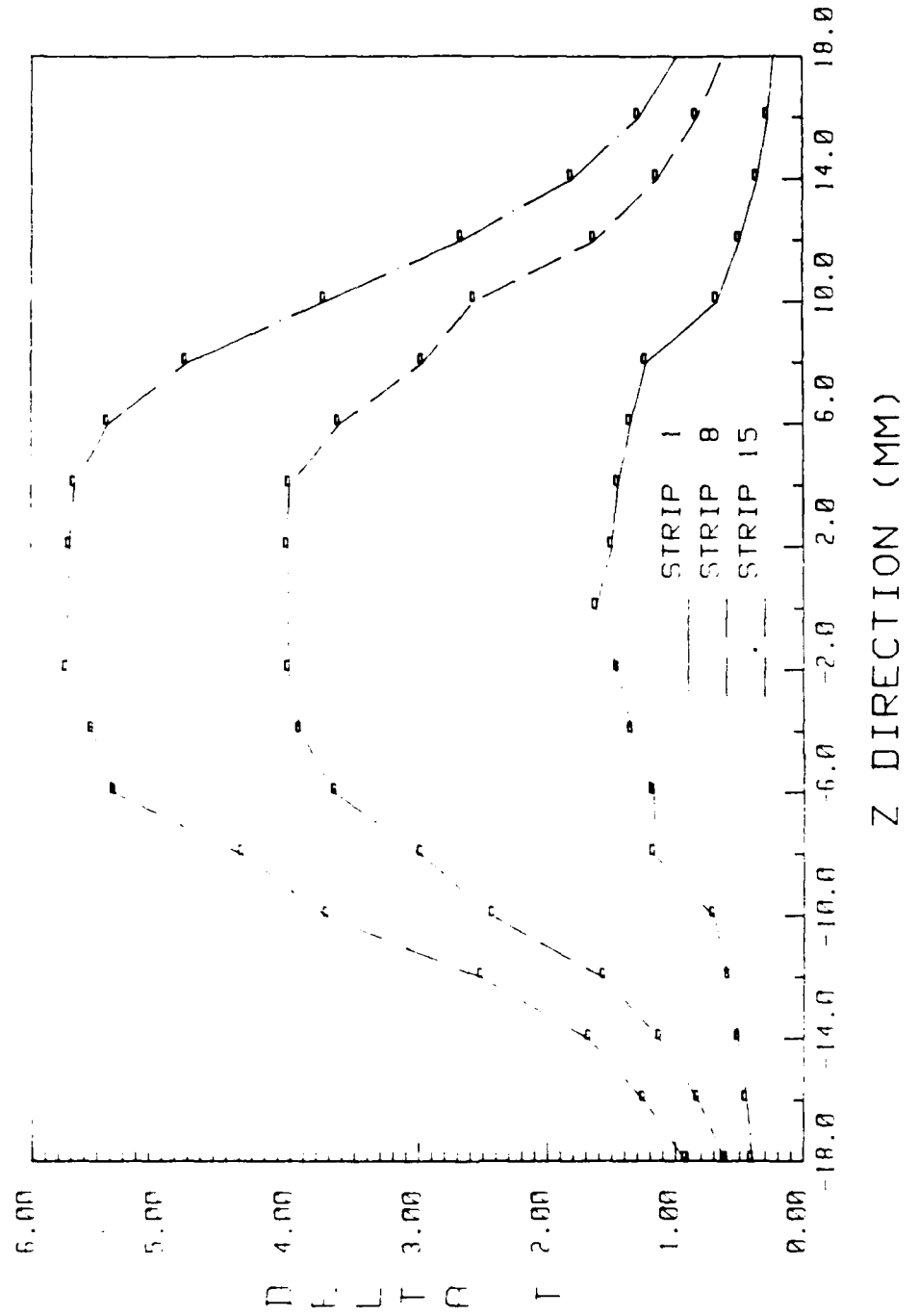

Figure 14. Spanwise Temperature Variation with 1Watt Input Power. Measurements Taken at y = 9 mm.

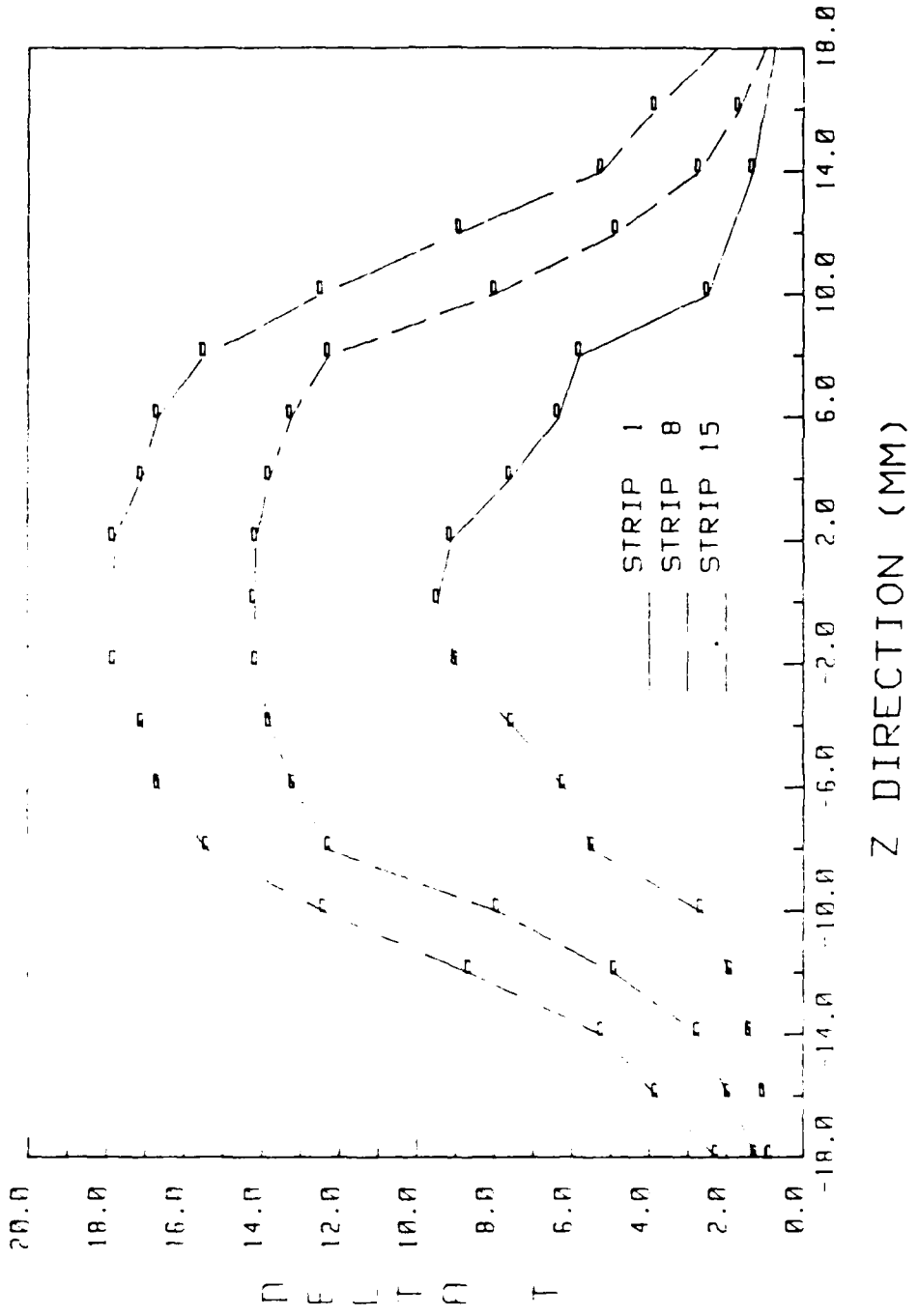

Figure 15. Spanwise Temperature Variation with 3 Watt Input Power. Measurements Taken at y = 9 mm.

positive and negative directions from the heater centerline. The heater spanned 17.9 mm in both directions, hence the data presented in these figures cover it's entire length.

From these figures, it is seen that the temperature rise of the fluid is symmetric about $z = 0$ where the highest temperature rise occurs. This symmetry is preserved for both one and three watt input power levels. Another trend seen at both power levels is the increase in the extent of the heated fluid as it proceeds toward the top heater. It is also observed that the ratio of temperature rise from the bottom to the top heater at a given z, increases with increasing power. This is in part due to the increasing rate of growth of the thermal boundary layer at higher levels of heat flux from the heater surface.

By traversing the probe normally to the heater surface, the thickness of the boundary layer was determined at each heater analyzed. For the experimental program, the normal probe runs were accomplished for the same heaters as was done for the spanwise runs. Additional temperature variations in the normal direction were obtained 6.35 mm above the top edge of these heaters in the unheated portion of the test surface. Once again two power levels were used; one and three watts.

Figures 16 and 17 are plots of normal fluid temperature variation away from the centers of heaters 1, 8 and 15. Referring to figure 16, it must be pointed out that the probe started recording fluid temperature measurements at a point .9 mm from the test surface. The values from 0 mm to .9 mm were plotted using the heater temperature recorded at the surface and extrapolating values in between these two boundaries. The same procedure was performed for the three watt input power case shown on figure 17. The only difference in this case is that the outward probe movement was started at a point 6 mm from the heater surface.

The thermal boundary layer was defined in the region within which 95% of the temperature drop between the surface and the ambient takes place. Figure 18 is a profile of the resulting boundary layer which was constructed using the thickness values obtained at

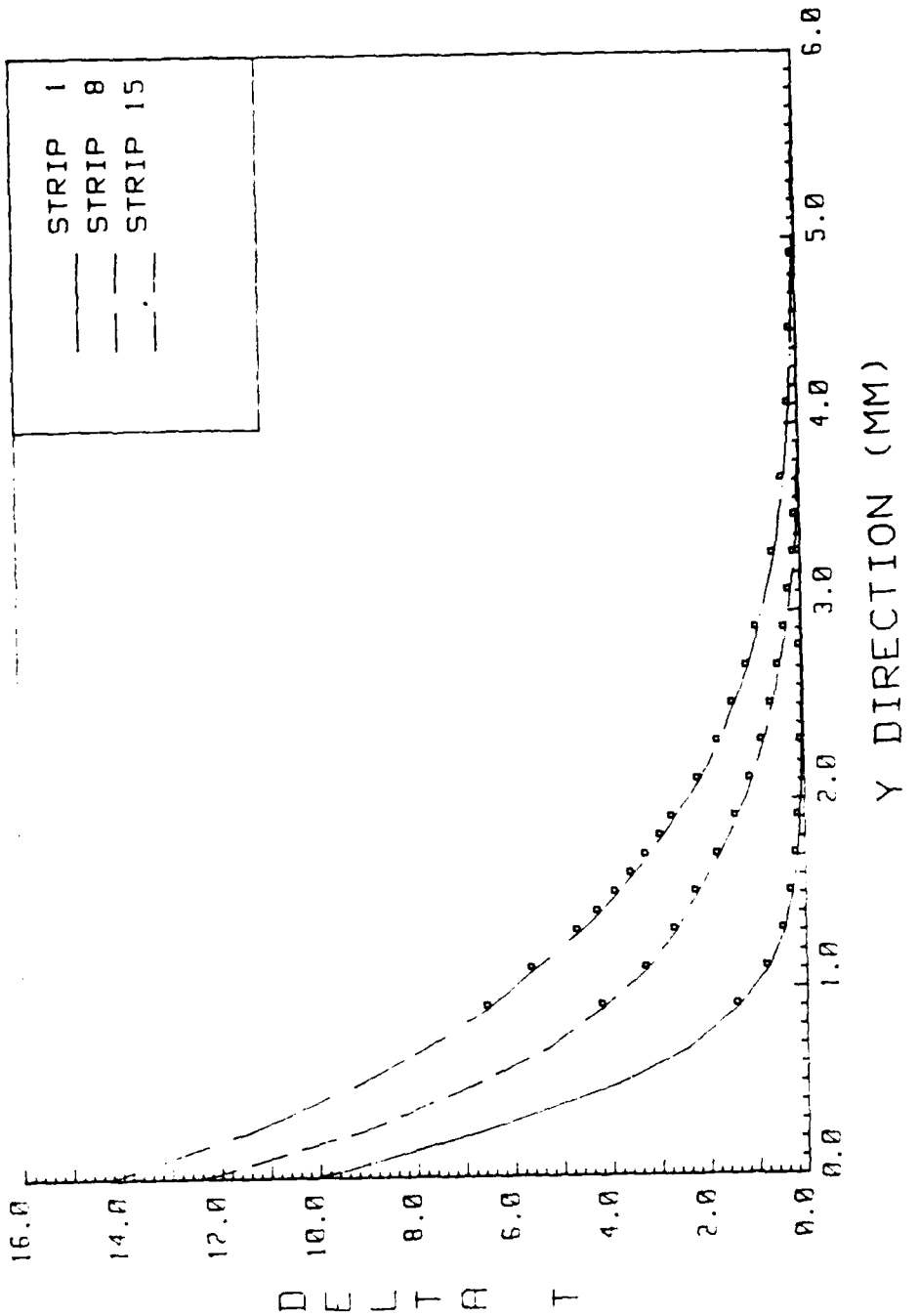

Figure 16. Normal Temperature Variation at Heater Centerline with 1 Watt Input Power.

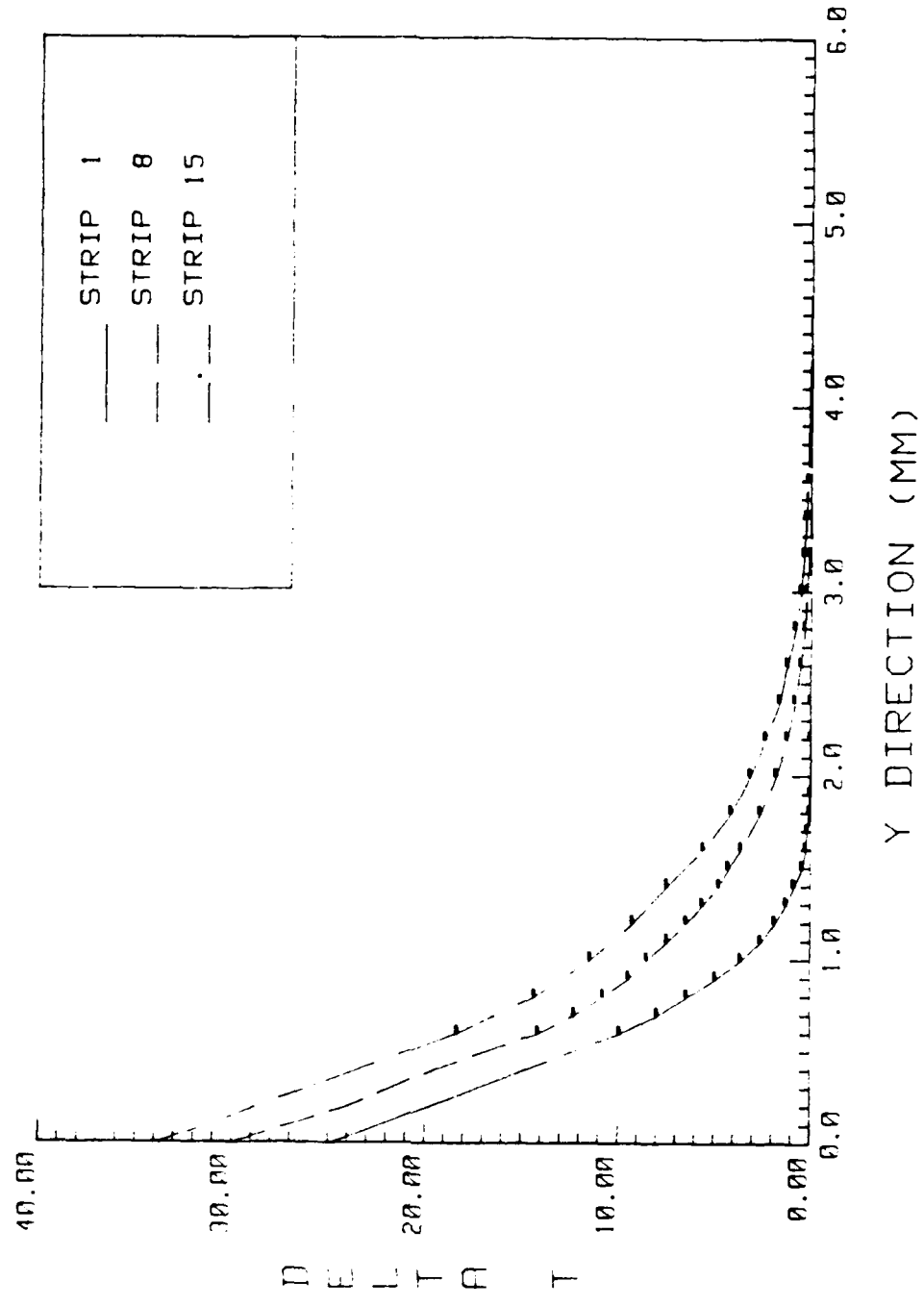

Figure 17. Normal Temperature Variation at Heater Centerline with 3 Watt Input Power

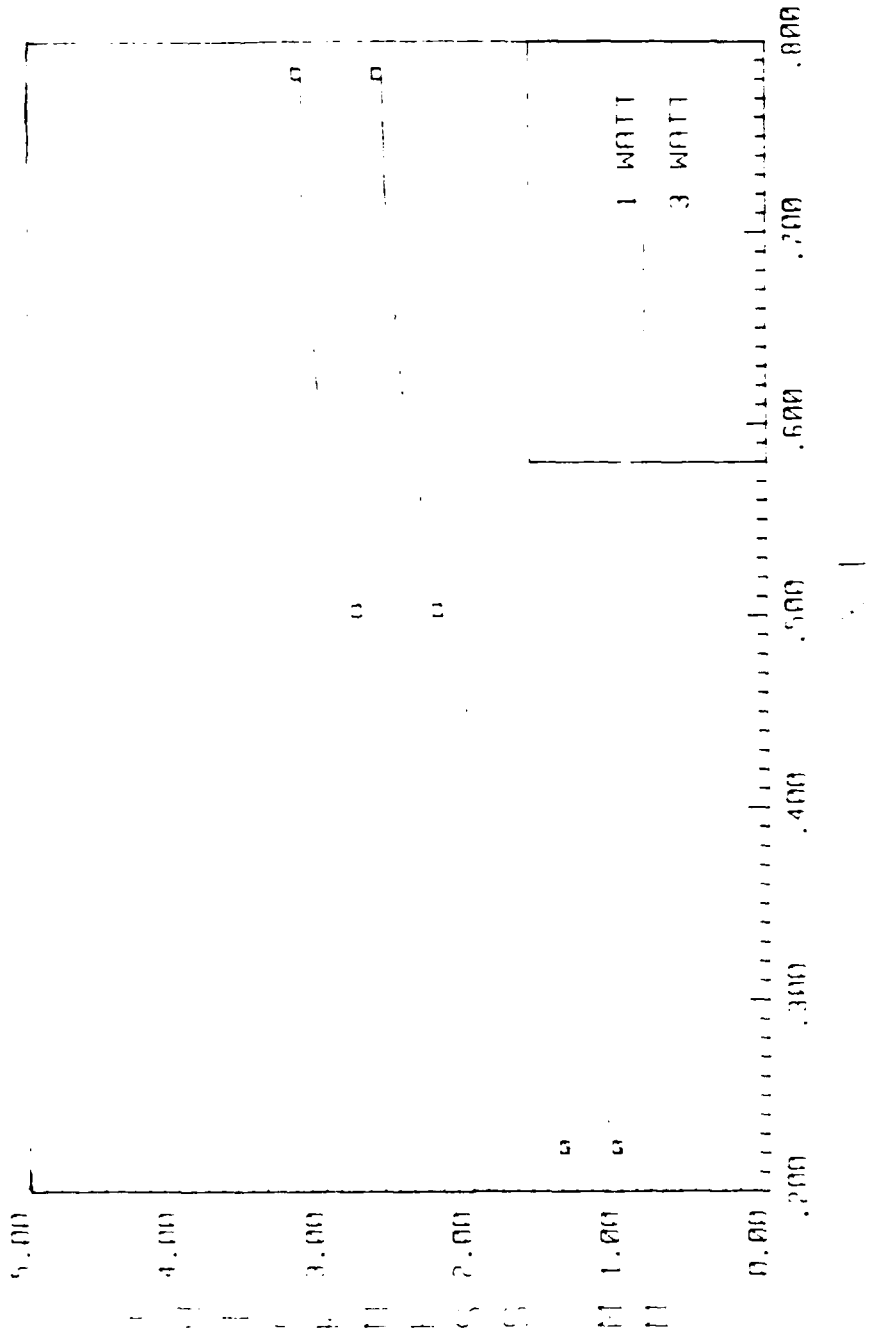

Figure 18. Thermal Boundary Layer Thickness vs. X/L

heaters 1, 8 and 15. From this figure it is seen that the thermal boundary layer decreases in thickness as the power level is increased at a given downstream location. This is in accordance with the 2-dimensional boundary layer theory.

The probe output for the positions 6.35 mm above heaters 1, 8, and 15 are plotted on Figures 19 and 20. The probe starting position for these cases was 0.4 mm away form the heater surface. From the curves shown on these plots, it is seen that the slope of the temperature vs. normal distance is slightly positive near the surface, leading to the conclusion that the non-heated portion of the test surface in between heaters receives heat from the fluid. This conclusion was confirmed with the surface colors produced with the liquid crystals. The heater surface displayed a dark blue color while the region inbetween heaters showed a light green. The color seen inbetween heaters indicate that thermal energy is present at this location, however it was shown previously that conducted energy is virtually one-dimensional in the direction normal to the test surface. Hence the fluid deposits energy onto the surface at unheated locations downstream.

3. Flow Visualization

Figures 21 and 22 are flow patterns showing the growth of the momentum exchange region in the x-y plane as the flow proceeds from the bottom heater to the top. Figure 21 displays the flow development along $z = 0$, as well as for $z = \pm 12$ mm at a power level of .2 watt. From this figure, the symmetry of the flow development along $z = \pm 12$ mm is evident.

Figure 22 shows the flow development along the same planes as in Figure 21 at a power input of 1 watt . Again for this case the flow visualization for $z = \pm 12$ mm display a symmetry about $z = 0$.

From the flow visualization pictures, the boundary layer thickness can be determined at any downstream location. These measurements are seen in Figure 23 as a function of position variable X/L. These curves are generated from the centerline and edge pictures

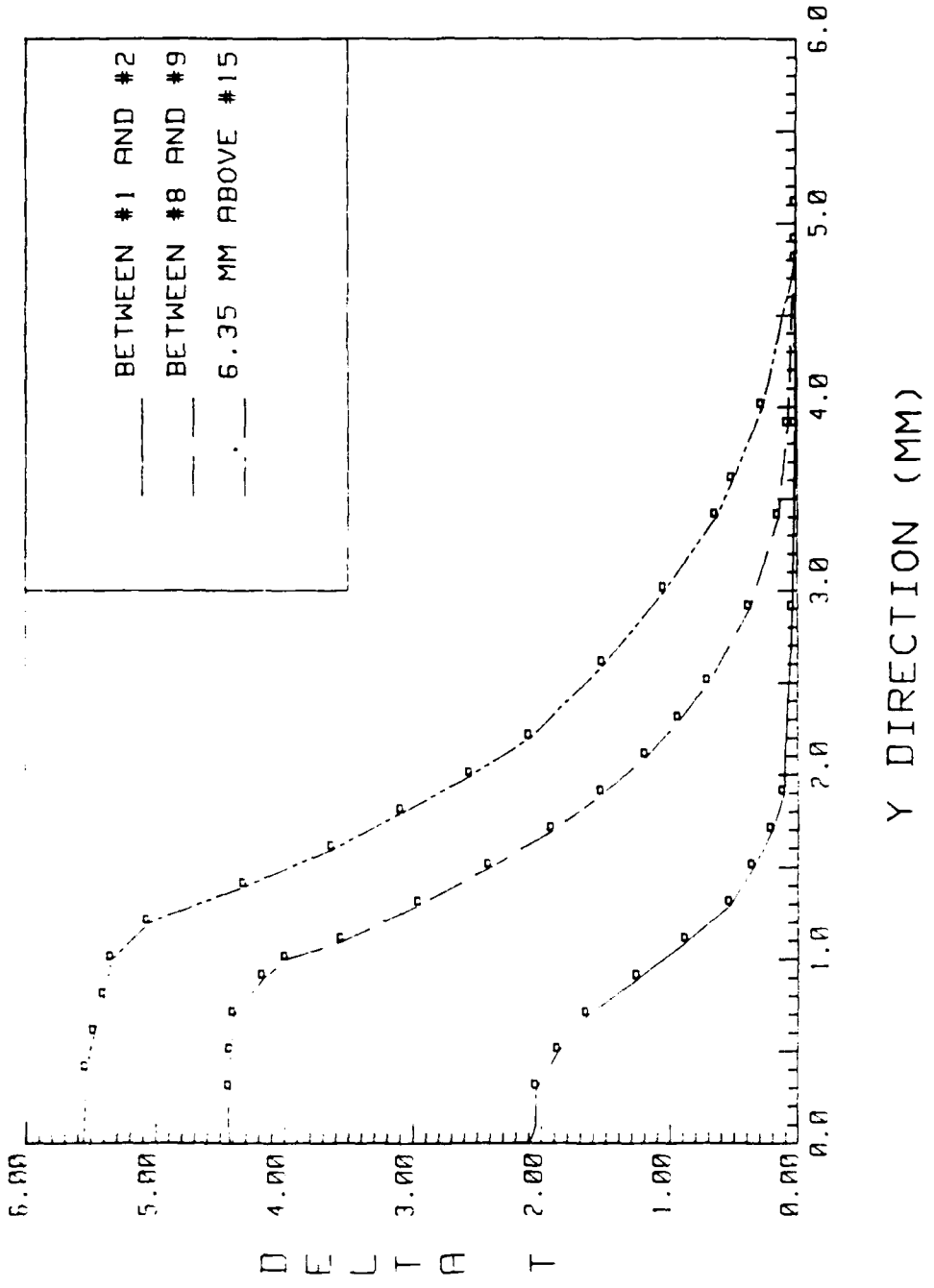

Figure 19. Normal Temperature Variation at 1 Watt Input Power for Positions 6.35 mm above Heaters

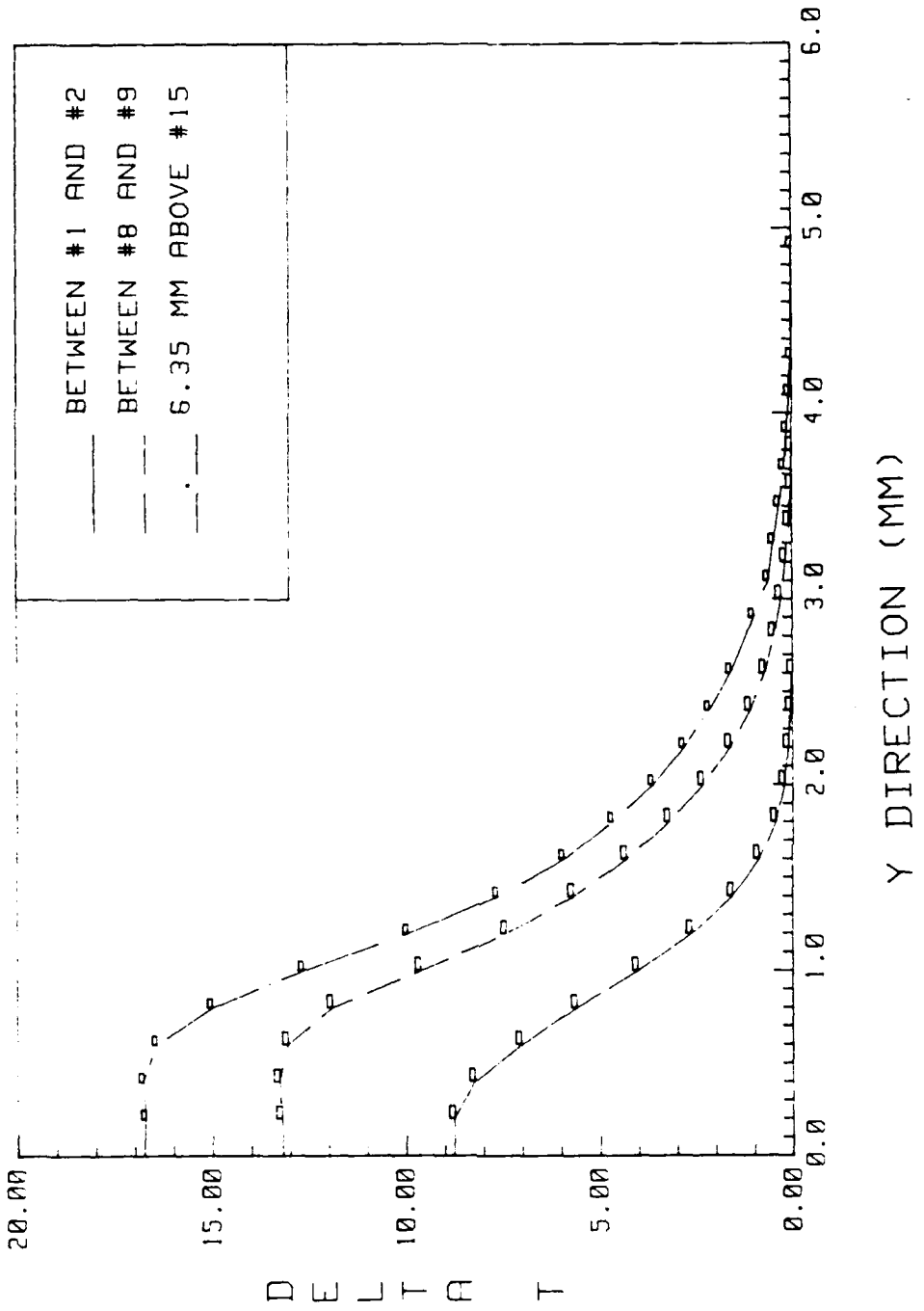

Figure 20. Normal Temperature Variation at 3 Watt Input Power for Positions 6.35 mm above Heaters

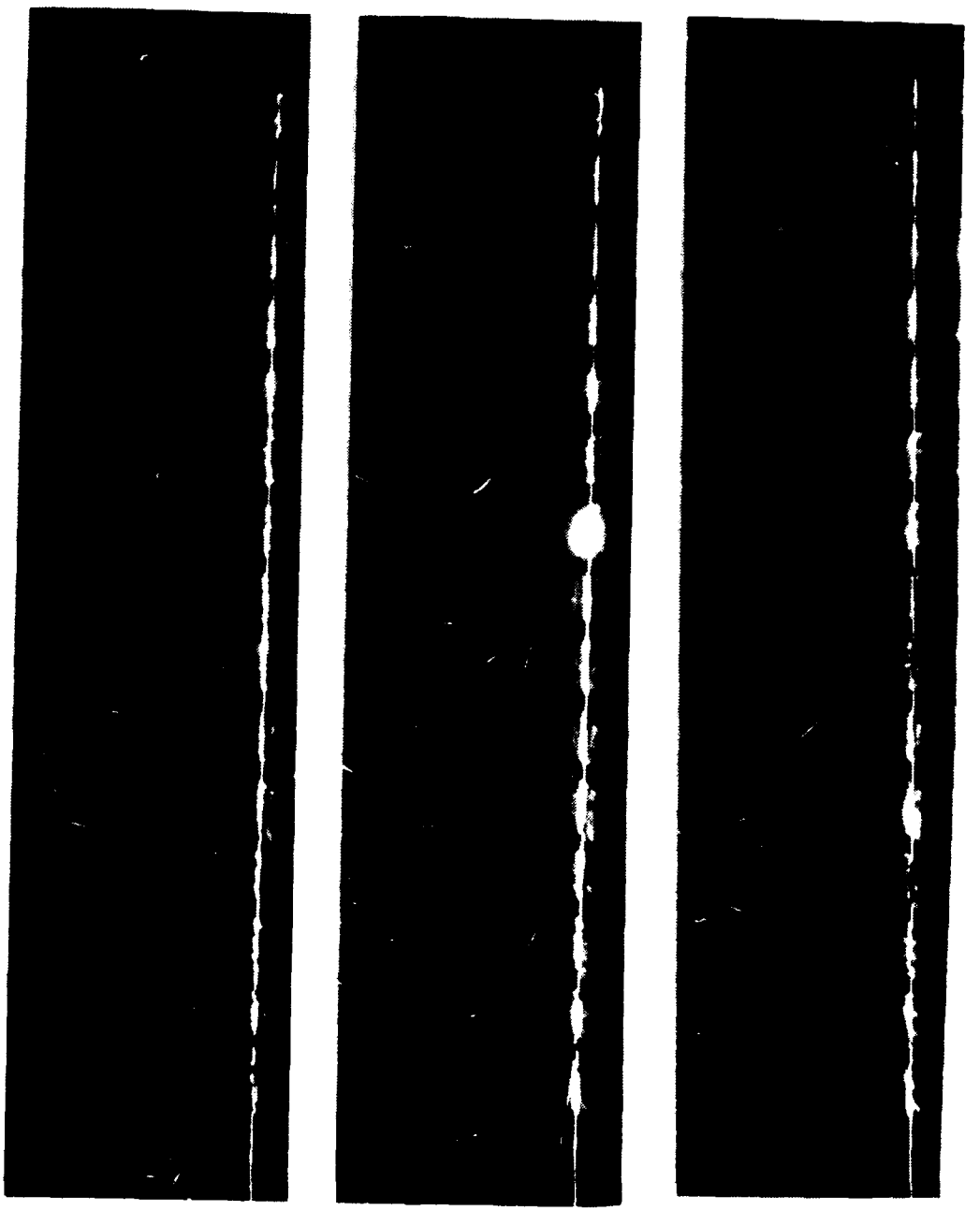

Figure 21. Steady Flow in the x-y Plane for .2 Watt Input Power

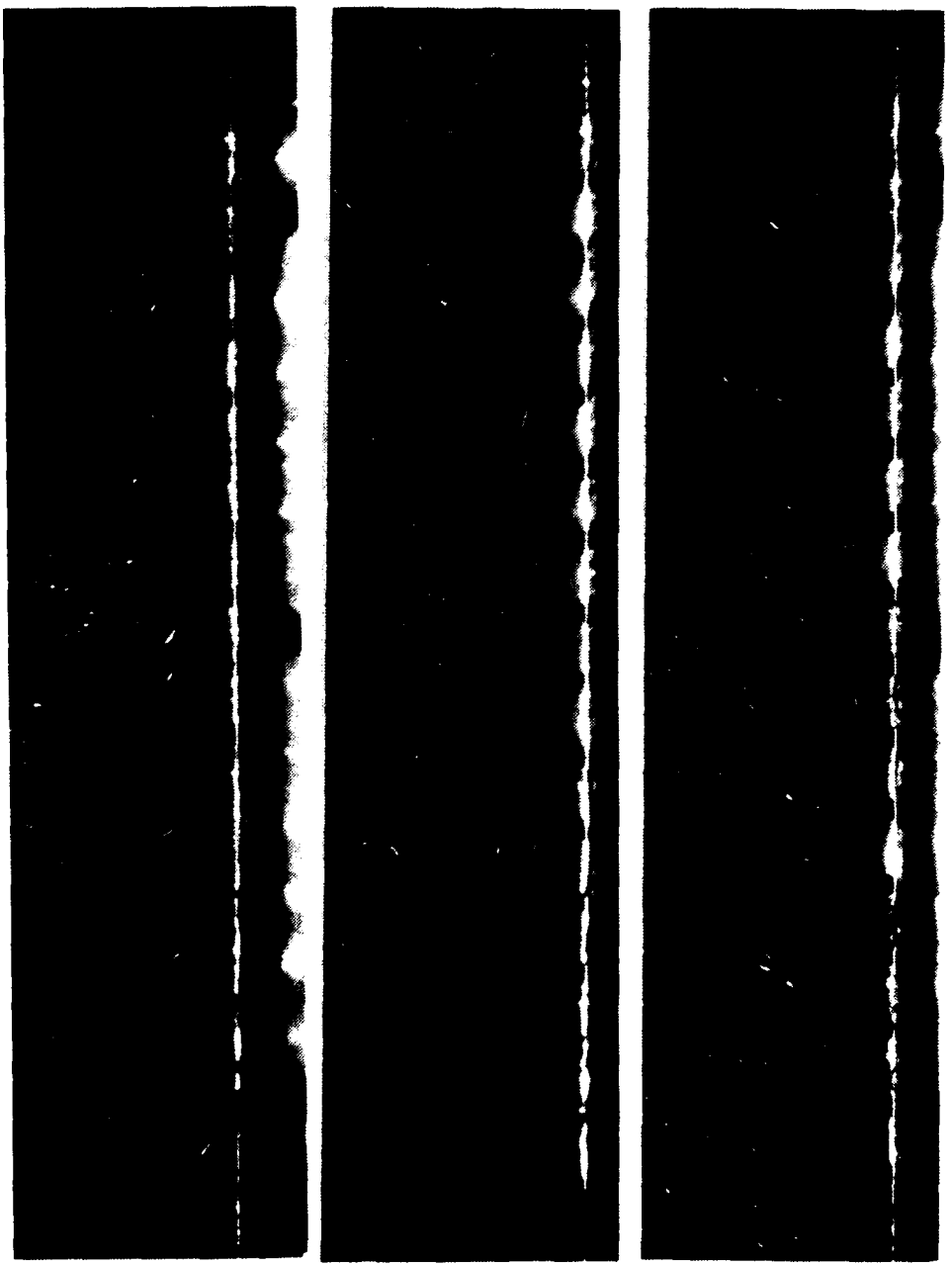

Figure 22. Steady Flow in the x-y Plane for 1 watt Input Power

for both .2 watt and 1 watt input power. From these figures, it is first seen that the boundary region is thicker at the heater edges than the heater centers at a given x. Another trend seen in a z = constant plane is that the boundary region at a given x becomes thinner as the power level is increased. As the power levels increase, the larger wall temperature gradient results in a thinner thermal transport region. This in turn causes a reduction in the thickness of the momentum exchange region.

4. Boundary Layer Effects

In order to verify the thicknesses of the boundary layer profiles, the data points obtained for the first heater at the bottom of the column were checked with values obtained from 2-D boundary layer theory [Ref. 7]. The 2-Dimensional theory predicted the thermal boundary layer thickness at x = 3.90 mm for an input power of 1 watt as 1.9 mm. The momentum layer thickness was predicted as 5.7 mm for the same position and same power input. From Figures 18 and 23, it is seen that the experimentally determined values reasonably match the predicted values thus verifying the probe data and flow visualization photographs.

Referring back to both Figures 18 and 23, it is apparent that the thermal boundary layer is well imbedded within the momentum boundary layer. A direct consequence of the difference in magnitude between the two layers is that the heat transfer characteristics of the system should not be greatly effected by placing a shroud wall in front of the test surface as long as the distance between the two surfaces is greater than the thermal boundary layer thickness. Hence, the heat transfer correlation developed above which relates Nu* and Gr* should also apply for shroud wall spacings which are larger than the greatest thermal boundary layer thickness. It is this hypothesis which is argued in the second portion of this chapter which investigates the effects of a shroud wall.

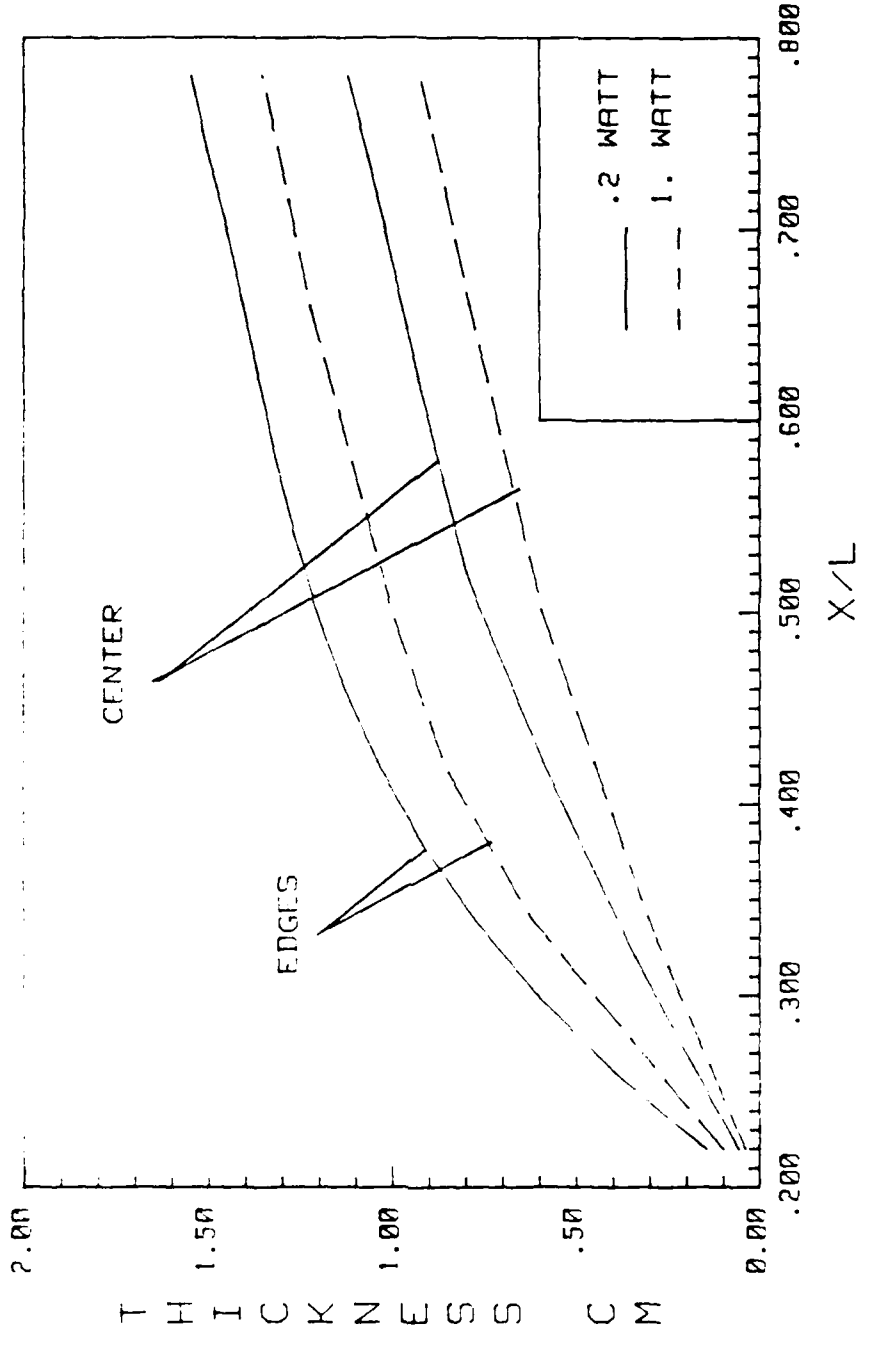

Figure 23. Momentum Boundary Layer Thickness vs. X/L

B. SINGLE COLUMN TRANSPORT WITH SHROUD

In the previous section, it was postulated that, based on the order of magnitude difference between the thermal and momentum boundary layers, the effects of the shroud on heat transfer should not be apparent until the shroud distance from the test surface is compressed to a point where it is smaller than the thermal boundary layer thickness. In order to investigate this prediction, a plexiglass shroud was placed in front of the test surface and heater temperature values were recorded for various power levels and shroud spacings. Flow visualization pictures were also taken in order to gain an understanding of the natural convection flow within the channel.

Figures 24, 25, and 26 are graphs of **NDT** values verses the position variable **X/L** at power levels of 1, 2 and 3 watts respectively for shroud spacings of 15, 12, 9, 6 and 3 mm. In each plot, all curves representing various shroud spacings with the exception of 3 mm, collapse together. The 3 mm shroud curve shows higher temperature values than the other spacings beyond the sixth heater element located at an X/L value of .420. As the power levels increase, the NDT values approach those for larger spacings. This trend is based on momentum and thermal boundary layer thicknesses. Since it was seen previously that at one watt input power the thermal boundary layer is approximately 3 mm thick at the sixth heater, the increase in **NDT** values is expected for the 3 mm shroud spacing. The thermal boundary layer thickness decreased with increasing power. As a consequence, it is also expected that the difference in **NDT** values shown by the 3 mm spacing decreases with increasing power. If it were possible to continue the experimental procedure for even higher power levels than those studied, the difference with the 3 mm spacing is unlikely to exist and in order to see any deviation, the spacing must be decreased further.

Another approach to study the effects of shroud spacing on temperature data is seen in Figure 27 where the dimensional temperature difference for each heater is plotted at the shroud spacings analyzed. From this plot it is again seen that the **delta T** remains constant

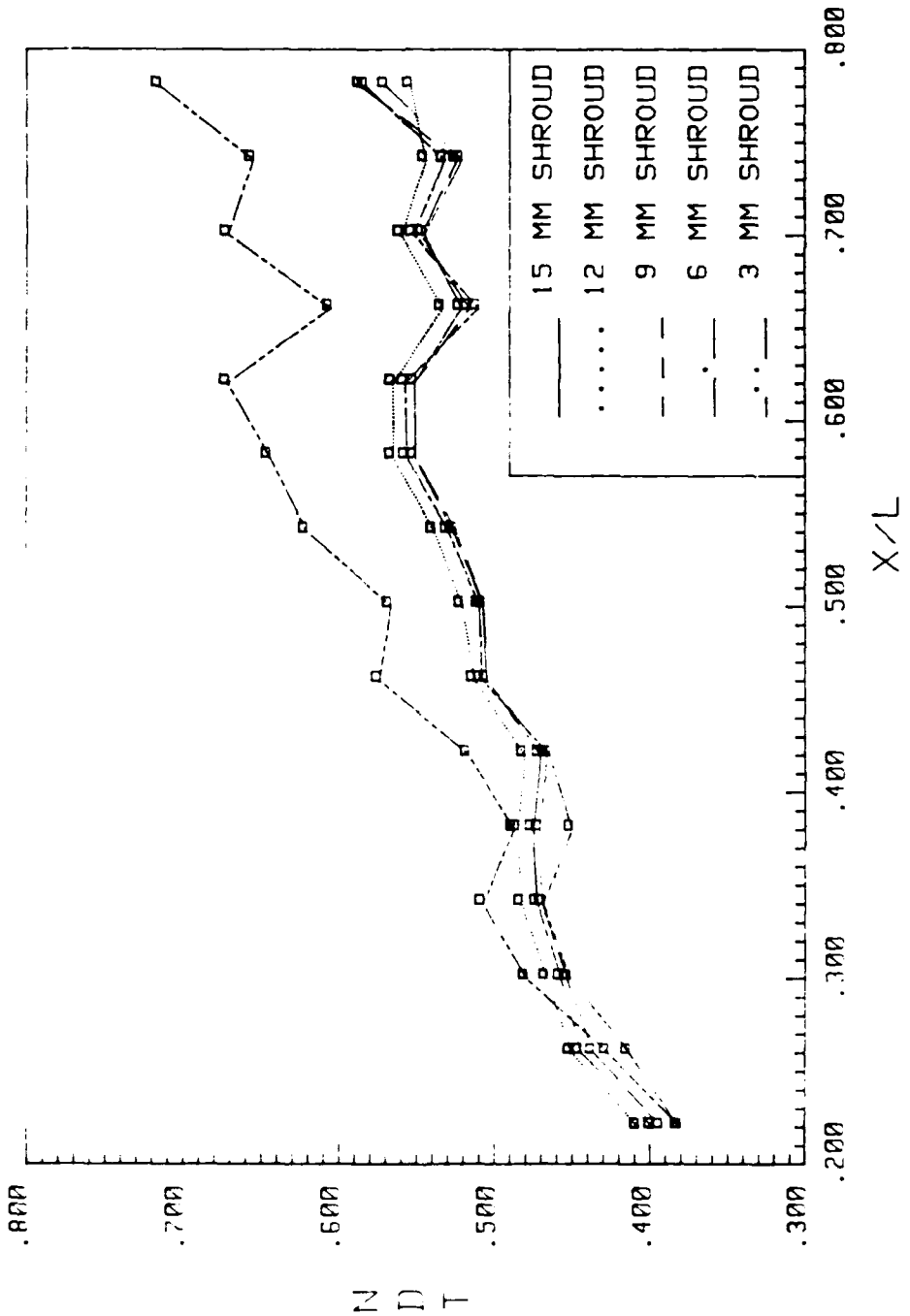

Figure 24. NDT vs. X/L for 1 Watt Input Power

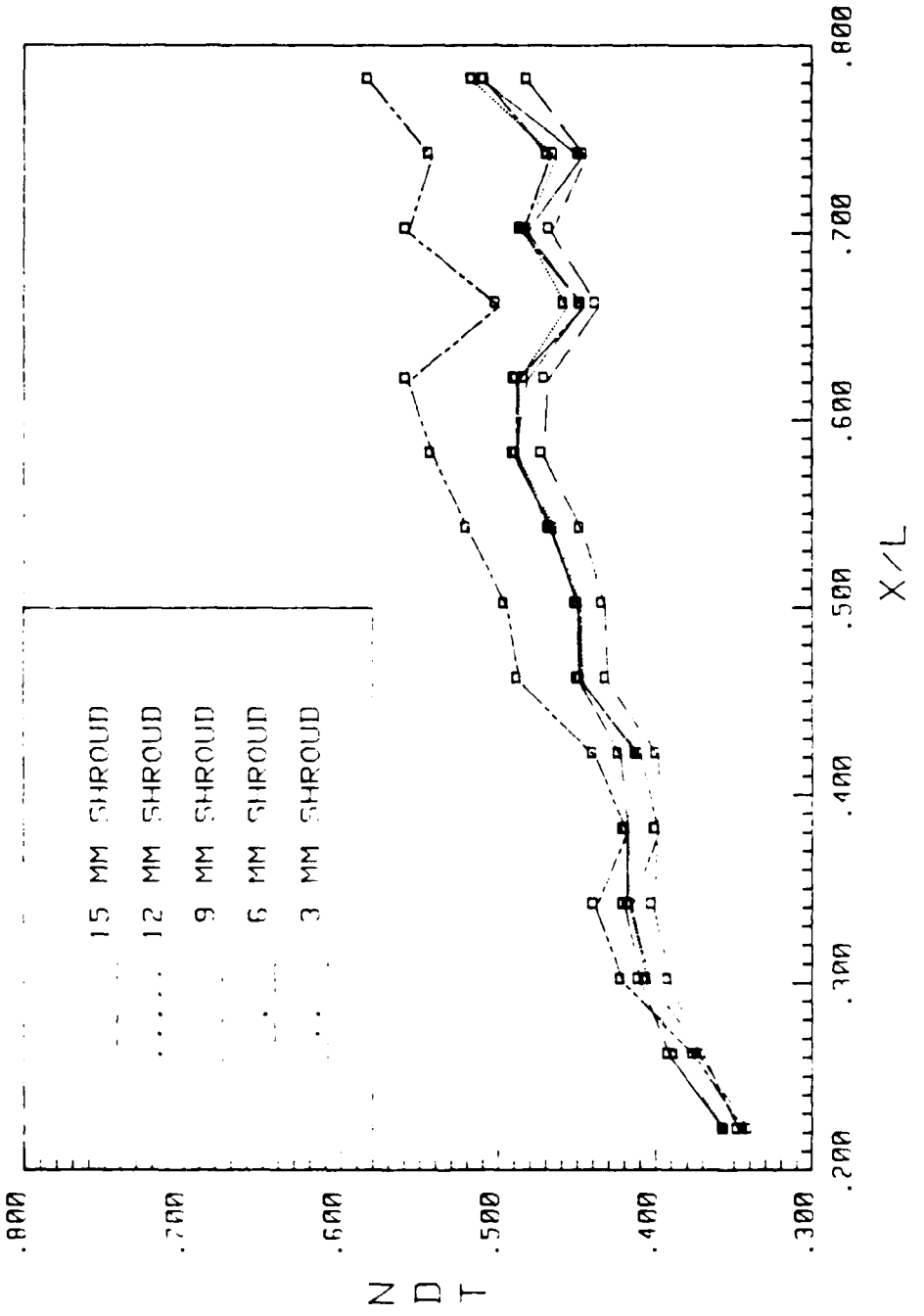

Figure 25. NDT vs. X/L for 2 Watt Input Power

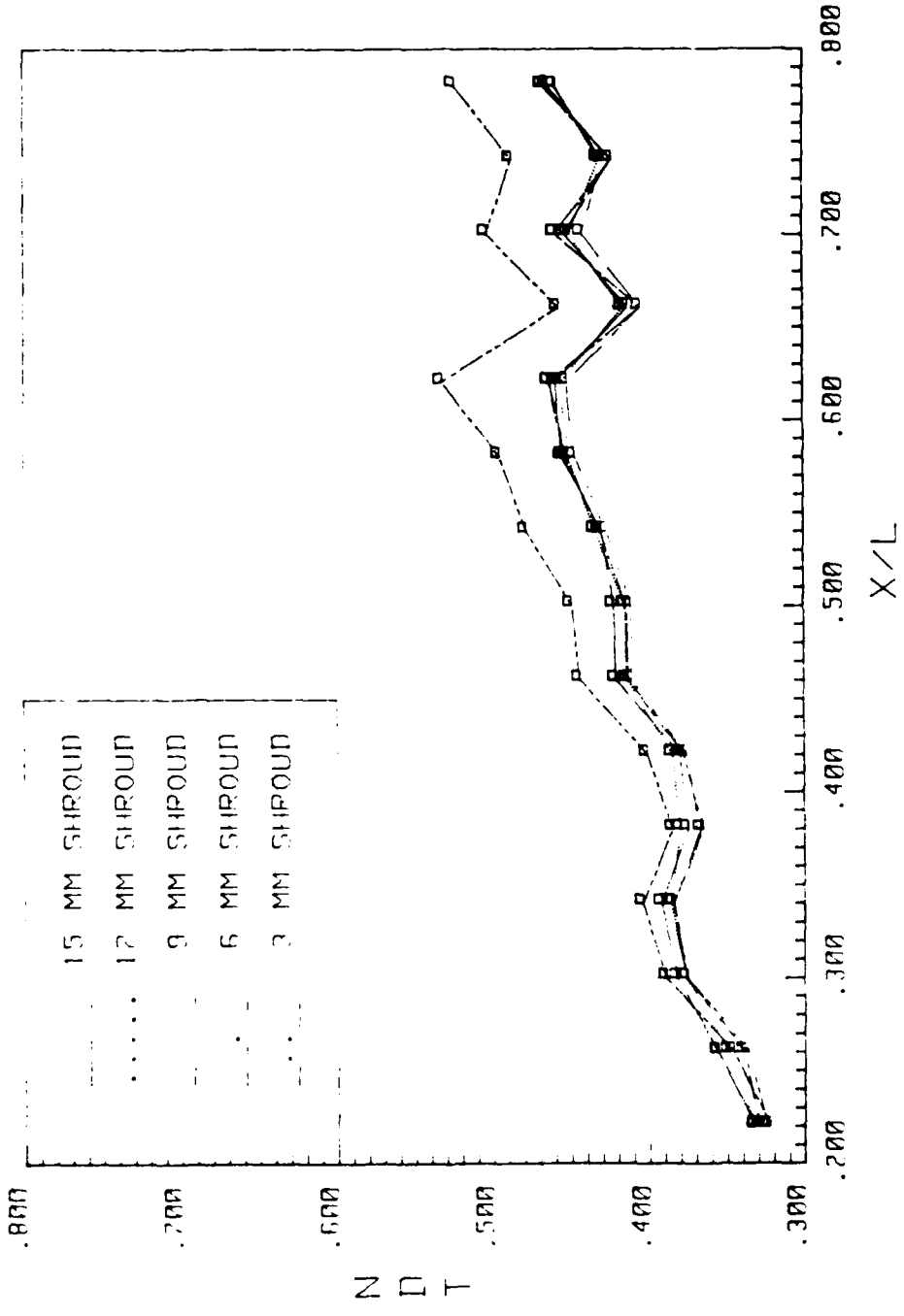

Figure 26. NDT vs. X/L for 3 Watt Input Power

for all spacings with the only exception at 3 mm. It will be shown in the following section, that the correlations developed earlier for the unshrouded test case still hold for shroud spacings up to 3 mm.

1. Quantitative Analysis

Figures 28, 29 and 30 are plots of the Nu^* vs. Gr^* on a logarithmic scale for shroud spacings of 12, 6 and 3 millimeters respectively. The values plotted were obtained from test runs at power levels of .5, 1.0, 1.5, 2.0, 2.5 and 3.0 watts. On each of these plots, the correlation developed for the unshrouded case and the 5% deviation lines are also plotted.

The first apparent trend is that as the shroud spacing is decreased, the spread of the data points increases leading to the conclusion that a smaller shroud distance causes the normalizing compression factor, $S_n^{1/13}$, to change. In order to compress the data at these smaller shroud spacings, the value of S_n will have to be raised to a slightly higher power.

Neglecting the case of 3 mm shroud spacing, it is seen that even though the spread of data increases with decreasing shroud spacing, the correlation developed for the unshrouded case still predicts the heat transfer characteristics of the system within $\pm$ 6% for the 12 mm shroud spacing and about $\pm$ 8% for the 6 mm shroud spacing.

Returning back to the 3 mm shroud case, it is seen that the data plotted clearly deviates from the values of the unshrouded correlation. This deviation was predicted previously from analysis of the thermal and momentum boundary layers conducted for the unshrouded test surface. A similar trend was observed by Knight for a single column of eight heaters [Ref. 3]. With the 3 mm shroud, the frictional resistance increases to the point where the flow is impeded within the channel. This in turn causes a decrease in convection heat transfer and as a result yields lower Nu and higher Gr^* values.

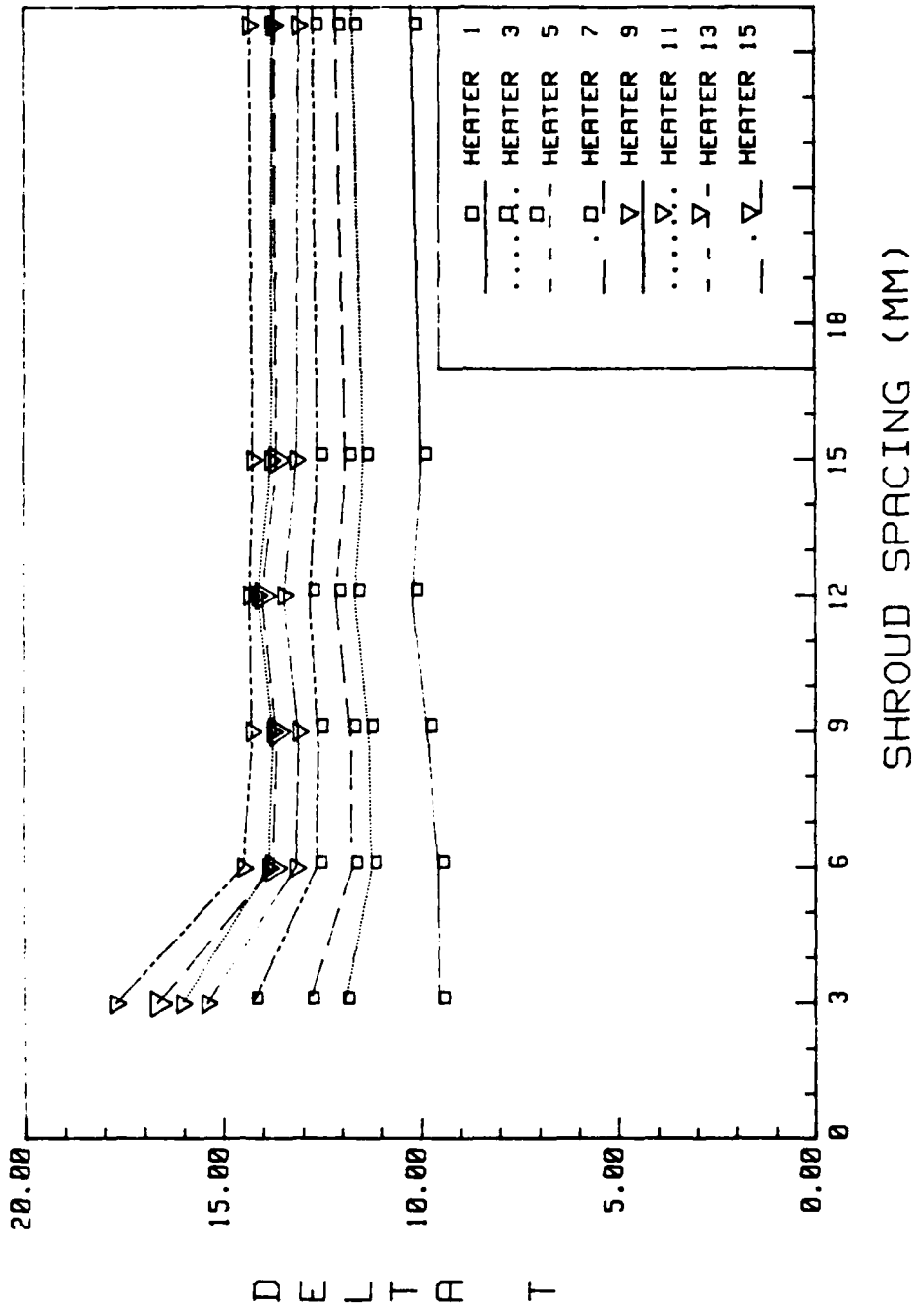

Figure 27. Delta T vs. Shroud Spacing

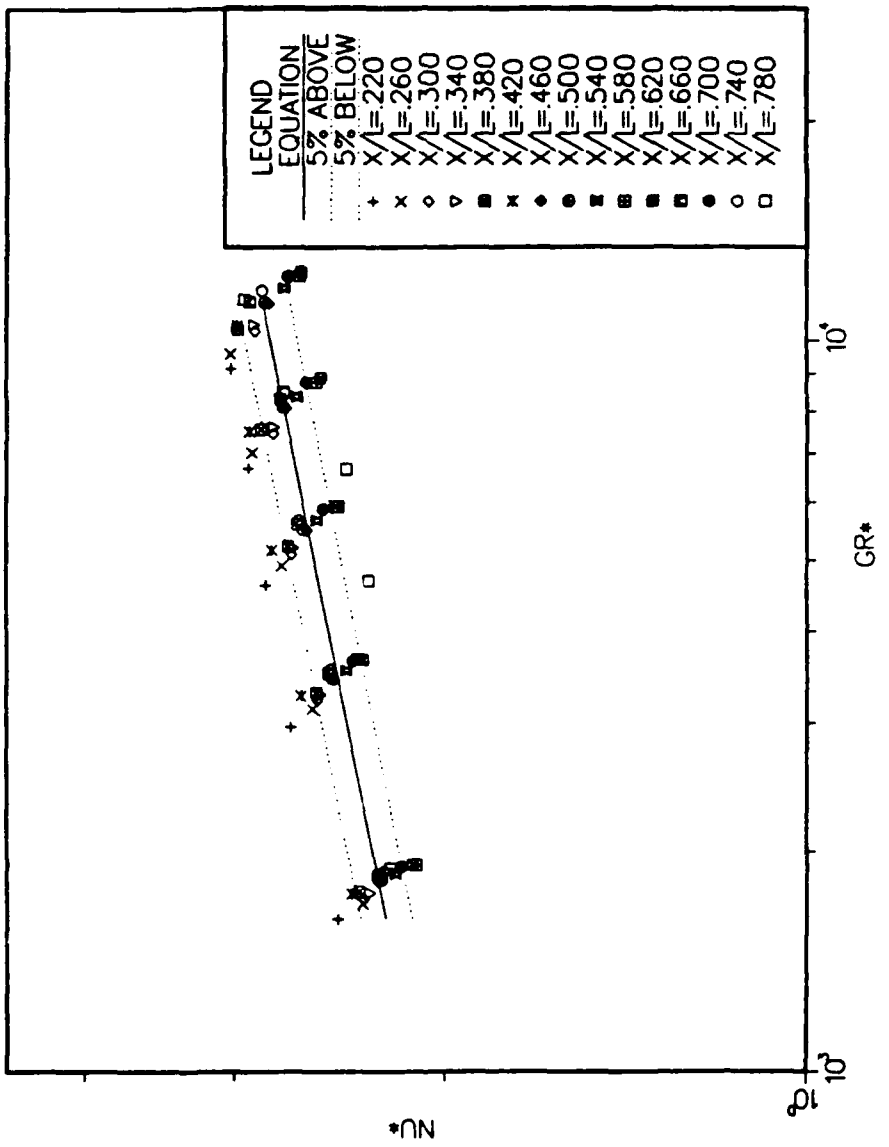

Figure 28. Nu* vs. Gr* for 12 mm Shroud Spacing

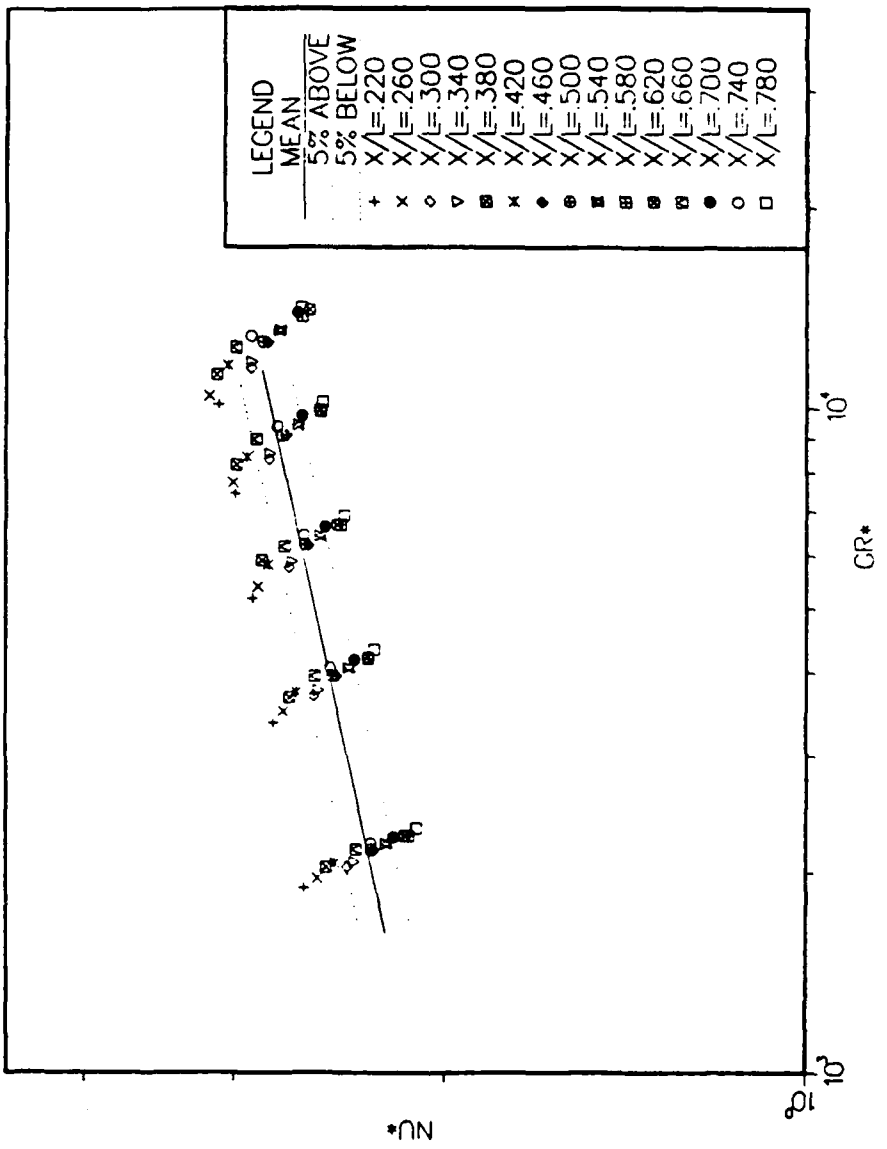

Figure 29. Nu* vs. Gr* for 6 mm Shroud Spacing

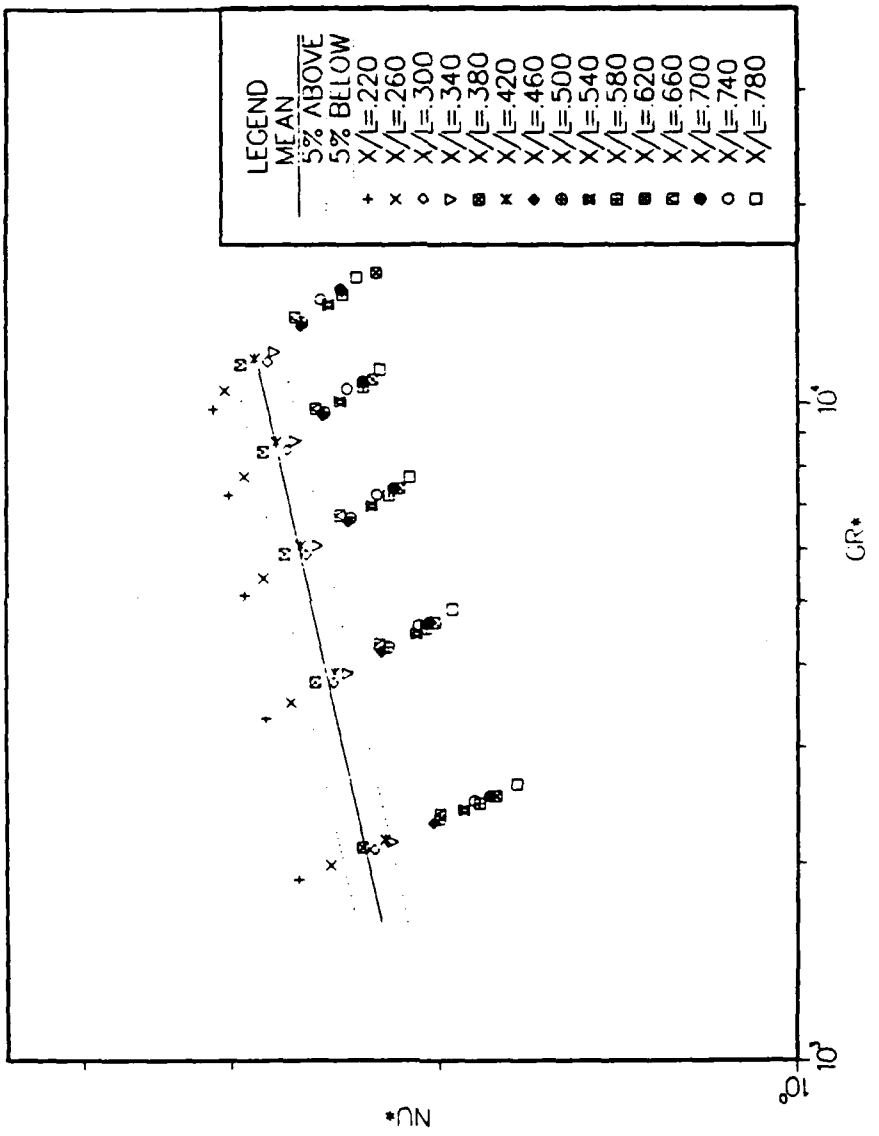

Figure 30. Nu* vs. Gr* for 3 mm Shroud Spacing

2. Flow Visualization

Flow patterns were visualized for shroud spacings of 15 and 9 mm at power levels of .2 and 1.0 watts. As with the unshrouded condition, both x-y and x-z planes were examined.

Figure 31 presents visualizations in the x-y plane through z = 0 for a shroud spacing of 15 mm. The picture on the left is for a power level of .2 watt while the other is for a power level of 1 watt. In both of these photographs, it is apparent that, starting at about the second heater, the developing boundary region adjacent to the test surface merges with the shroud wall and a channel flow begins. Figure 32 displays the same flow patterns in the same plane with the spacing reduced to 9 mm. The same general trends are evident as in Figure 31.

Figures 33 and 34 are flow patterns in the x-z plane near y = 0 for 15 mm shroud spacing at .2 and 1.0 watt respectively. From these pictures, it is seen that the column of heaters entrains considerable fluid flow out from the edges of the test board as well as from the channel inlet into a large buoyant upflow which covers the entire center portion of the test surface. It is also apparent that the higher input power produces a stronger flow. Figures 35 and 36 are the x-z plane visualizations for a 12 mm shroud spacing at .2 and 1 watt input power. These pictures indicate that the flow also becomes stronger with decreasing shroud spacing.

For both the 15 and 9 mm shroud spacings, the thermal boundary layer apparently remains intact even though no flow normal to the board can exist. Since the spacings are larger than the thermal boundary layer thickness, the heat transfer characteristics of the system can be described with the same properties that were seen for the unshrouded case.

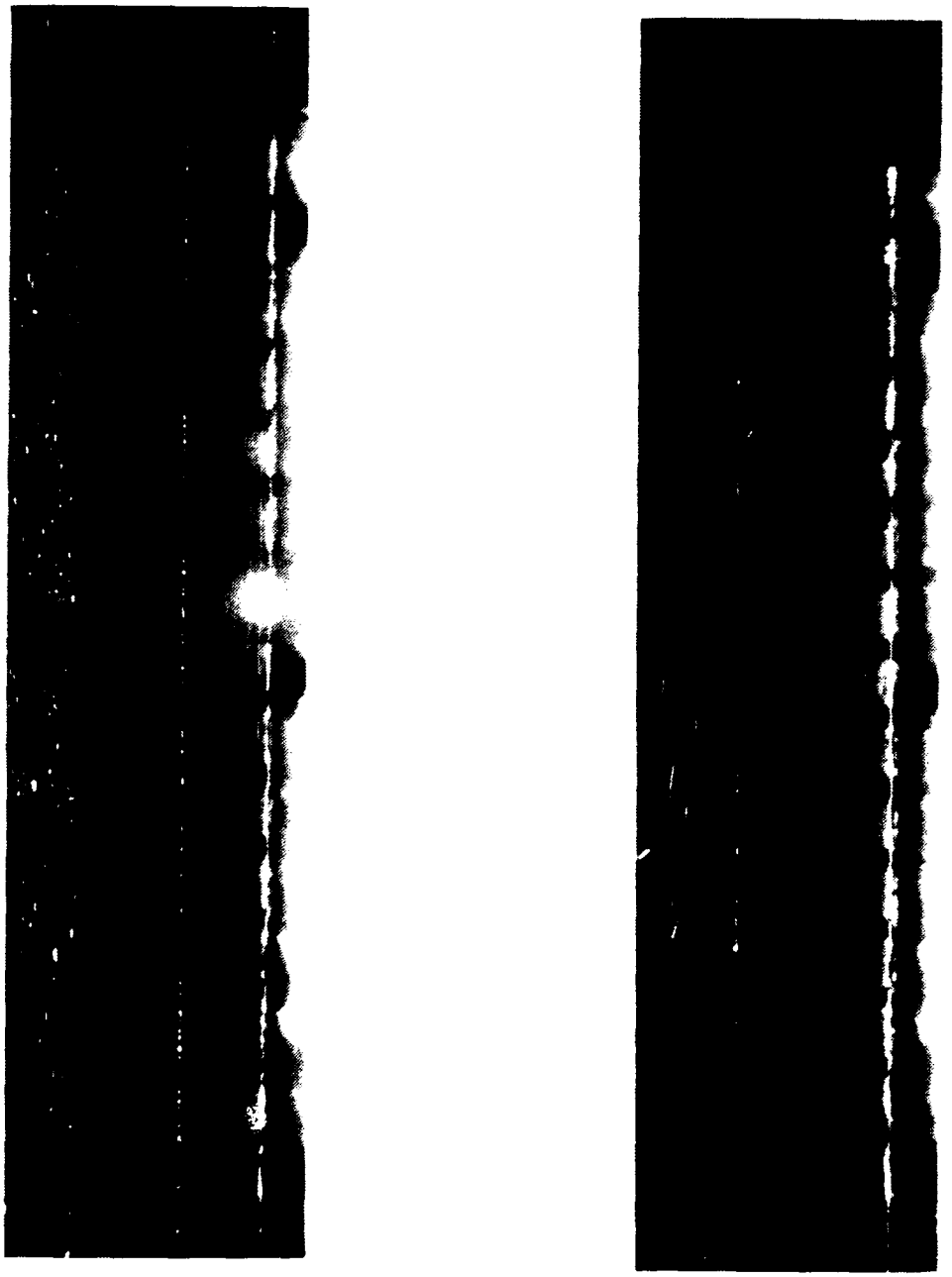

Figure 31. Steady Flow in the x-y Plane for Power Levels of .2, 1 watt with 15 mm Shroud

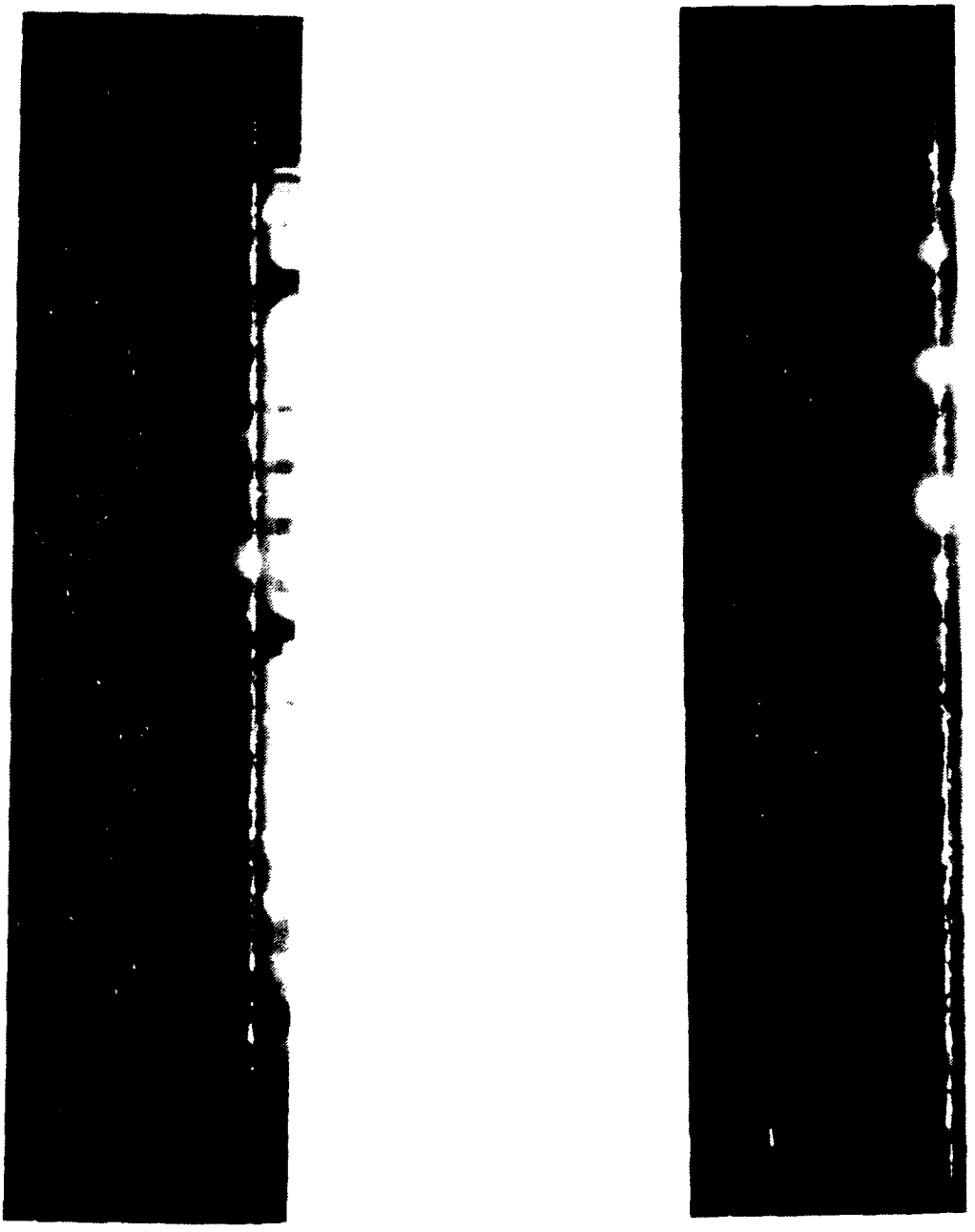

Figure 32. Steady Flow in the x-y Plane for Power Levels of .2, 1 Watt with 9 mm Shroud

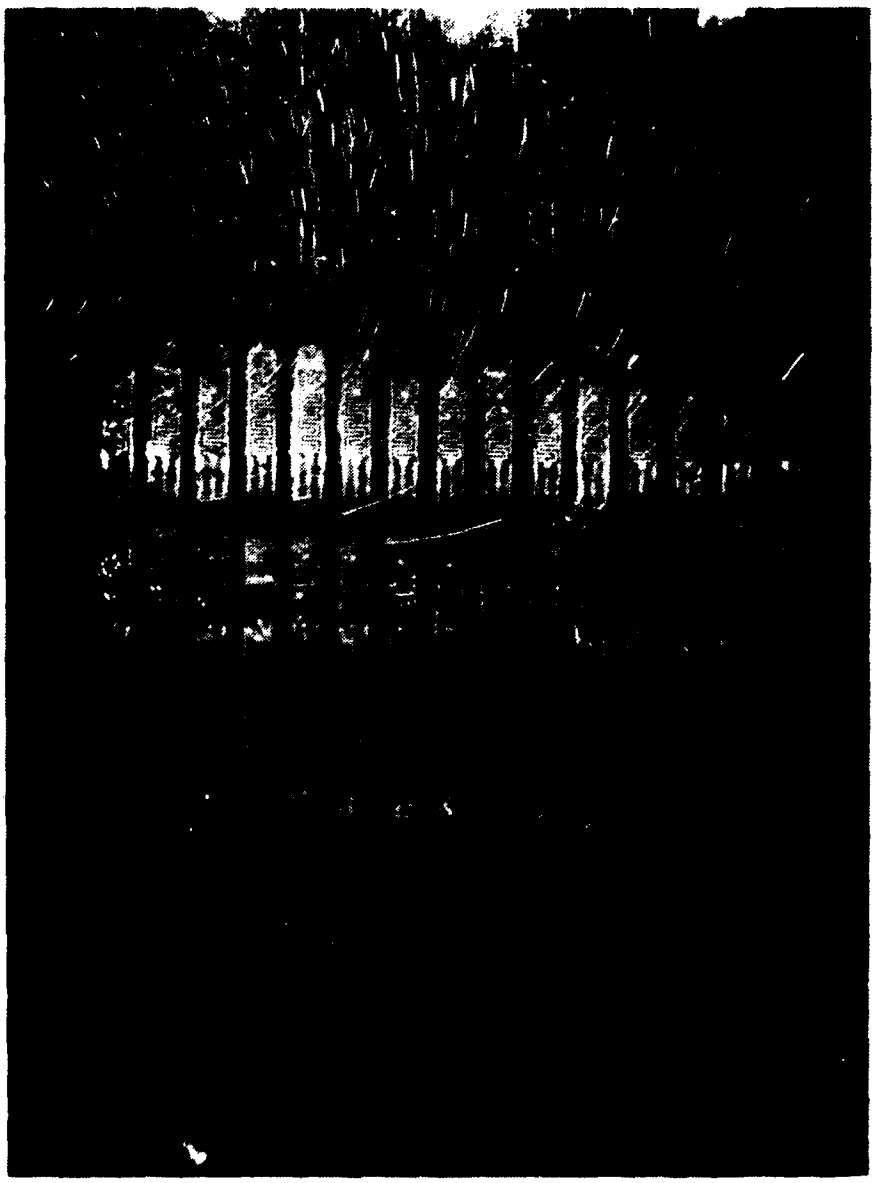

Figure 33. Steady Flow in the x-z Plane at Power Level of .2 Watt with 15 mm Shroud

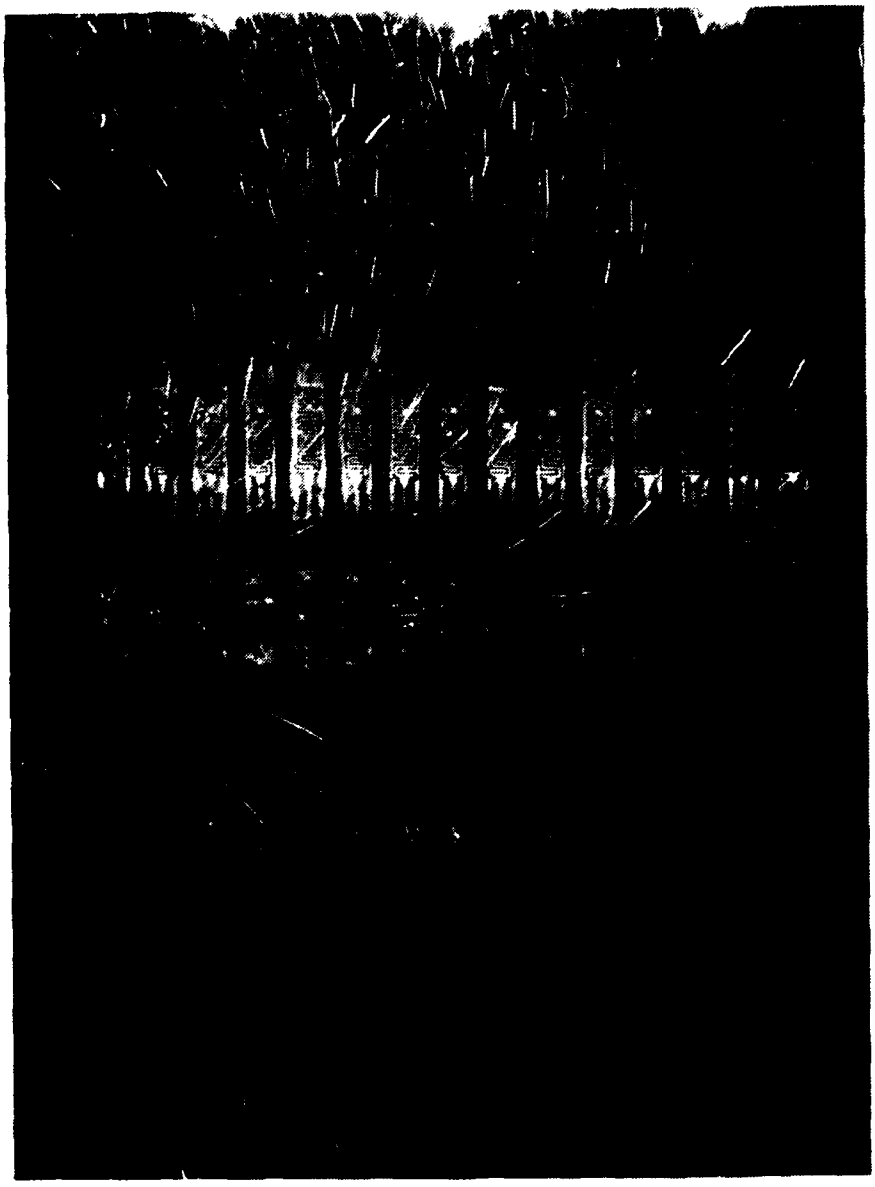

Figure 34. Steady Flow in the x-z Plane at Power Level of 1 Watt with 15 mm Shroud

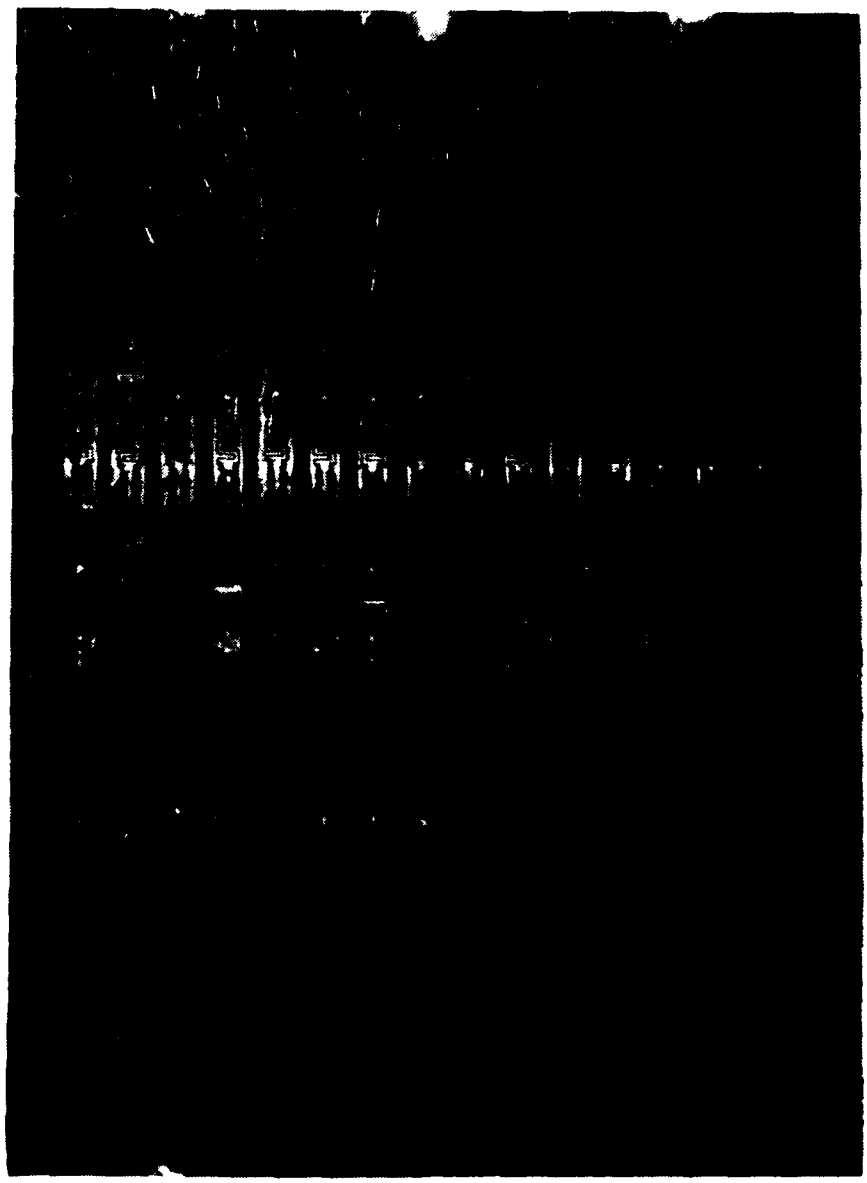

Figure 35. Steady Flow in the x-z Plane at Power Level of .2 Watt with 9 mm Shroud

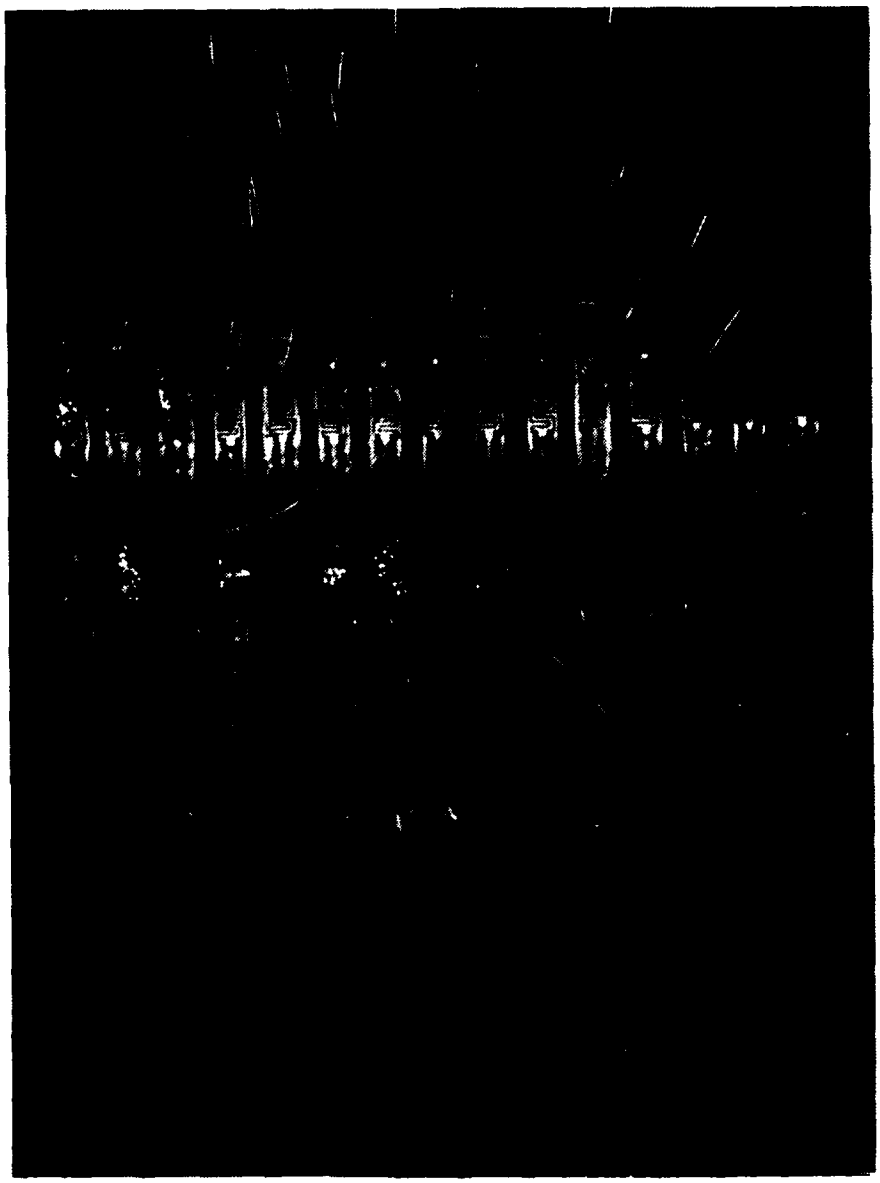

Figure 36. Steady Flow in the x-z Plane at Power Level of 1 watt with 9 mm Shroud

V. TRANSPORT WITH THREE COLUMNS POWERED

The second major area of study conducted during the experimental program was to evaluate the effects of placing flanking columns of heaters alongside the single column considered previously. The same experimental procedure that was followed for the single column study was used in the three column case and the data produced helped provide an understanding of the heat transfer characteristics for this new arrangement. The presentation of the three column results will follow the same format that was used for the single column. This chapter is broken down into two main sections; the first discusses the unshrouded test condition, while the second section will pertain to the case where a shroud wall was used.

A. Three Column Transport without Shroud

The main point of interest for the unshrouded multi-column test surface is the effect that the two flanking columns have on convective heat transfer as compared with single column transport.

Figures 37, 38 and 39 are **NDT** verses **X/L** plots at power levels of one, two and three watts respectively for both flanking and central columns. From these plots it is seen that the left and right flanking column temperatures are symmetric about the central column. It is also seen that the central column produces slightly higher **NDT** values when compared to the flanking columns at **X/L** values greater than .500. Even though the central column shows higher values for downstream positions, this difference is very small and the **NDT** values for the three columns all fall within a narrow band for the entire range of **X/L**. Referring back to Figure 11 where **NDT** verses **X/L** is plotted for a single column, it is

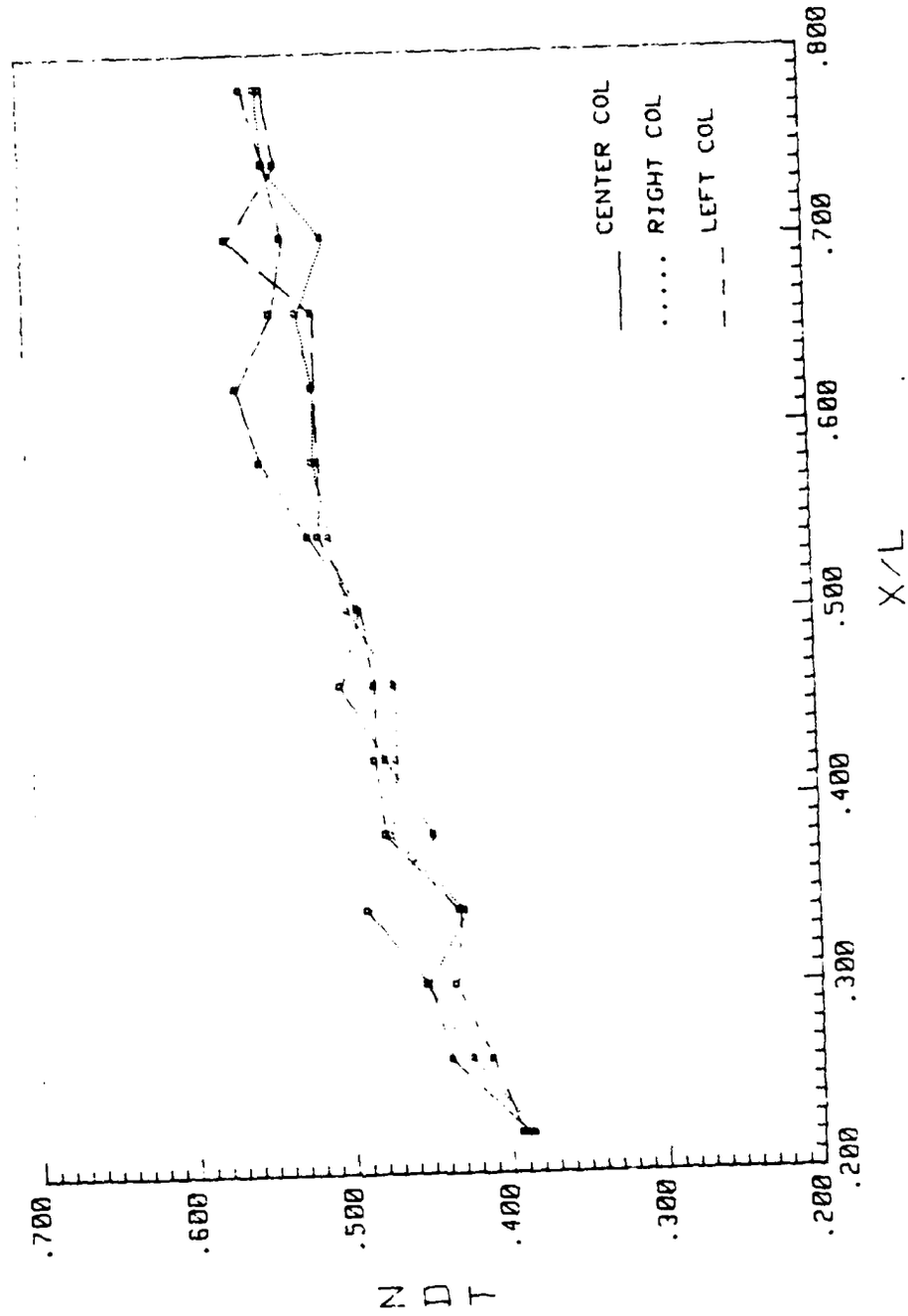

Figure 37. Non-Dimensional Temperature Excess vs. X/L with 1 Watt Input Power

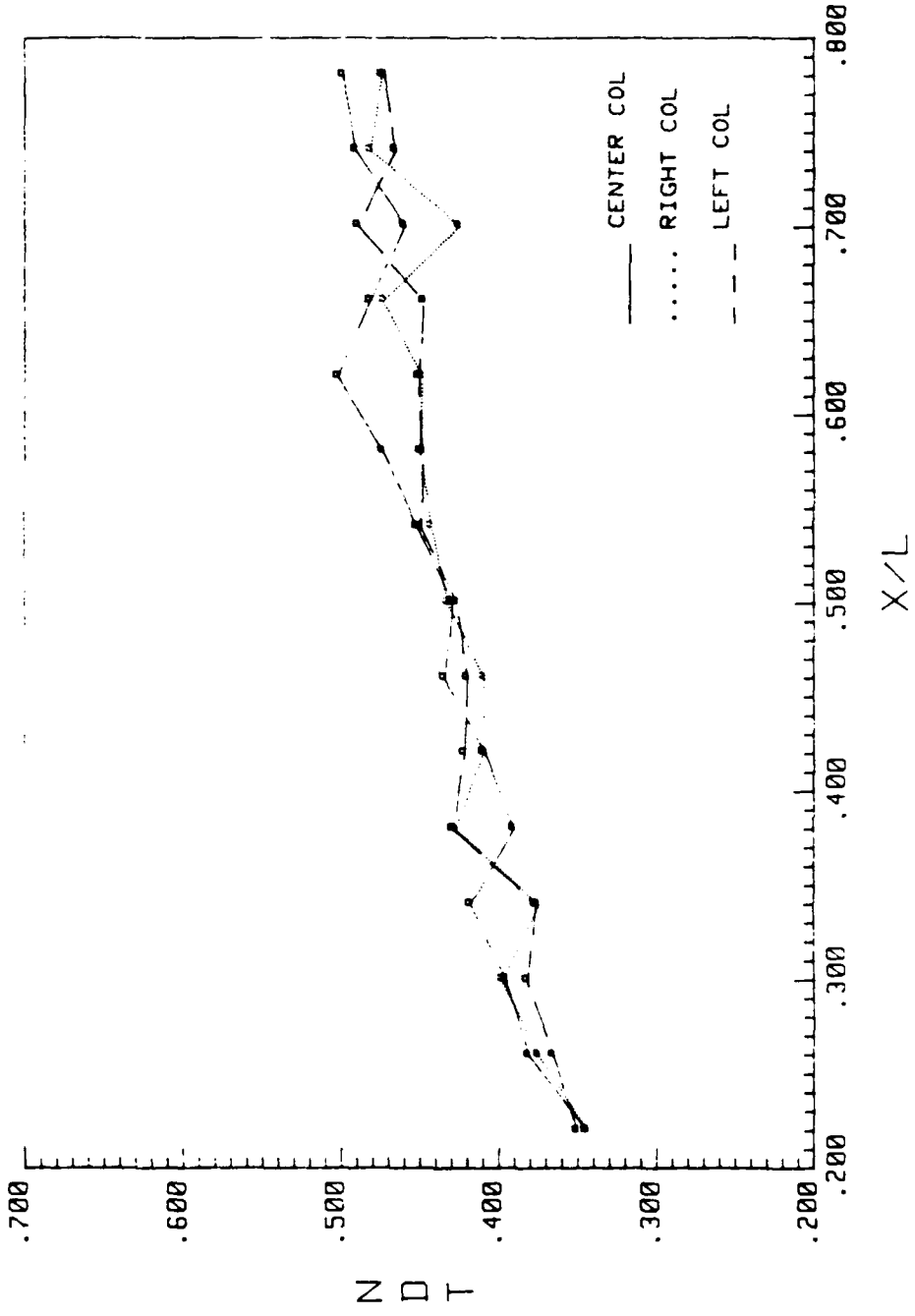

Figure 38. Non-Dimensional Temperature Excess vs. X/L with 2 Watts Input Power

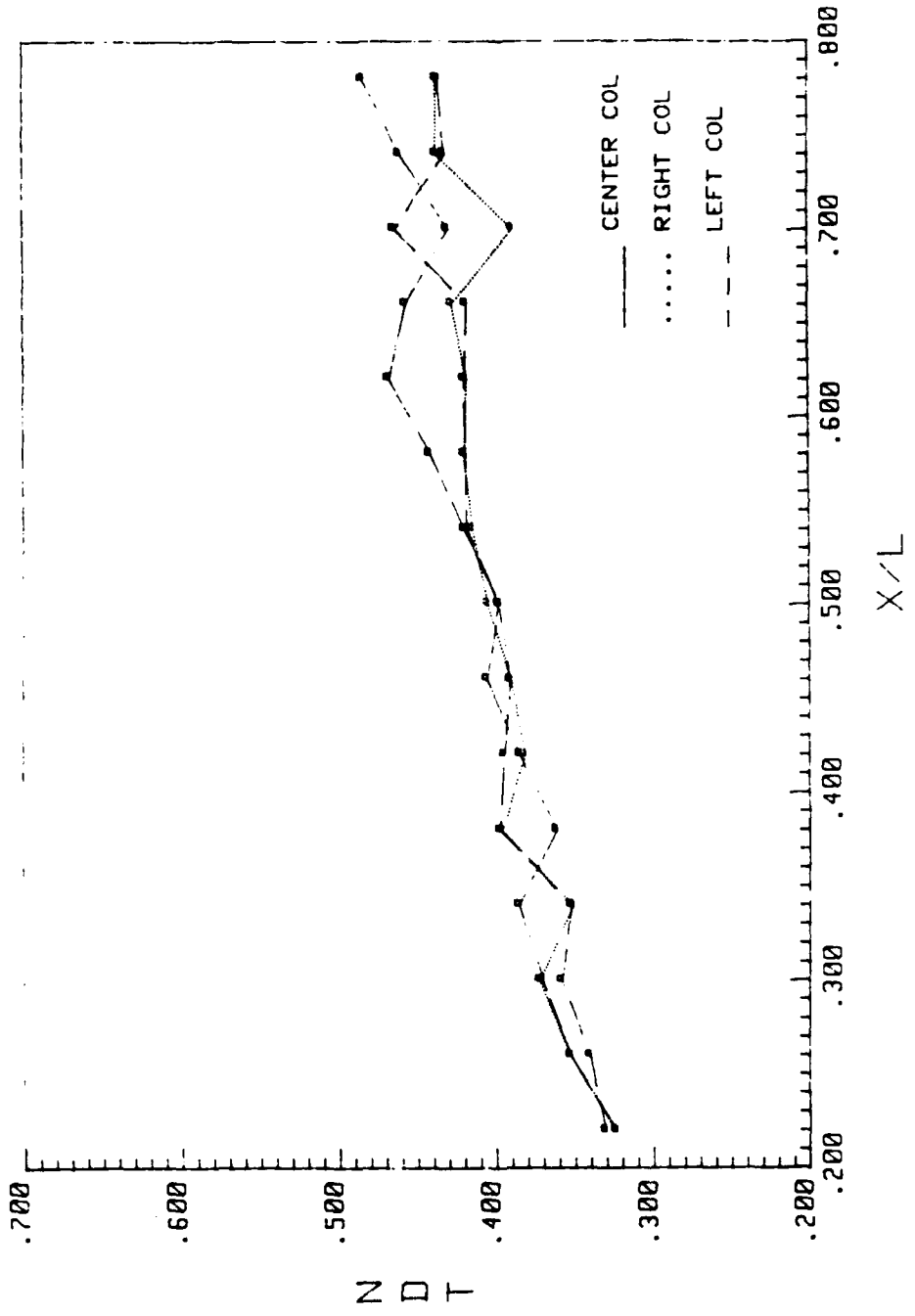

Figure 39. Non-Dimensional Temperature Excess vs. X/L with 3 Watts Input Power

apparent that the NDT band for three columns has values which are similar to the values obtained for a single column.

From the information conveyed from the NDT plots, it is initially hypothesized that the three unshrouded columns act independently from one another at lower positions along the test surface. At higher positions, the flanking columns interact with the center column slightly and will alter the heat transfer characteristics. Since the columns for the most part act independently, it is expected that the single column correlation relating Nu^* and Gr^* should also apply within acceptable accuracy for each of the three columns. This hypothesis is the basis of discussion in the following paragraphs.

1. Quantitative Analysis

The temperature data from the three column experimental runs were reduced using the equations presented in chapter two into local heat transfer coefficients, Nusselt numbers, and Grashof numbers.

The local heat transfer coefficients for each column at a given x are within 3% of one another. The difference between the three columns increases in the downstream direction. The local values of **h** for each of the three columns indicate a decreasing trend moving from the bottom heater to the top. It was also seen that the **h** values increase with rising power level. These trends are expected since the values of **h** at each heater location are inversely proportional to the NDT values. Comparing the heat transfer coefficients for three columns with the single column values it is seen that for low values of X/L, the three column data produce slightly higher **h** values.

Figure 40 and 41 are logarithmic scatter plots of Nu^* verses Gr^* for the center and right columns respectively. Also plotted for comparison is the single column correlation and its 5% deviation lines. From the two plots, it is seen that the values for the lower heaters are the same for the central and right columns. These values tend to deviate from

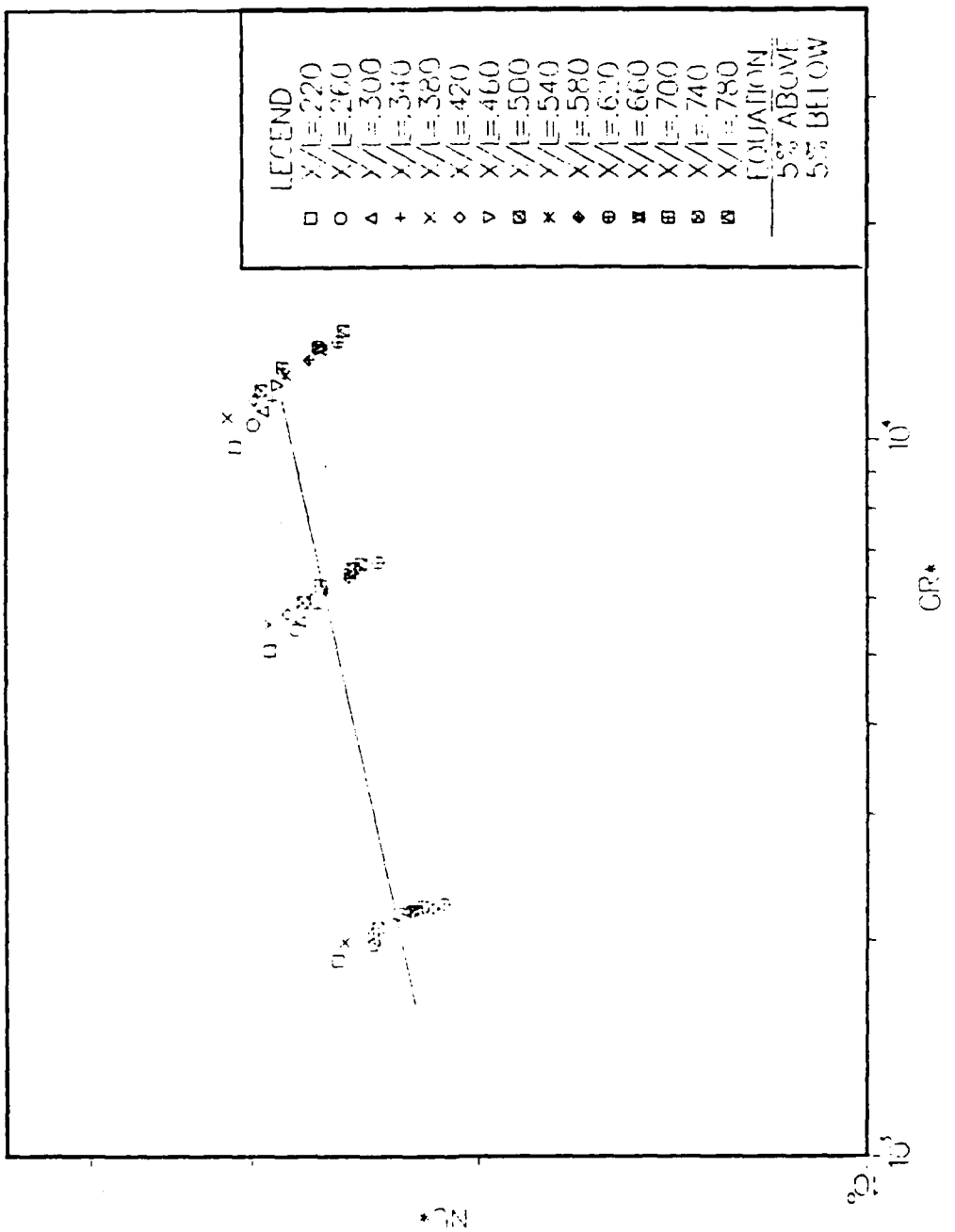

Figure 40. Nu* vs. Gr* for Center Column

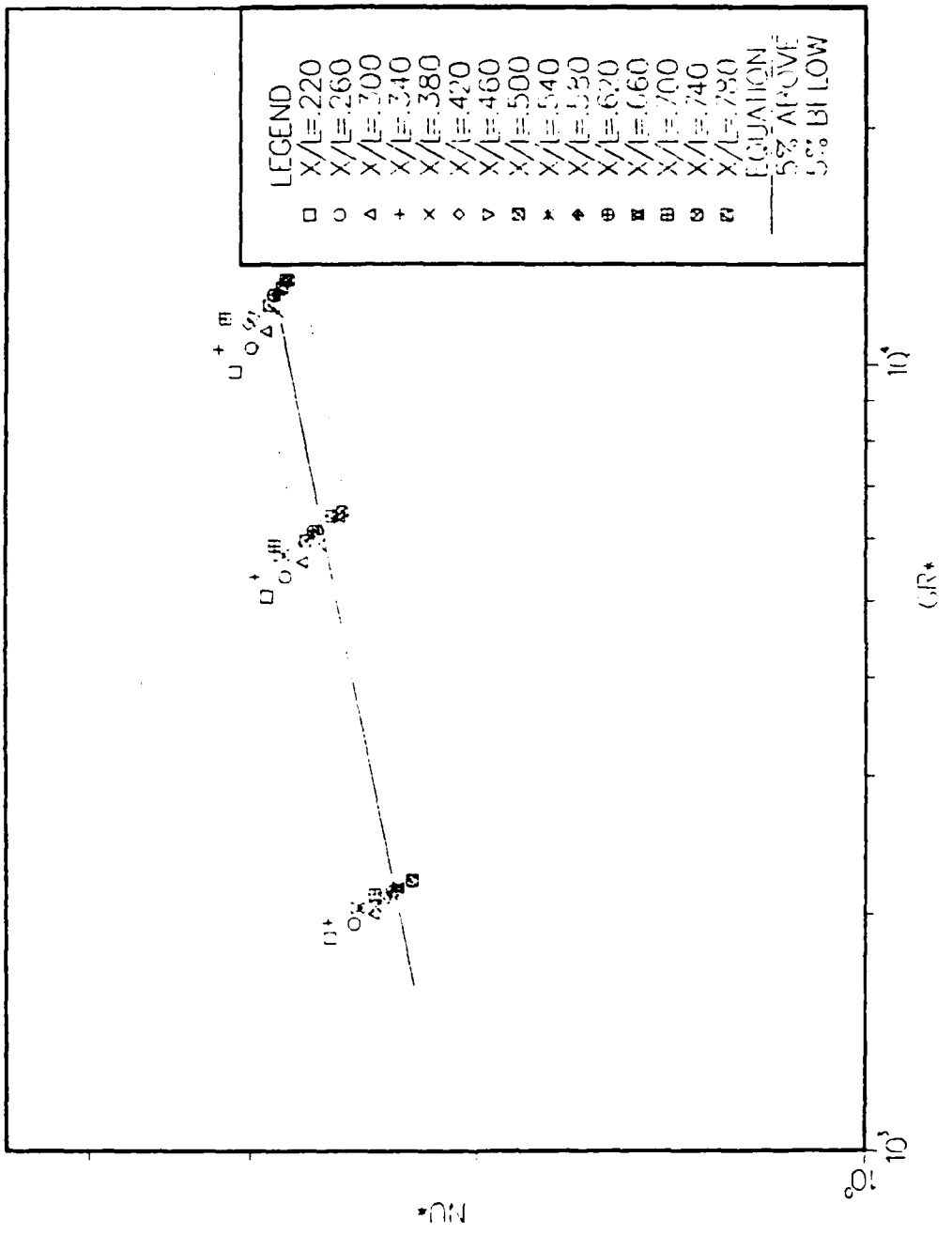

Figure 41. Nu* vs. Gr* for Right Column

one another at an X/L of .500 from where the central column produces lower Nu^* and higher Gr^* values. This verifies the independence of the columns at lower X/L positions while indicating how the columns interact at higher positions. Starting at an X/L value of .500, some fluid is entrained from the side columns toward the central column. The entrainment of fluid from the sides aids the flanking columns in dissipating heat, however since the fluid reaching the central column has been heated, the warmer fluid hinders the heat transfer causing lower Nusselt numbers.

Comparing the single column correlation relating Nu^* and Gr^* with the values obtained for the three columns it is seen that the correlation describes the mean for the central column data and is slightly lower than the right column data. The correlation does fit both the central and right column data within $\pm$ 10% vise the $\pm$ 5% seen for the 1 column case. In order to fit the data more accurately, the correlation would have to be modified. The comparison between the three and one column cases indicates that initially the starting heaters for the three column case have higher heat transfer. Starting at an X/L of .500, the heat transfer is slightly lower for the central column while at the same time the right column transfer of energy improves, as compared with the single column data. In general, the single column correlation still produces acceptable results for all three columns and can be used in most practical situations. The correlation will give conservative values for all heaters in the flanking columns and the lower heaters of the central column, while continuing to give reasonable values for the upper heaters of the central column as well.

2. Probe Measurements

As was done with the single column analysis, a thermocouple probe measured the temperature of the fluid adjacent to the test surface at precise locations in order to evaluate how the thermal boundary layer developed as the flow proceeded downstream. Once again the probe was moved both in the normal and spanwise directions in the vicinity of the test surface.

The spanwise plot of the fluid temperature in the x-z plane at 1 watt input power is shown in Figure 42. From this figure it is seen that the unheated region between heaters remains relatively cool as compared to the heater surfaces. However, it is apparent that some energy is being transferred in this unheated region due to the fact that the **delta T** is not zero and increases with rising **X. The delta T** between heaters is negligible for first heater row, but must be accounted for at the middle and top heater rows. The fact that a **delta T** exists in the unheated region between heaters in a row verifies the conclusion that the central column entrains some fluid from the two flanking columns. This accounts for the slightly higher temperatures seen for the central column at the eighth and fifteenth rows.

Figures 43 and 44 are normal plots of the fluid temperature in the x-y plane at 1 watt for the center and right columns respectively. From these plots, it is seen that the central column has slightly higher values for heater strips eight and fifteen. The difference between the two figures is so small on the scale used to plot the values, that it is extremely hard to distinguish the two plots from one another. The same trends seen for the 1 watt plots are also seen in Figures 45 and 46 which are normal plots in the x-y plane at 3 watts input power. Referring back to Figures 16 and 17 which are normal plots for the single column case at 1 and 3 watts, it is apparent that there is no noticeable difference between the one column and three column cases. Hence this leads to the conclusion that even though there is a difference between the three columns and the single column with respect to heat transfer characteristics as was shown above, this difference is negligible when it comes to thermal boundary layer thicknesses.

3. Flow Visualizations

Figures 47 and 48 show the flow patterns for the three columns in the x-z plane near $y = 0$ at power levels of .2 and 1 watt respectively. From these figures it is seen that starting at heater row two, the three columns form three large individual buoyant upflows. Some flow interaction between the center and flanking columns is seen in the .2 watt

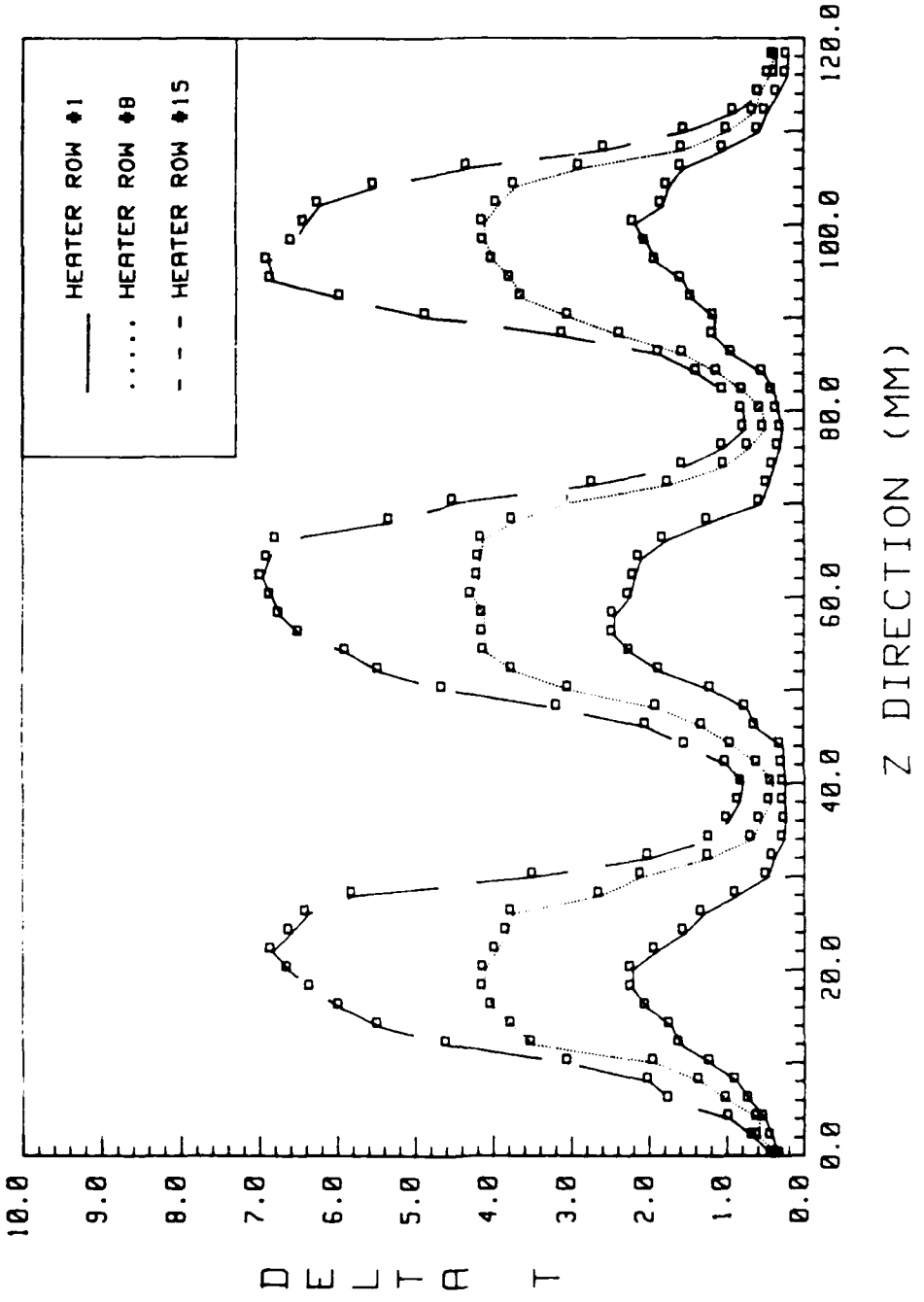

Figure 42. Spanwise Temperature Variation with 1 Watt Input Power. Measurements Taken at Y = 9 mm.

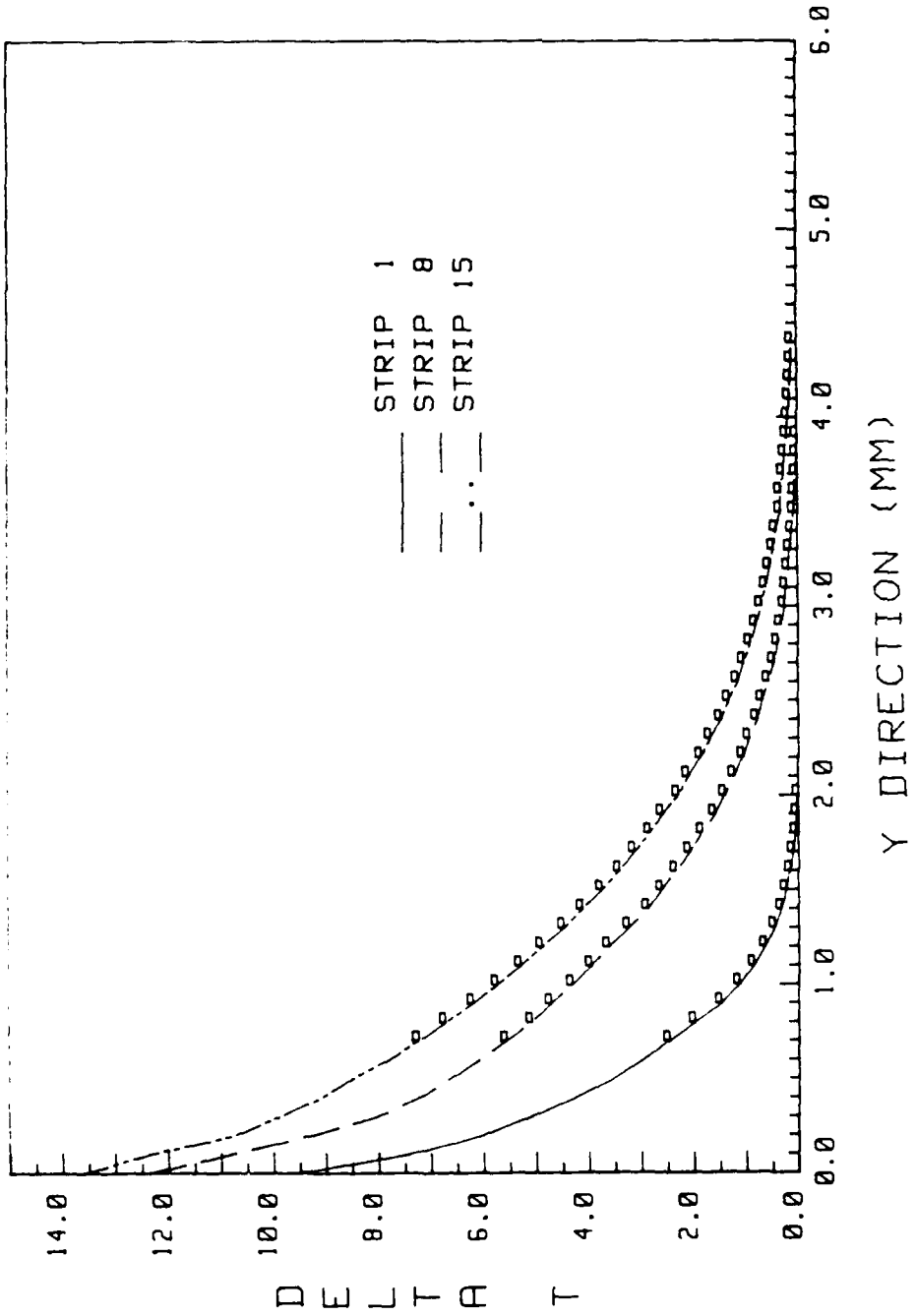

Figure 43. Normal Temperature Variation at Heater Centerline with 1Watt Input Power for Center Column

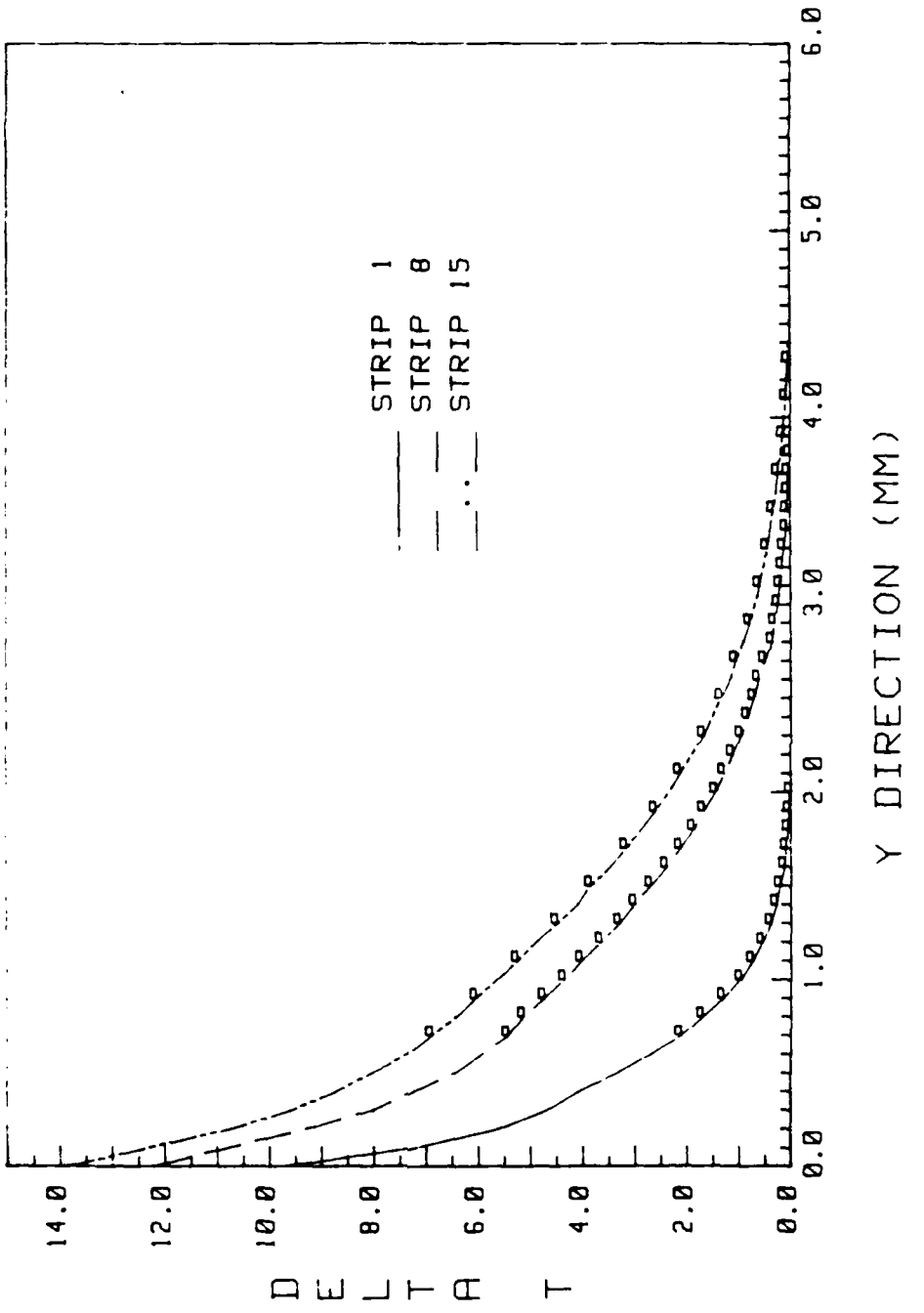

Figure 44. Normal Temperature Variation at Heater Centerline with 1 Watt Input Power for Right Column

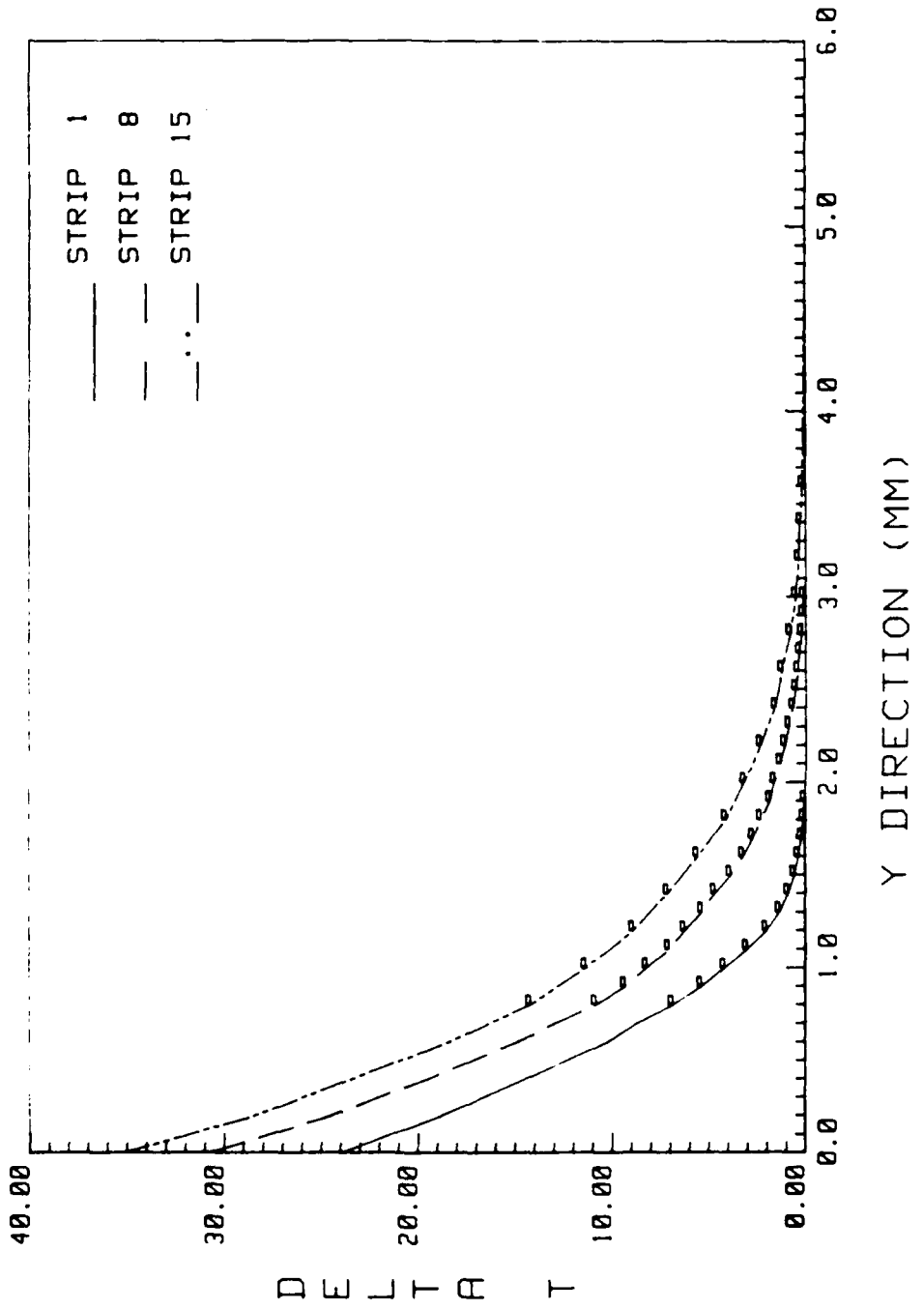

Figure 45. Normal Temperature Variation at Heater Centerline with 3 Watt Input Power for Center Column

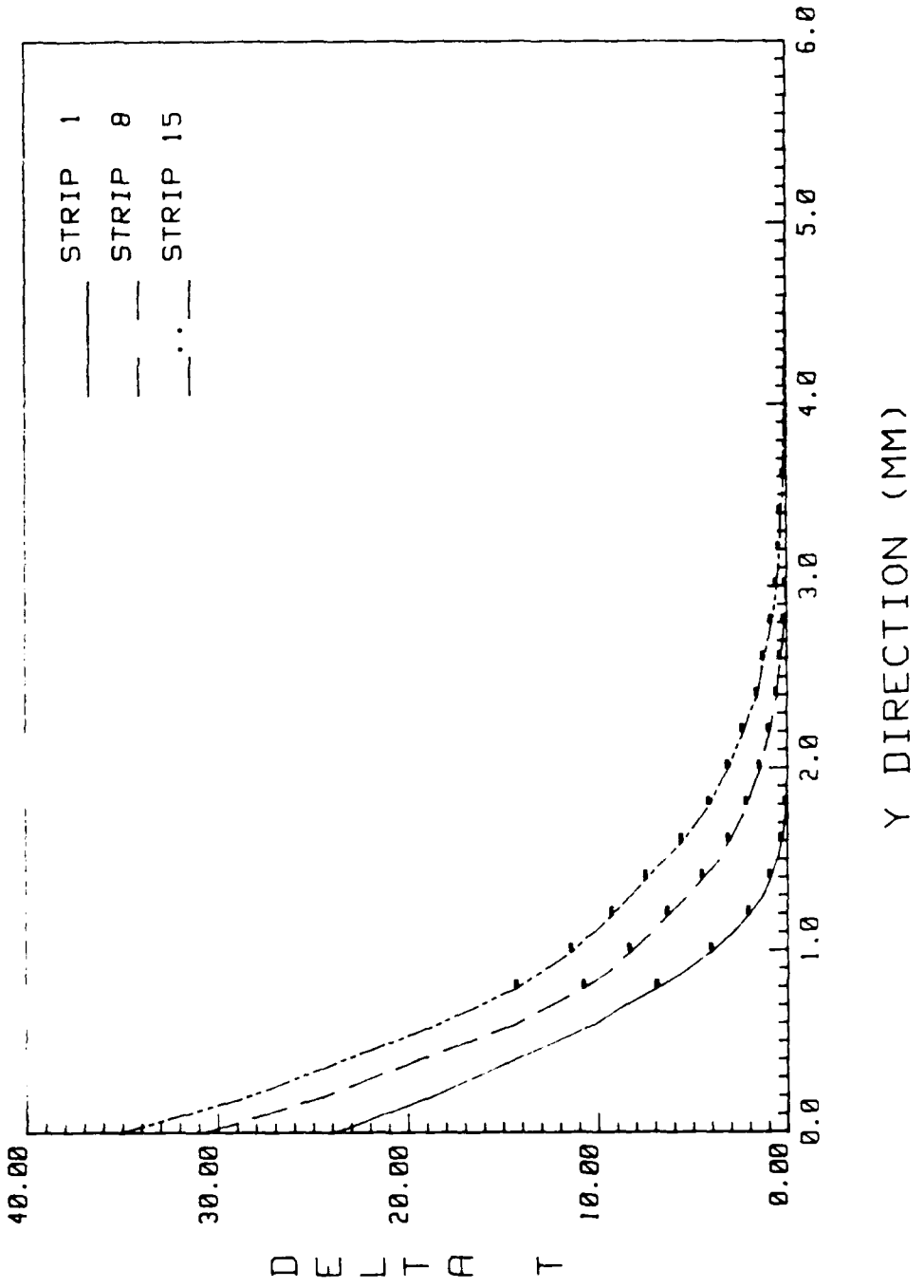

Figure 46. Normal Temperature Variation at Heater Centerline with 3 Watt Input Power for Right Column

picture. This interaction is seen as the shifting of the particle traces over the flanking columns toward the central column. For the 1 watt picture, only the strong buoyant upflow is visible. The interaction seen at .2 watt input power verifies the flow interaction predicted with the thermocouple probe.

Figures 49 and 50 display the normal flow patterns in the x-y plane for the right and center columns at .2 watts. In these figures the z values correspond to the right, center and the left edges of the heater columns. The same views are shown in Figures 51 and 52 with 1 watt input power. The flow patterns for the right and left edges of the central column are identical confirming the flow symmetry about $z = 0$. Referring to the right column patterns it is seen that the flow patterns for the two edges and the center match with those for the central column. This indicates that the interaction between the three columns is relatively weak.

From the normal flow profiles in the x-y plane, boundary layer thicknesses were evaluated and plotted in Figure 53 for the central column. Comparing the plot with Figure 26 where the single column boundary layer thicknesses are plotted for the column center and edges, it is seen that the thicknesses for the three column case are approximately equal to those for the single column. This again supports the conclusion that the development of the velocity boundary layer in the x-direction over a particular column in this three column system, is independent of what happens for the other two columns.

B. Three Column Transport with Shroud

The second experimental arrangement analyzed with the three columns powered was accomplished by placing a shroud at a given normal spacing from the test surface. The objective was to evaluate the effects of this shroud on heat transfer characteristics. Referring back to the single column shrouded case, it was seen that the shroud wall had minimal effects on the heat transfer up to a shroud spacing of 3 mm. For spacings equal to

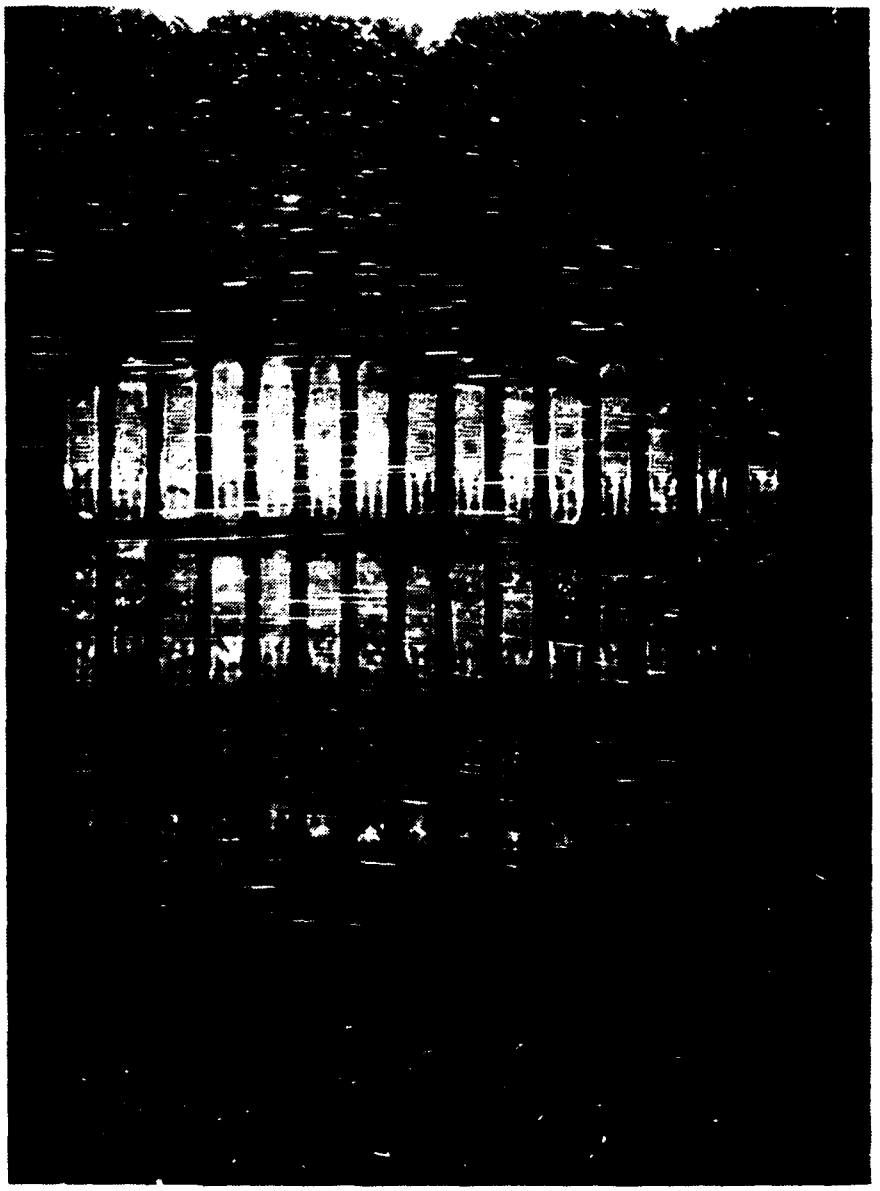

Figure 47. Steady Flow in the x-z Plane for .2 Watt Input Power

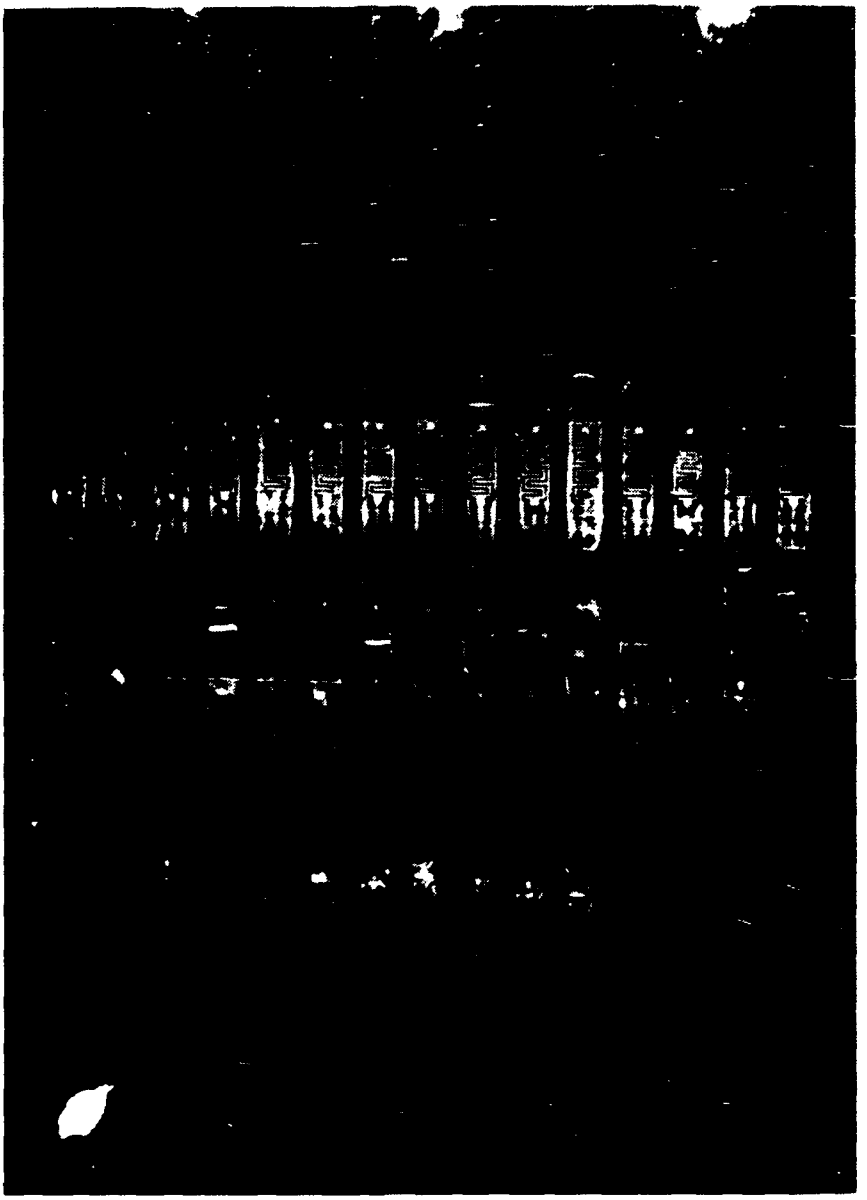

Figure 48. Steady Flow in the x-z Plane for 1 Watt Input Power

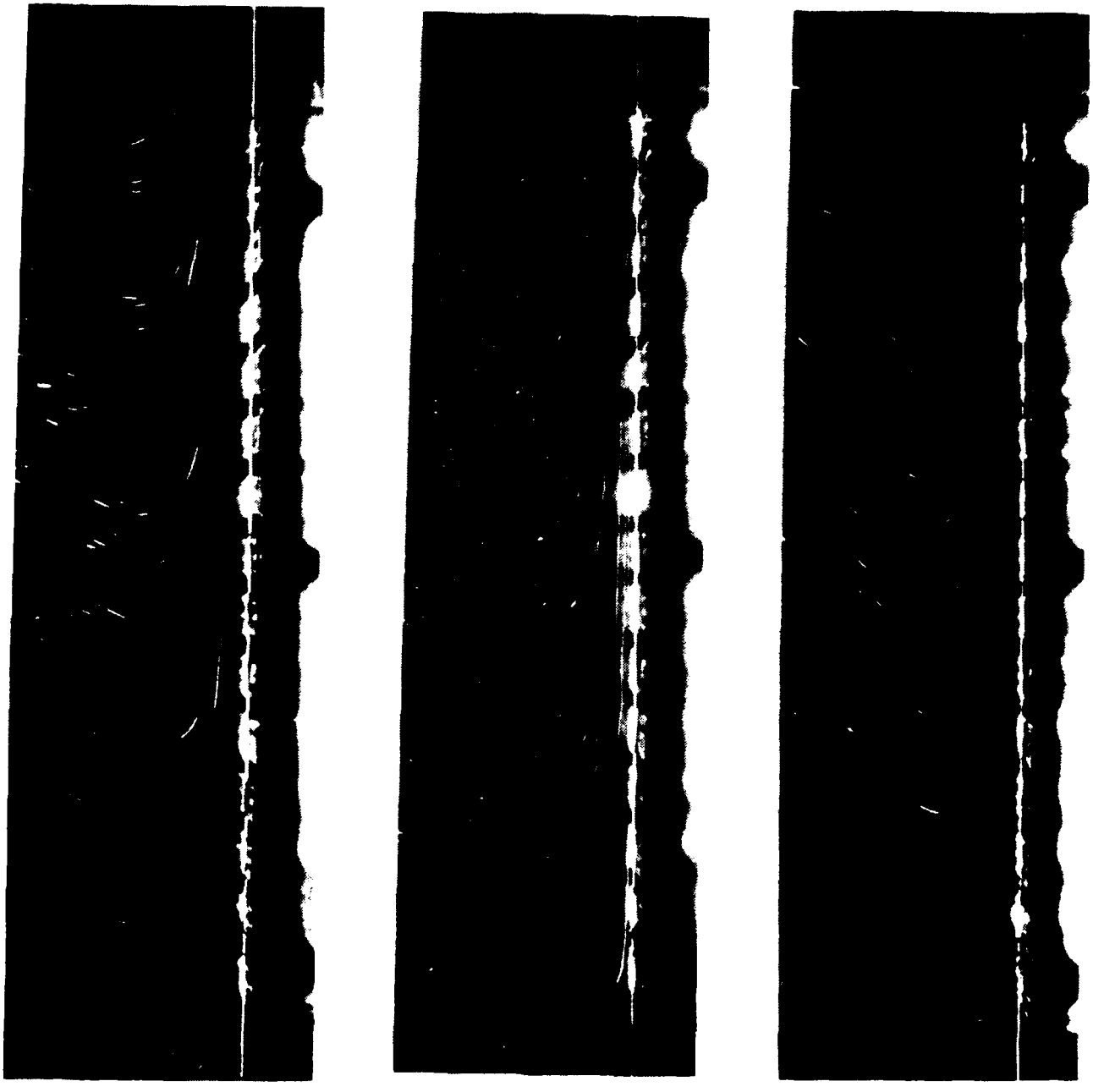

Figure 49. Steady Flow in the x-y Plane with .2 Watt Input Power for Center Column

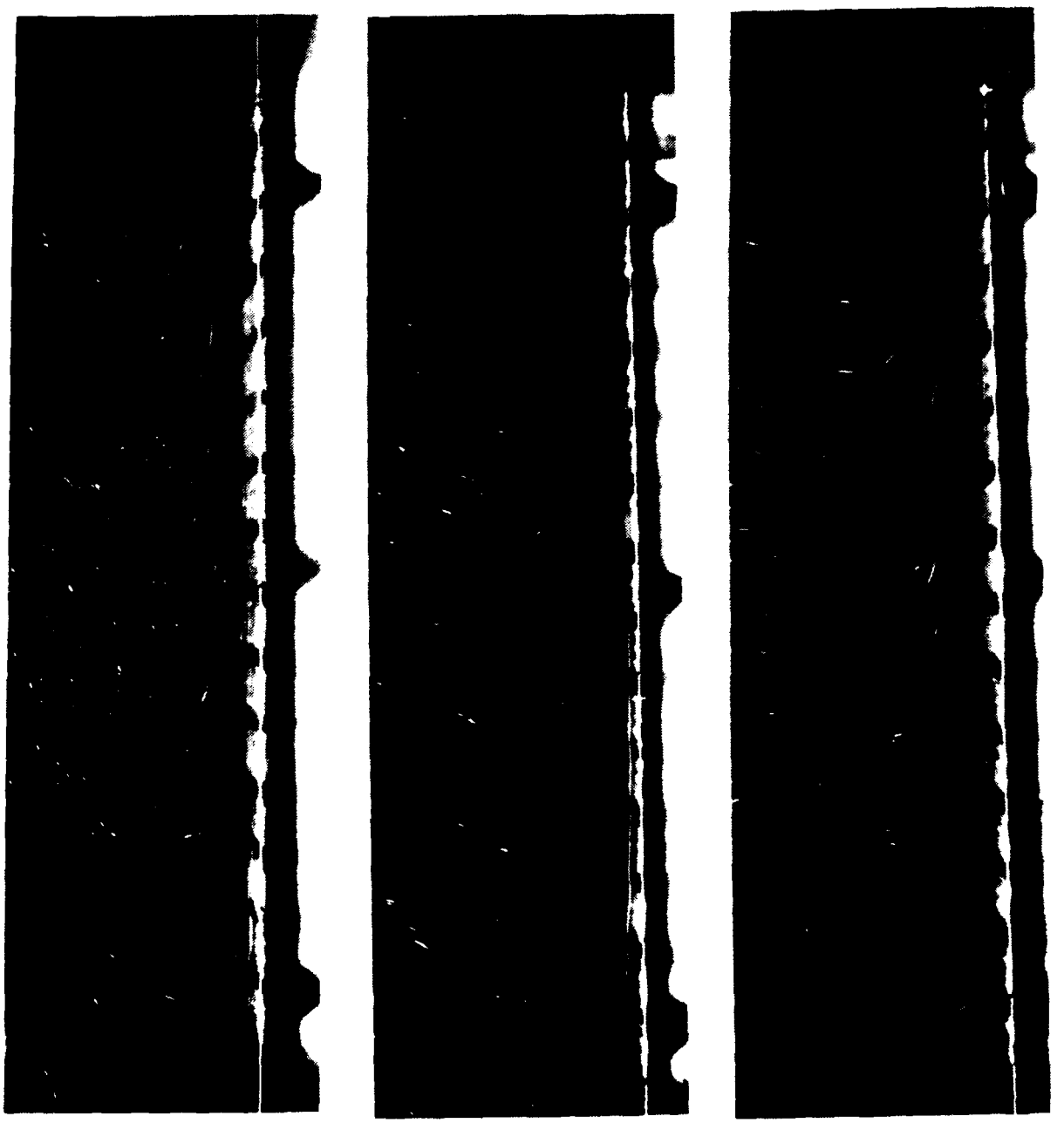

Figure 50. Steady Flow in the x-y Plane with .2 Watt Input Power for Right Column

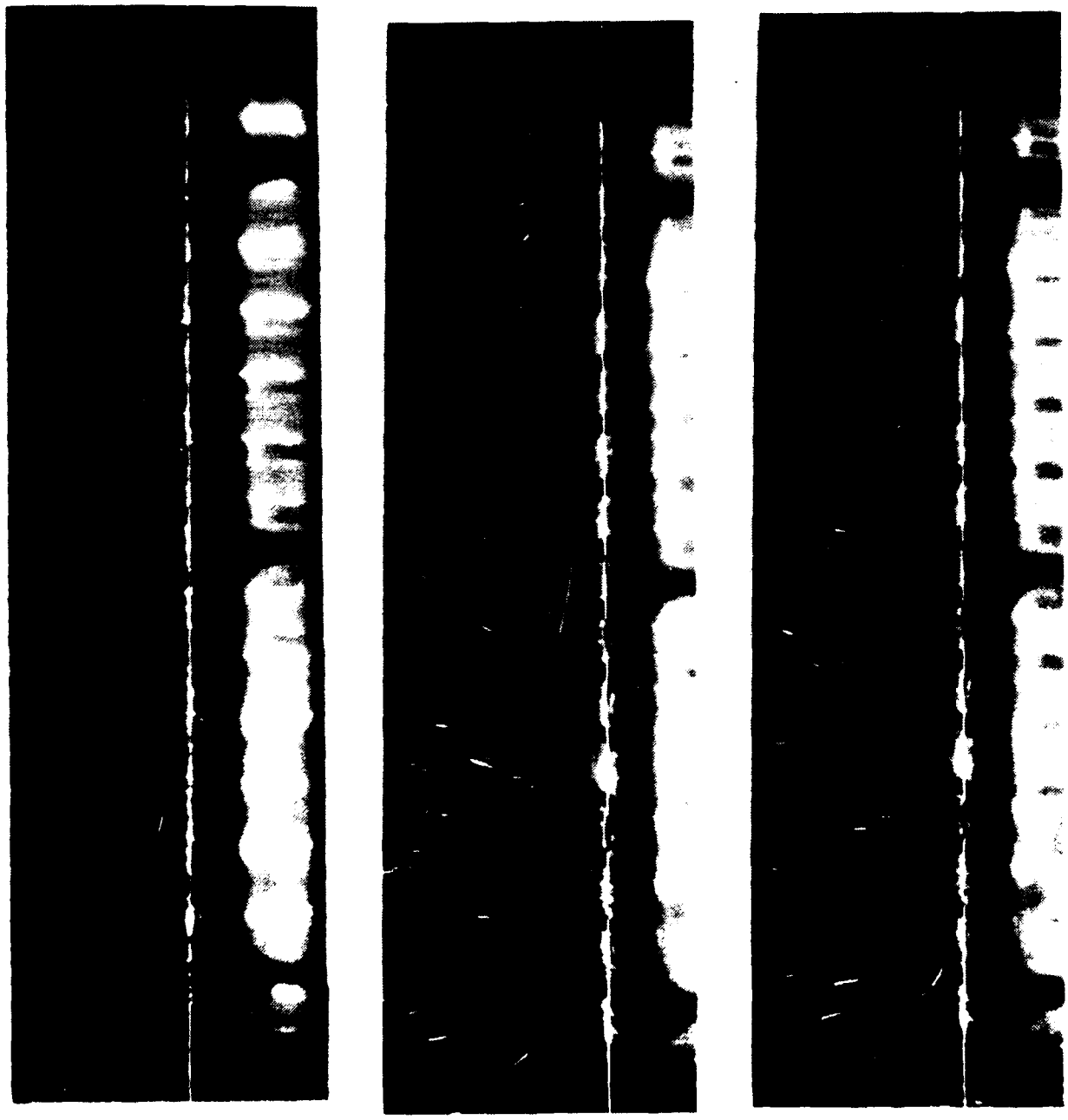

Figure 51. Steady Flow in the x-y Plane with 1 Watt Input Power for Center Column

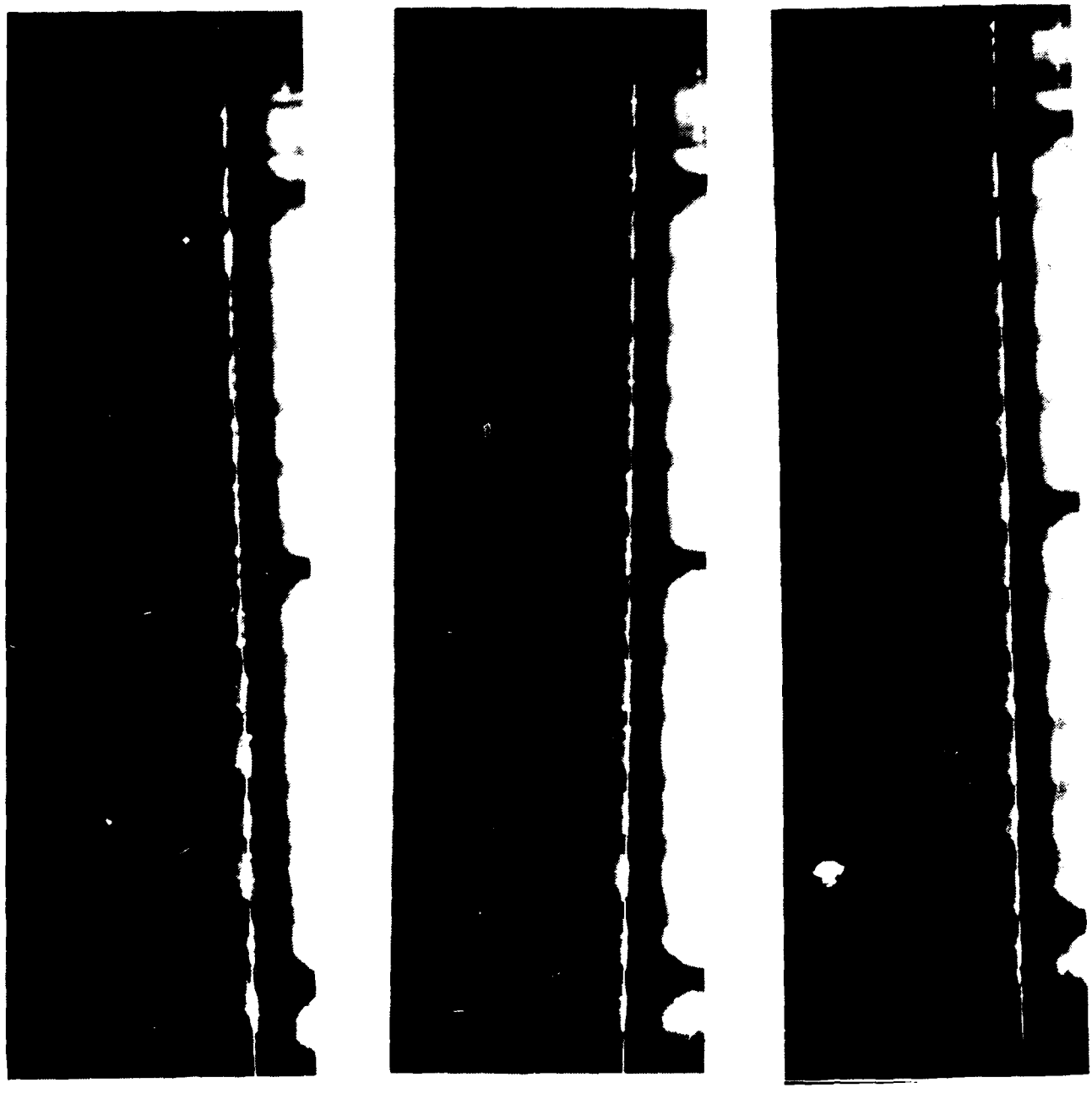

Figure 52. Steady Flow in the x-y Plane with 1 Watt Input Power for Right Column

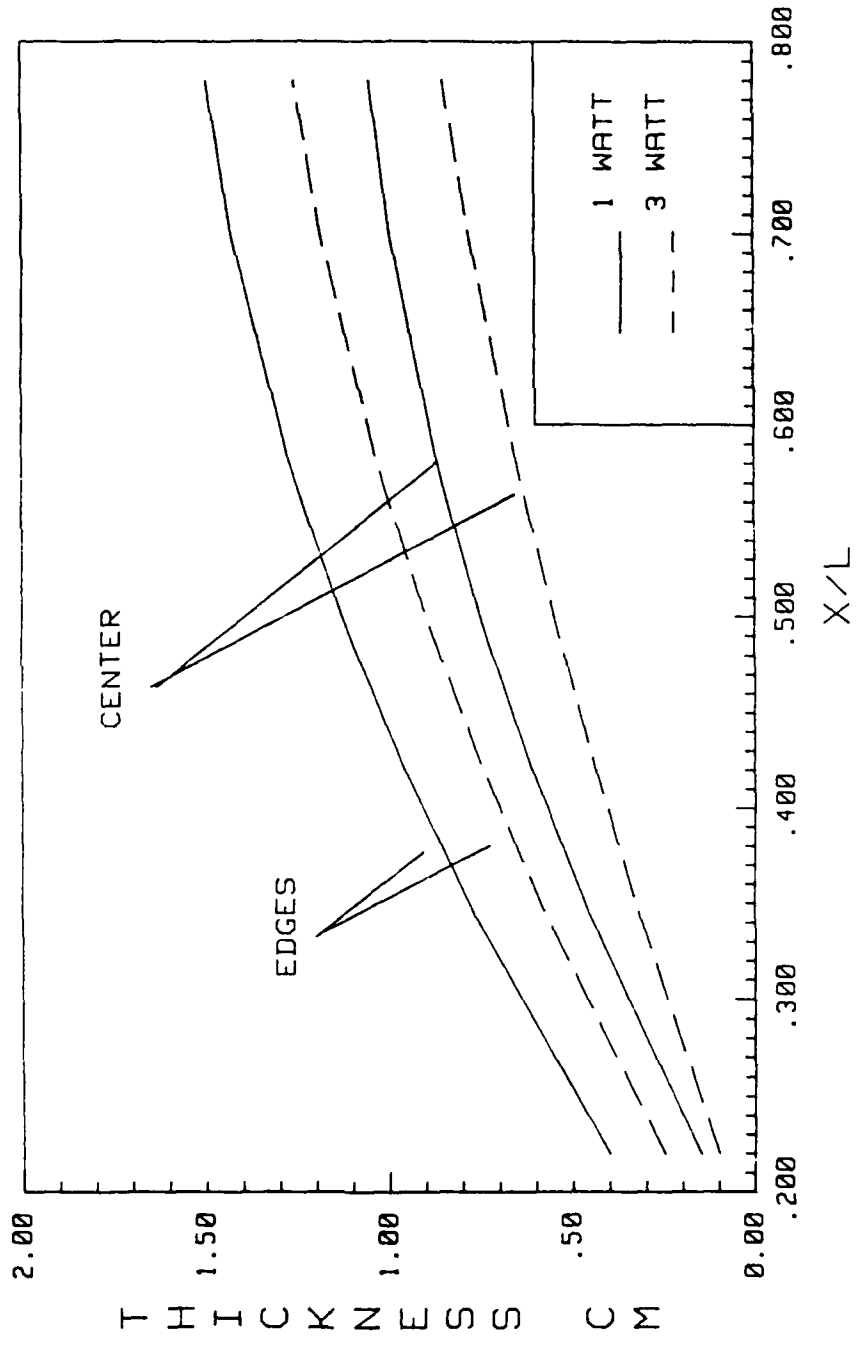

Figure 53. Momentum Boudary Layer Thickness for Center Column

and less than 3 mm, the flow resistance increased to a point where the heat transfer characteristics of the system were effected. It was also seen that the shroud wall at the thinner spacings caused considerable fluid entrainment from the side regions.

These trends seen for the single column analysis will be considerably different for the three column case due to the fact that the fluid flowing over the flanking columns is entrained by the central column and interacts more vigorously with the central column flow. This destroys the individuality of the flow over each column that was seen for the unshrouded condition.

Figures 54, 55 and 56 are central column variations of delta T verses X/L for power levels of 1, 2 and 3 watts. For each figure the data are plotted for shroud spacings of 12, 6, and 3 mm. For comparison the unshrouded single column and three column experimental data are also plotted. From these plots, several trends are observed. First, it is seen that for X/L values less than .420, the heater temperatures are lower for the central column in a three column arrangement than for single column operating alone without a shroud. For one watt input power, the remaining X/L positions beyond .420, separate into two catagories depending on the shroud spacing. For spacings greater than 6 mm, the heater temperatures are approximately equal to the single column unshrouded test case. For spacings equal to or less than 6 mm, it is seen that the heater temperatures rise above the single column unshrouded values. The same general trends are seen for the 2 and 3 watt cases. The only exception to this is that the 6 mm curve follows the same pattern established with the one watt curve, however at an X/L of .700, the curve deviates downward toward the band containing the higher shroud spacing and unshrouded values.

Figures 57, 58 and 59 are right column plots of delta T verses X/L at power levels of 1, 2 and 3 watts. From these curves, it is seen that the unshrouded single column gives the highest heater temperatures for all values of X/L. The values for the unshrouded three column 12 mm shroud and 6 mm shroud are lower than the single column values and are

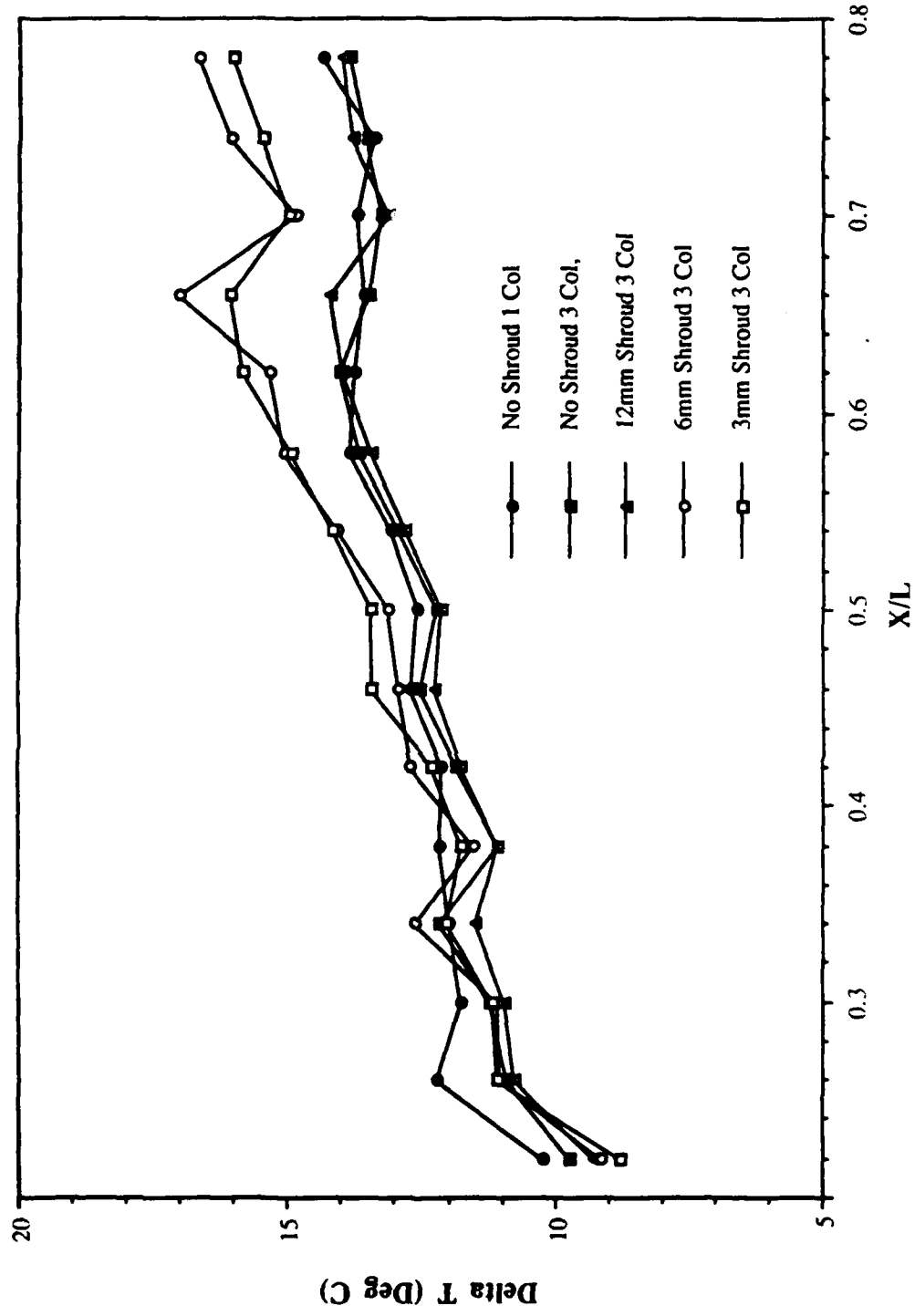

Figure 54. Delta T vs. X/L with 1 Watt Input Power for Center Column

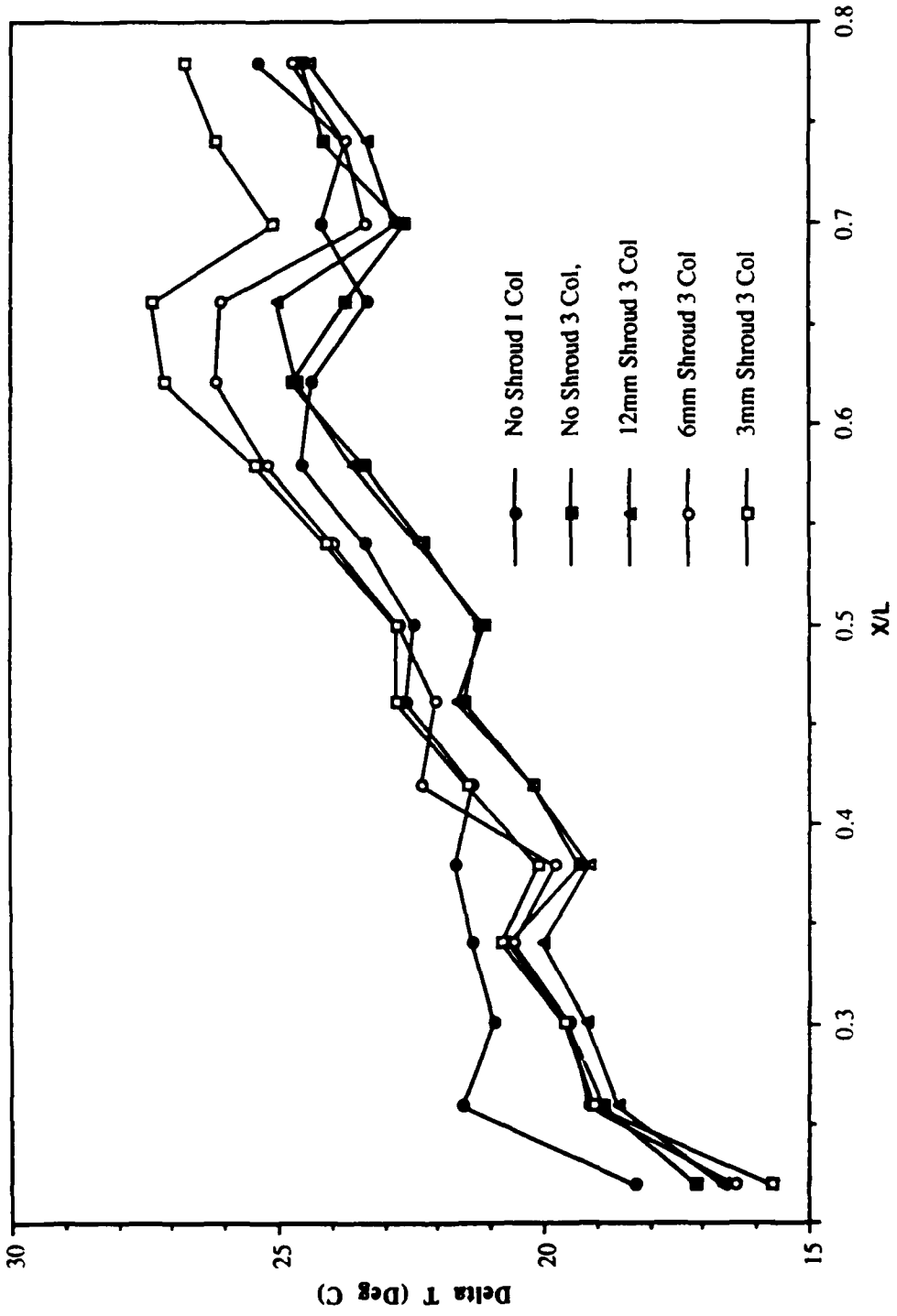

Figure 55. Delta T Vs. X/L with 2 Watt Input Power for Center Column

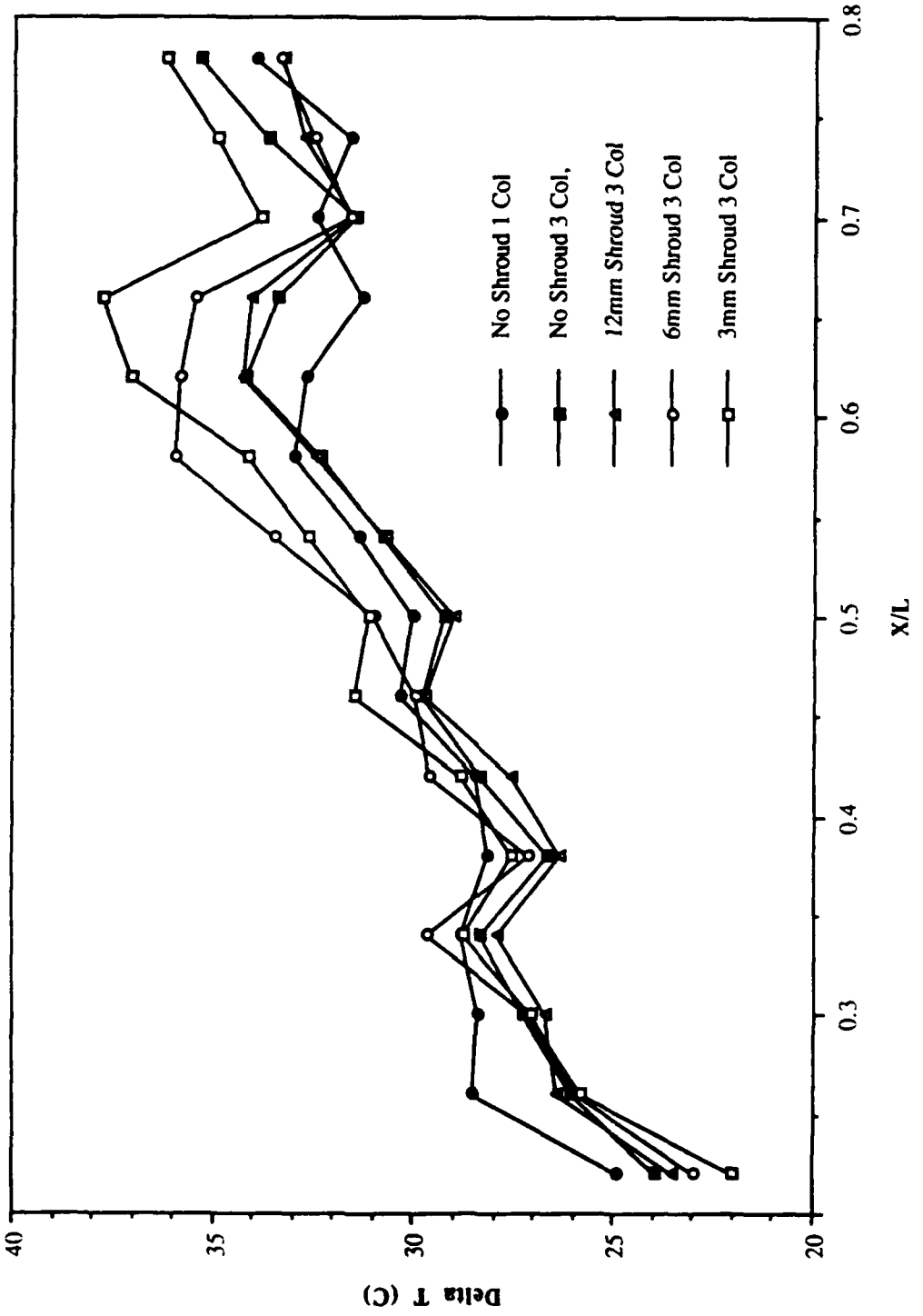

Figure 56. Delta T vs. X/L with 3 Watt Input Power for Center Column

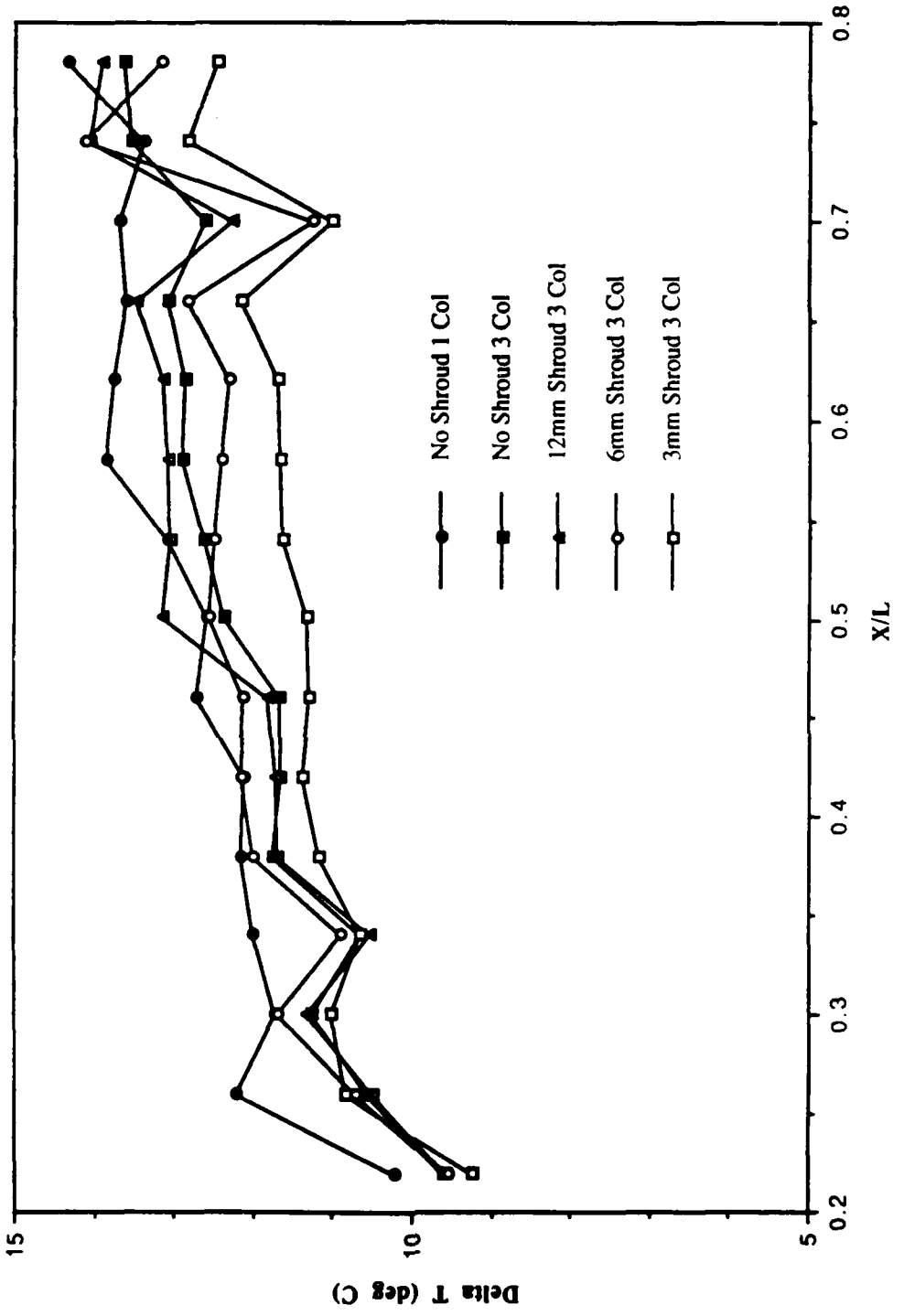

Figure 57. Delta T vs. X/L with 1 Watt Input Power for Right Column

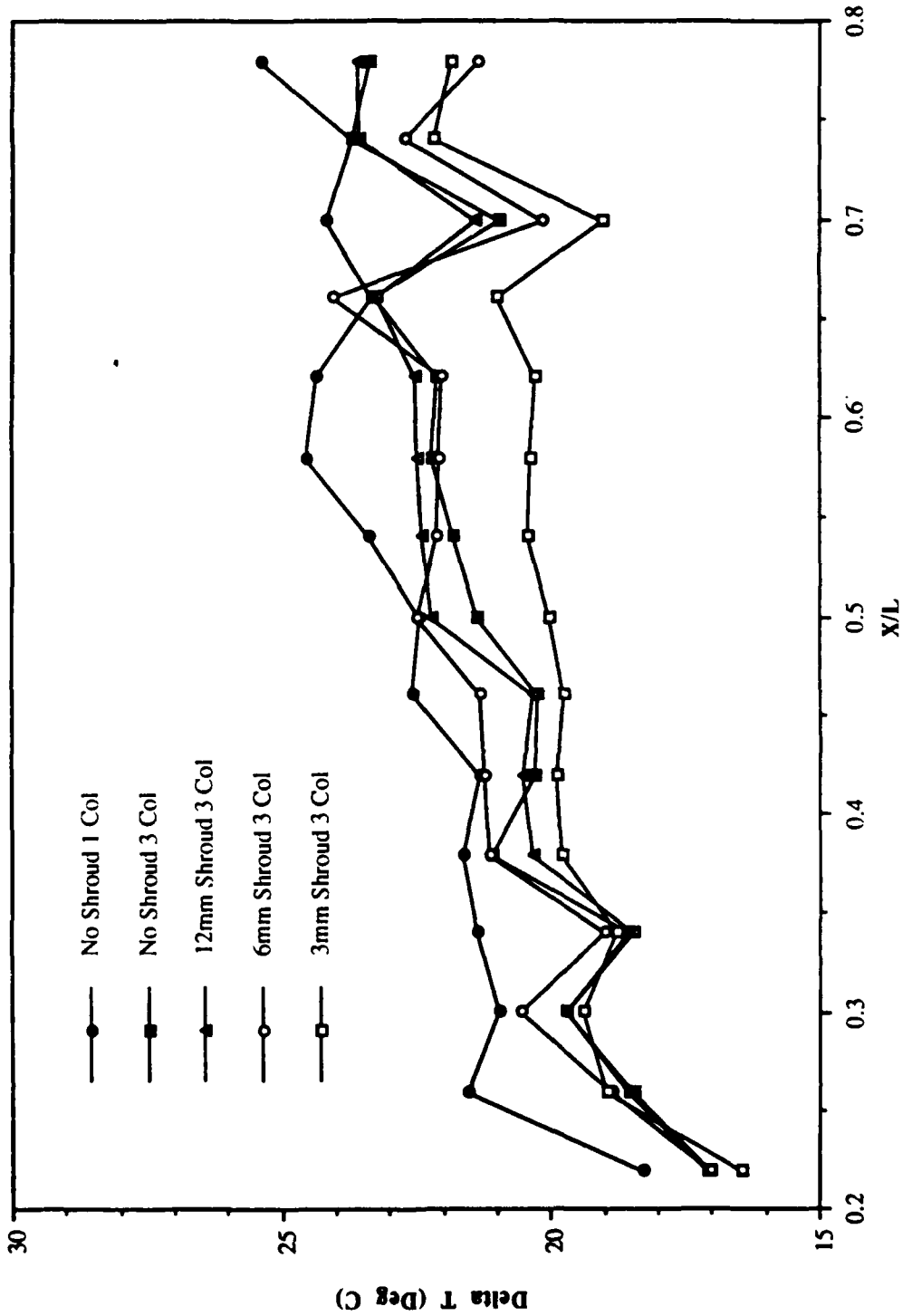

Figure 58. Delta T vs. X/L with 2 Watt Input Power for Right Column

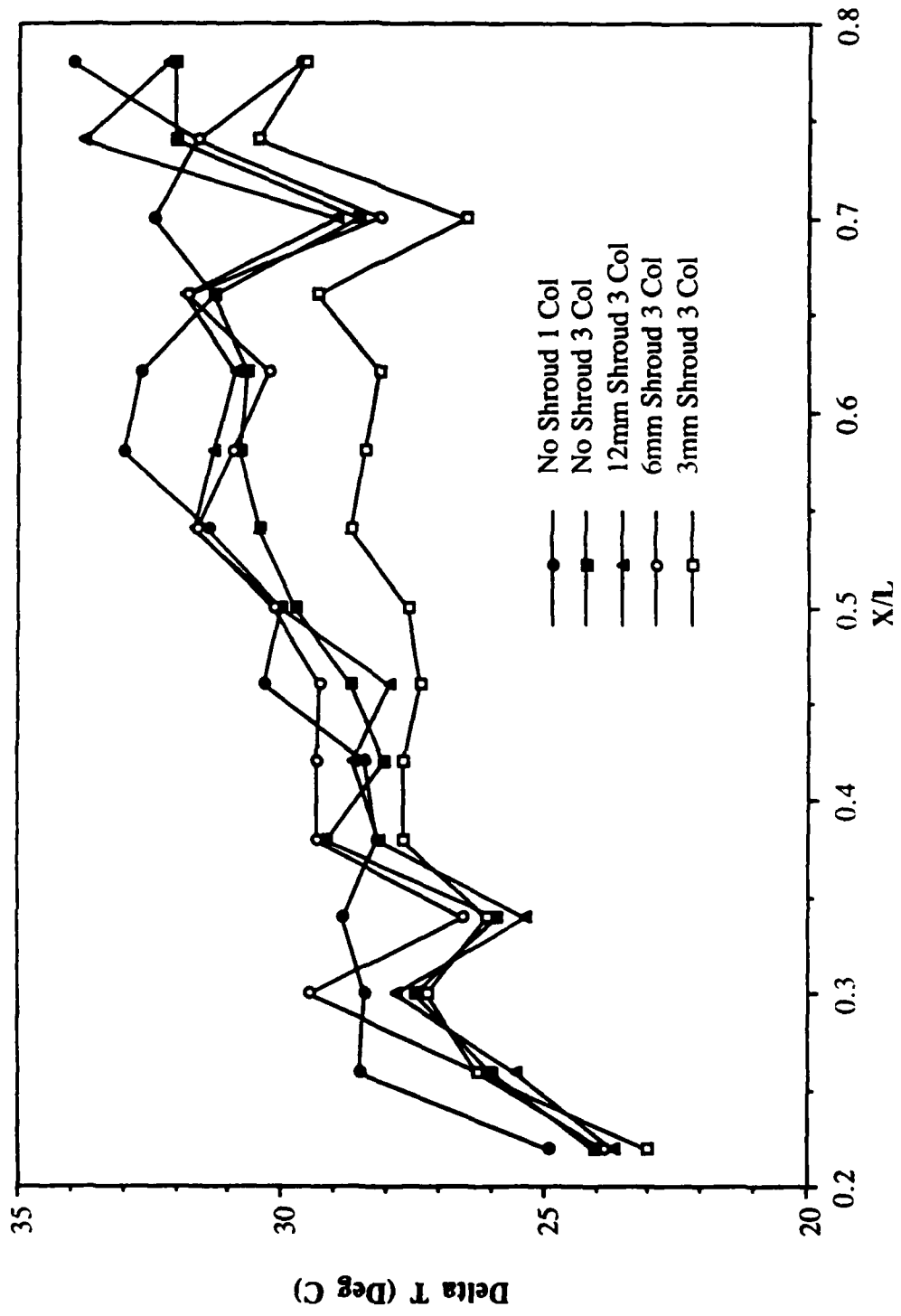

Figure 59. Delta T vs. X/L with 3 Watt Input Power for Right Column

also similar, hence they form a band which lies slightly below the single column curve which starts from the first heater in the right column all the way to the top heater. Initially the 3 mm shroud values fall within this temperature band up to an X/L value of .380. Beyond this location, the 3 mm shroud curve lies below the band.

The trends seen from the plots above indicate several important features of the three column shrouded test surface measurements. It is suspected that as the shroud spacing is decreased, the entrainment of fluid by the central column from the two flanking columns increases. This in turn causes the component temperatures in the flanking columns to decrease since the fluid entrained by the central column is replaced by the cooler fluid drawn from the ambient medium. The warm fluid received by the central column tends to increase the heater temperatures. Also, the warmer fluid temperatures increase the buoyancy force and the fluid velocities near the elements. The net effect on heater temperatures will be the combination of these contributions. At a shroud spacing of 6 mm, the heater temperatures along the central column increase significantly due to the entrainment of surrounding warm fluid. With an even smaller spacing of 3 mm, the flanking column component temperatures decrease further while the center column components become the warmest.

The above temperature measurements of the three columns configuration with the shroud in place form the basis for the following discussion. The temperature data were again used to calculate Nu* and Gr*. These variations are described next. Visualizations of the resulting flow patterns are then presented.

1. Quantitative Analysis

Figures 60 and 61 are Nu* verses Gr* logarithmic scatter plots for a 12 mm shroud spacing for the right and central columns respectively. Figures 62 - 65 are also Nu* verses Gr* plots with the reduced shroud spacings of 6 and 3 mm for the same two columns.

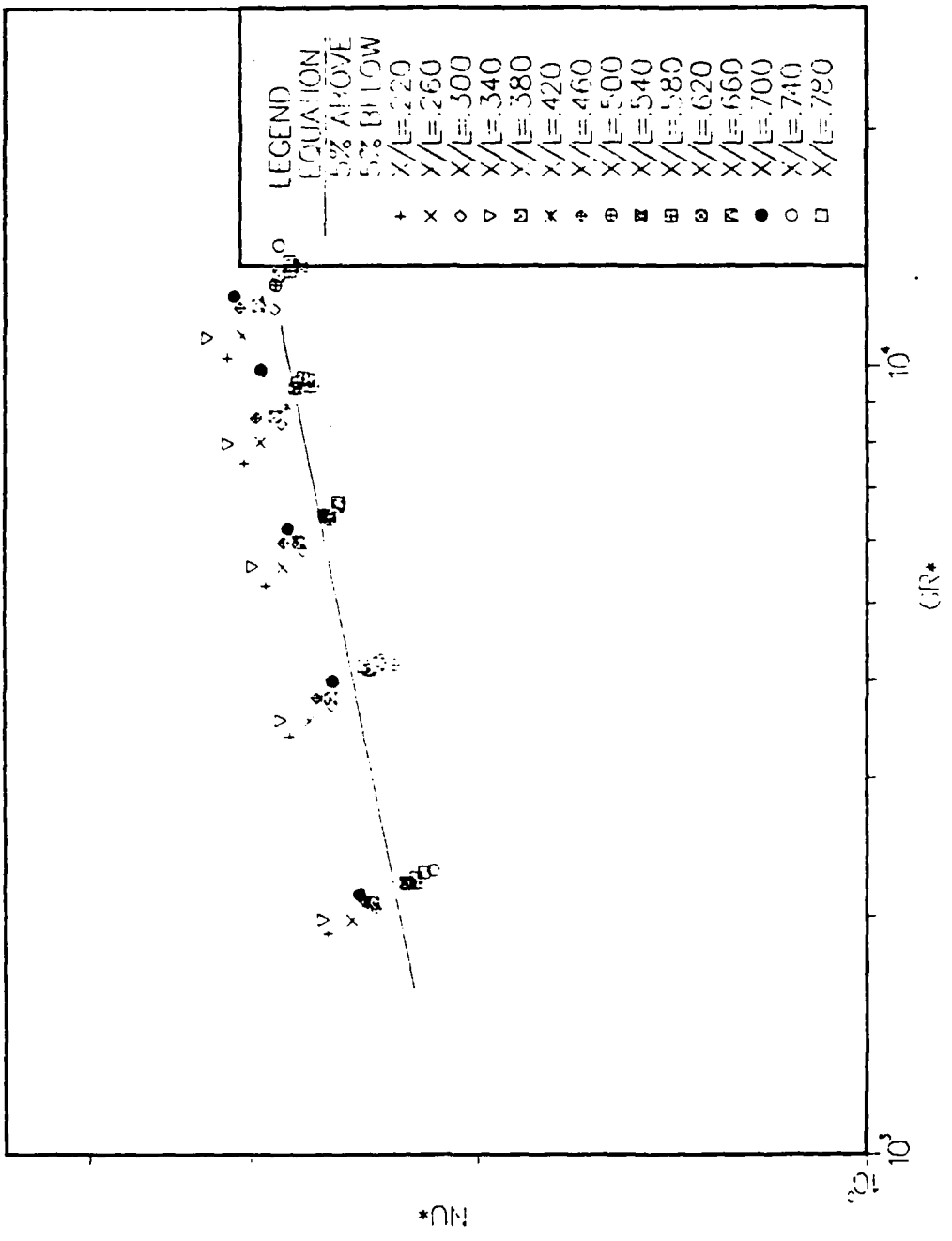

Figure 60. Nu* vs. Gr* for Right Column with 12 mm Shroud

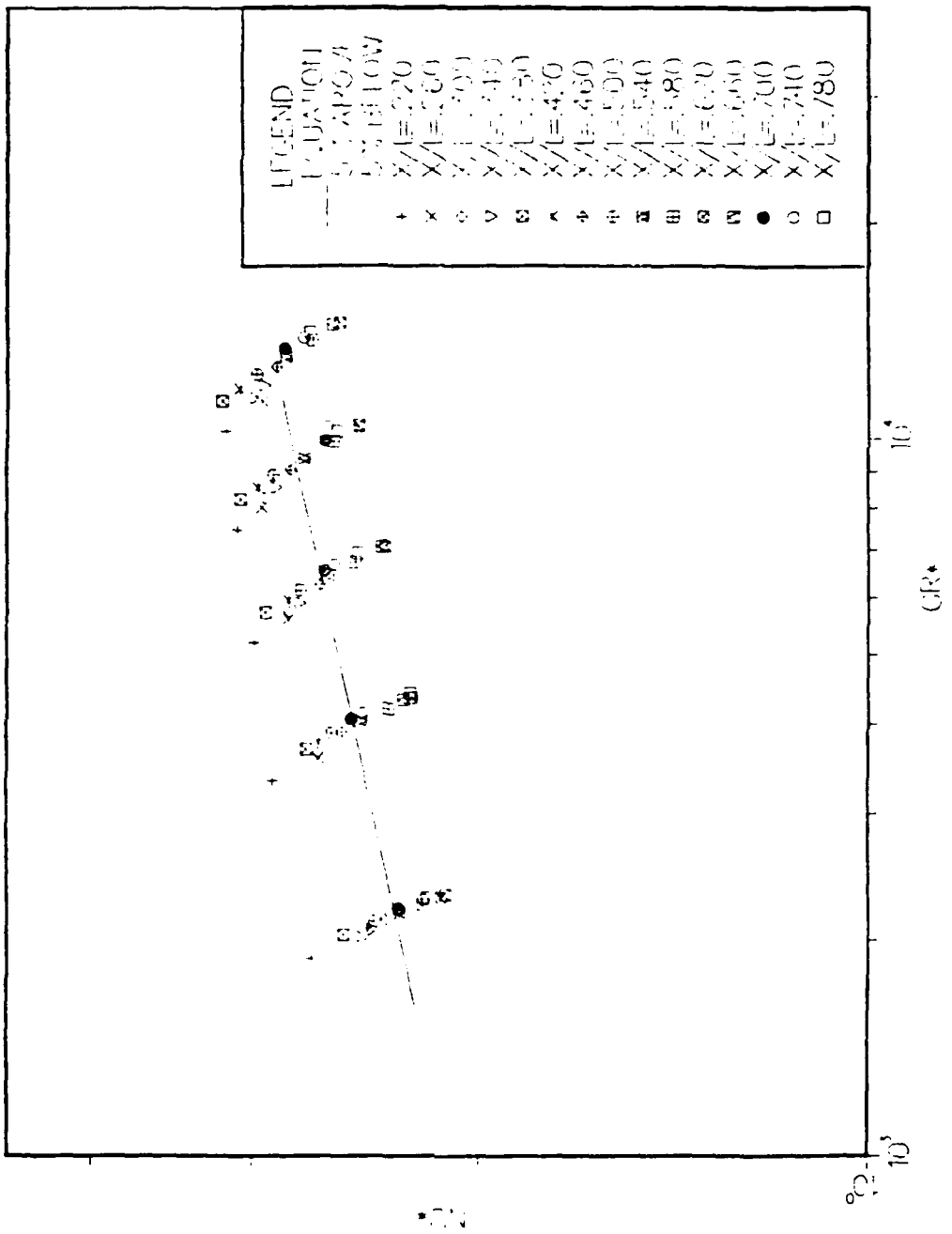

Figure 61. Nu* vs. Gr* for Center Column with 12 mm Shroud

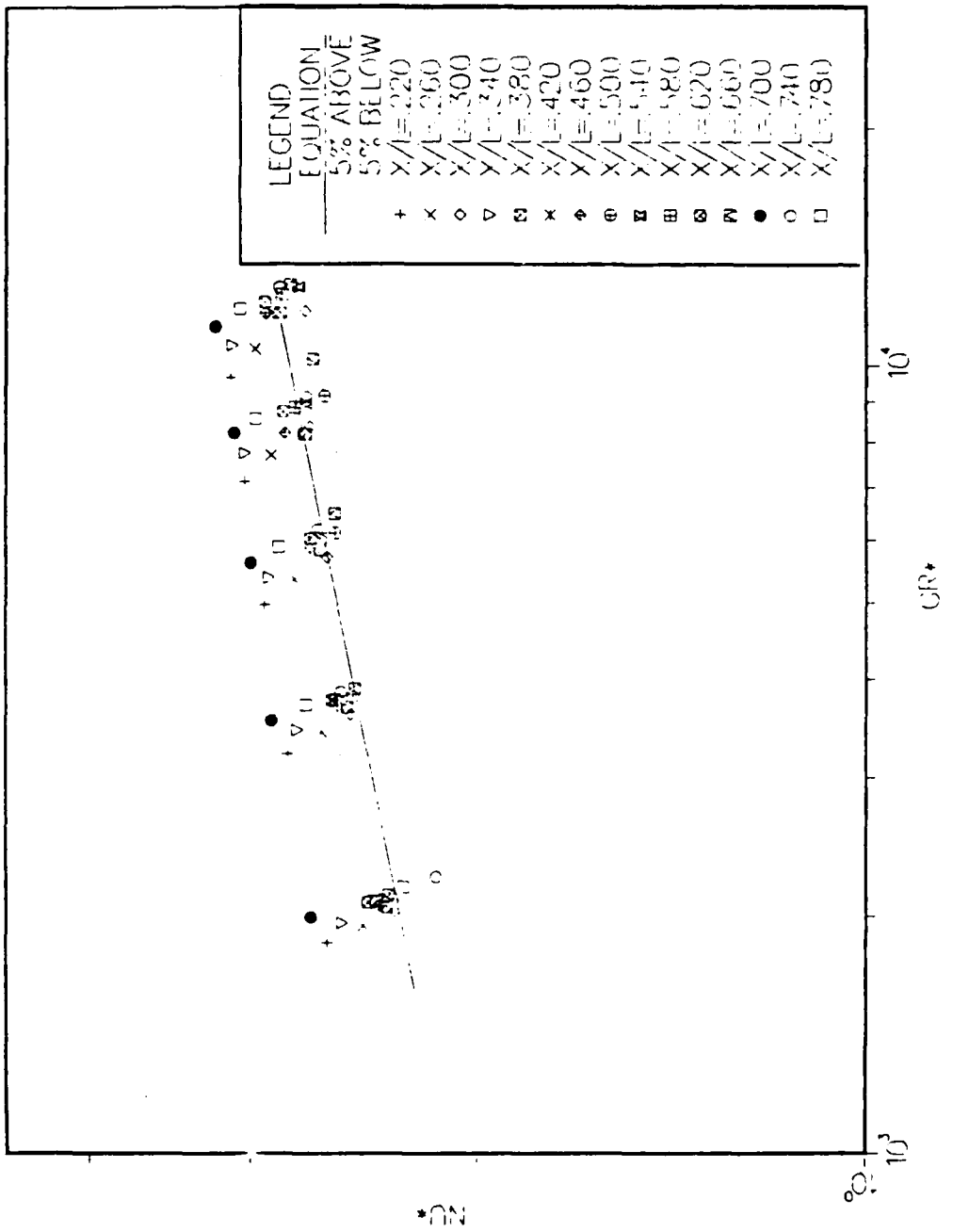

Figure 62. Nu* vs. Gr* for Right Column with 6 mm Shroud

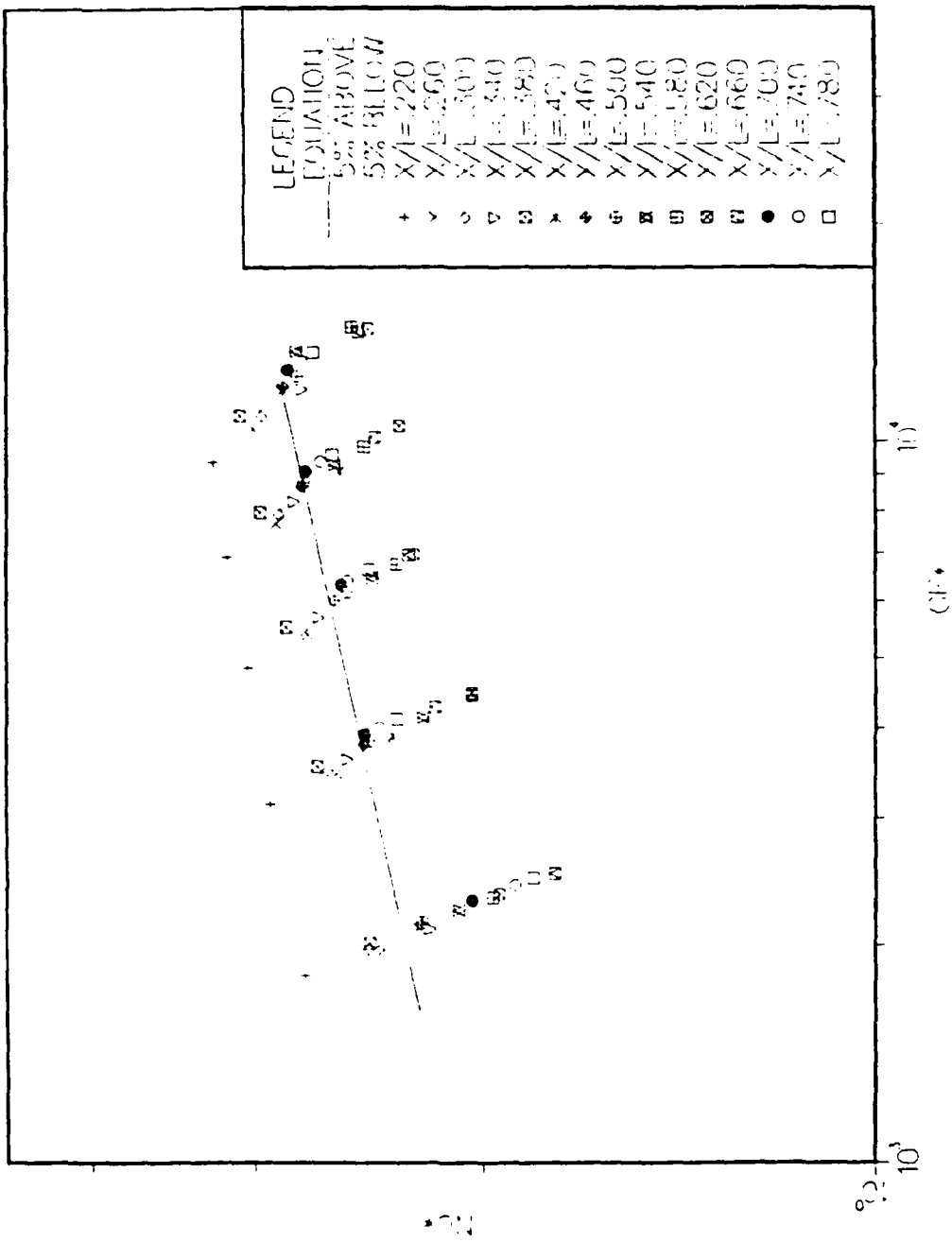

Figure 63. Nu* vs. Gr* for Center Column with 6 mm Shroud

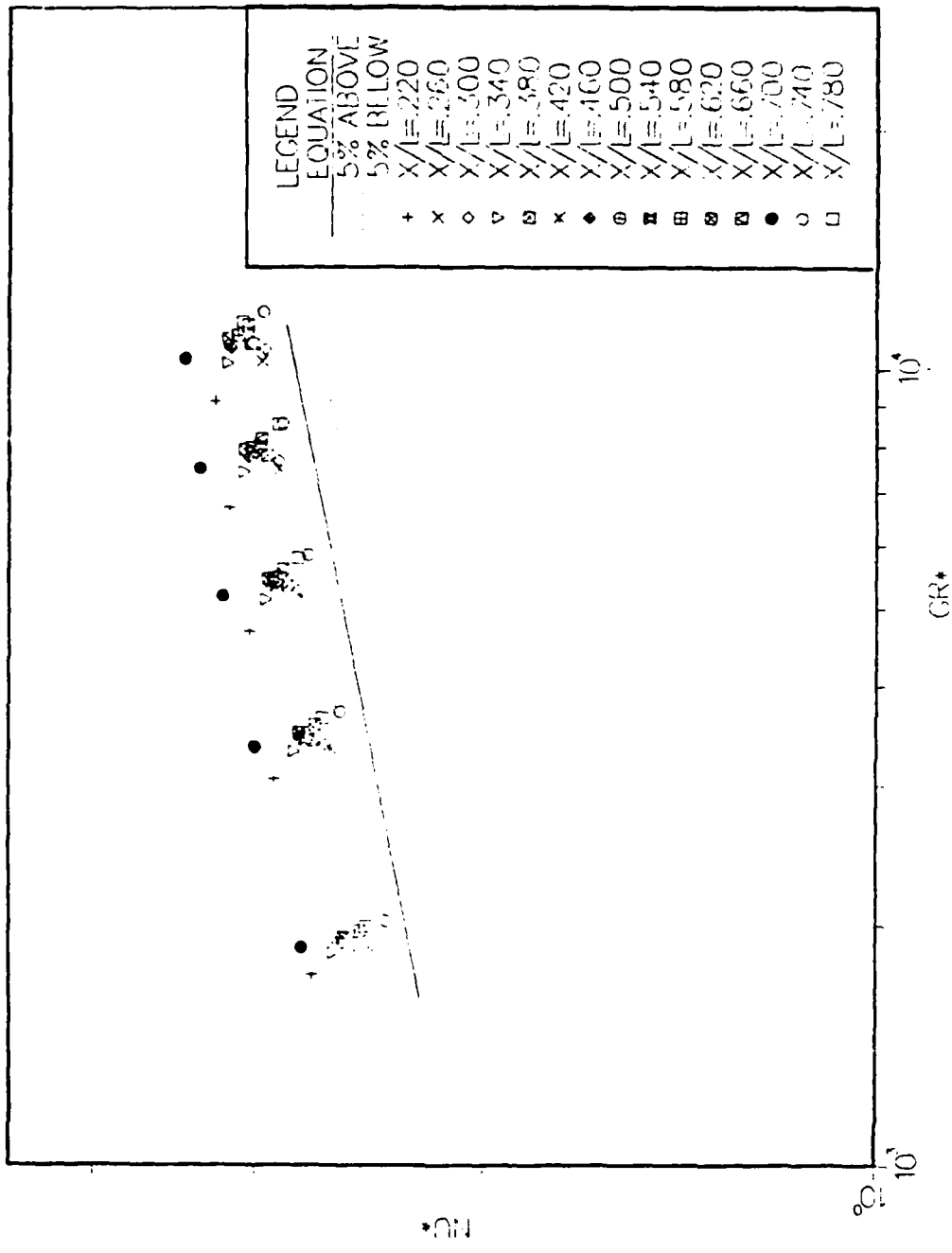

Figure 64. Nu* vs. Gr* for Right Column with 3 mm Shroud

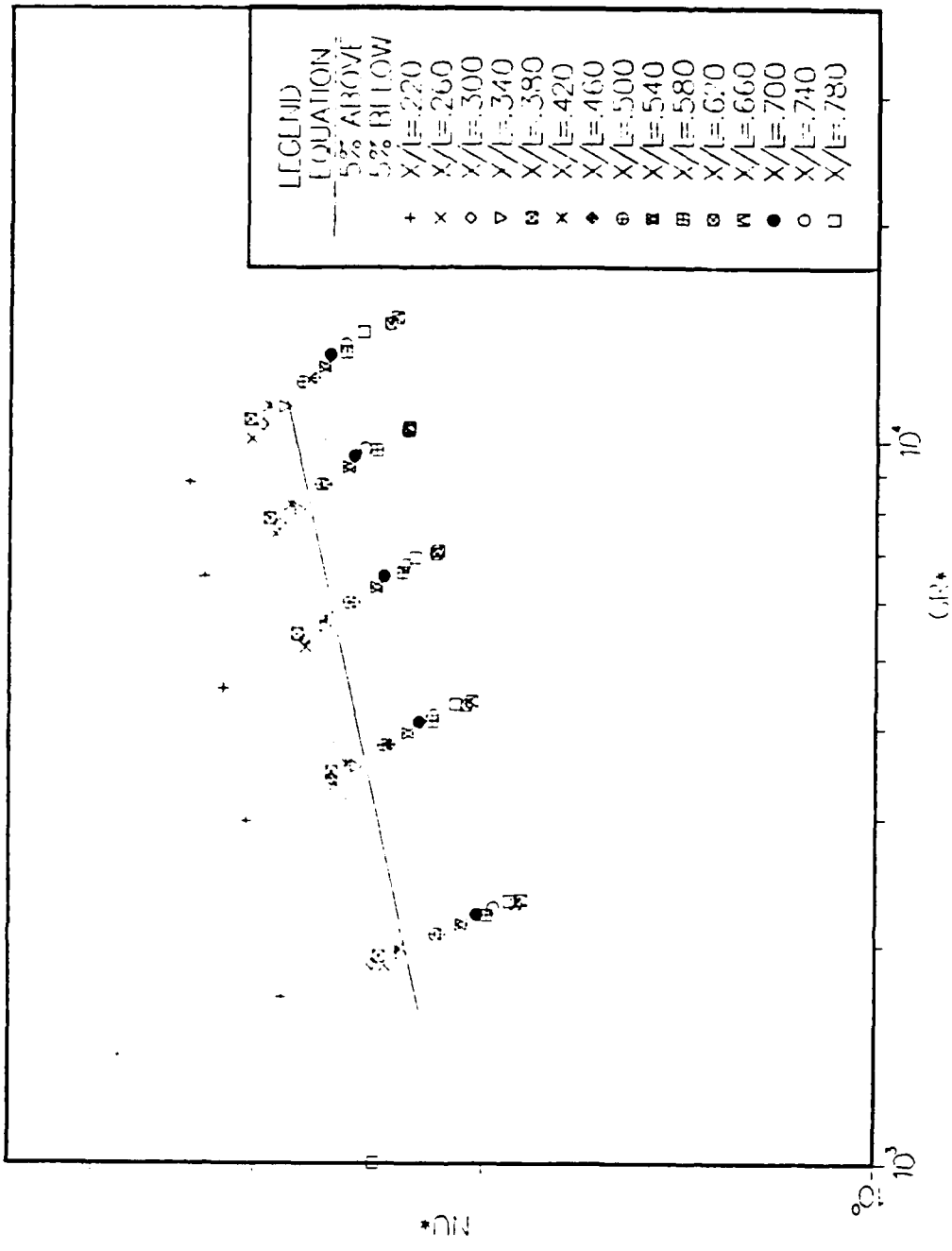

Figure 65. Nu* vs. Gr* for Center Column with 3 mm Shroud

For comparison purposes, the single column correlation obtained earlier is also shown along with the ± 5% deviation lines.

Starting with the data plotted for the 12 mm shroud spacing, it is seen that the points representing the lower heaters in both plots match the data for the unshrouded condition. However, the higher heaters for the right column show higher Nu* values than the unshrouded case. The upper heaters for the central column tend to show a larger spread at a particular power level as compared to the unshrouded case. This trend indicates that in the vicinity of the upper heaters, fluid is being entrained from the flanking columns toward the center causing higher temperatures in the central column as compared to the flanking columns. Figures 62 and 63 for the 6 mm shroud spacing show the same general trends. At a yet smaller spacing of 3 mm in Figures 64 and 65, these effects are even stronger.

In order to predict the heat transfer, it is seen that the single column correlation can be used with 10% accuracy for all three columns as long as the shroud distance is not decreased below 12 mm. If the spacing is 12 mm or greater, the correlation will provide conservative values for the flanking columns and will give reasonable values for the central column. For the cases where the shroud spacing is less than 12 mm, the single column correlation should not be used. In order to match the data obtained in this experimental study, a separate correlation needs to be developed for both the flanking and central columns. This correlation will have to incorporate the effects of shroud spacing and power level in order to properly model the system.

2. Flow Visualization

Visualization pictures were obtained in the x-y and the x-z planes as described earlier. As was seen with the single column powered, the central x-y plane indicated a developing channel flow. The pictures in the x-z plane near the surface provided details of the entrainment development process which supported the heat transfer measurements. Figures 66 and 67 display the flow patterns in the x-z plane near $y = 0$ with a 15 mm

shroud spacing for power levels of .2 and 1 watt respectively. From these figures, it is obvious that the central column entrains fluid from the two flanking columns. This effect becomes more pronounced for the upper heaters. Comparing the two figures, the effect is also stronger as the power is increased. Comparing shrouded three column figures with the unshrouded case in Figures 47 - 50, it is seen that the main effect of the shroud is to hinder the formation of individual columns of upward flowing fluid adjacent to the two flanking columns. Instead, the flow over the flanking columns comes in from the two unheated sides and from the bottom of the test board and is slightly pulled toward the center as it upward. The central column on the other hand, initially receives flow from the bottom and is supplemented with flow from the two flanking columns.

Figures 68 and 69 display flow patterns in the x-z plane near y = 0 for .2 and 1 watt input power with a 9 mm shroud spacing. These pictures indicate that a decrease in shroud spacing enhances the entrainment of flanking column fluid by the central column. It also is apparent that the flow velocities are higher at this smaller spacing compared to Figures 66 and 67.

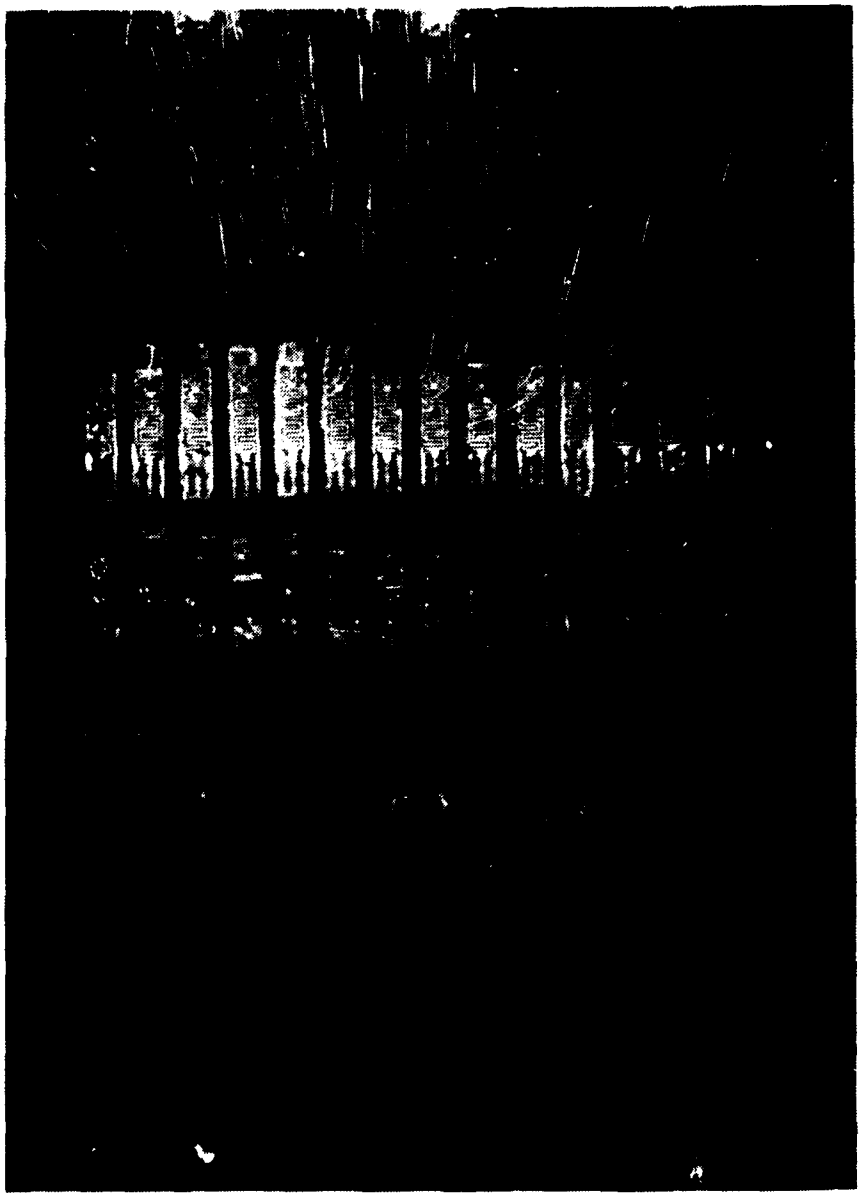

Figure 66. Steady Flow in the x-z Plane for 15 mm Shroud with .2 Watt Input Power

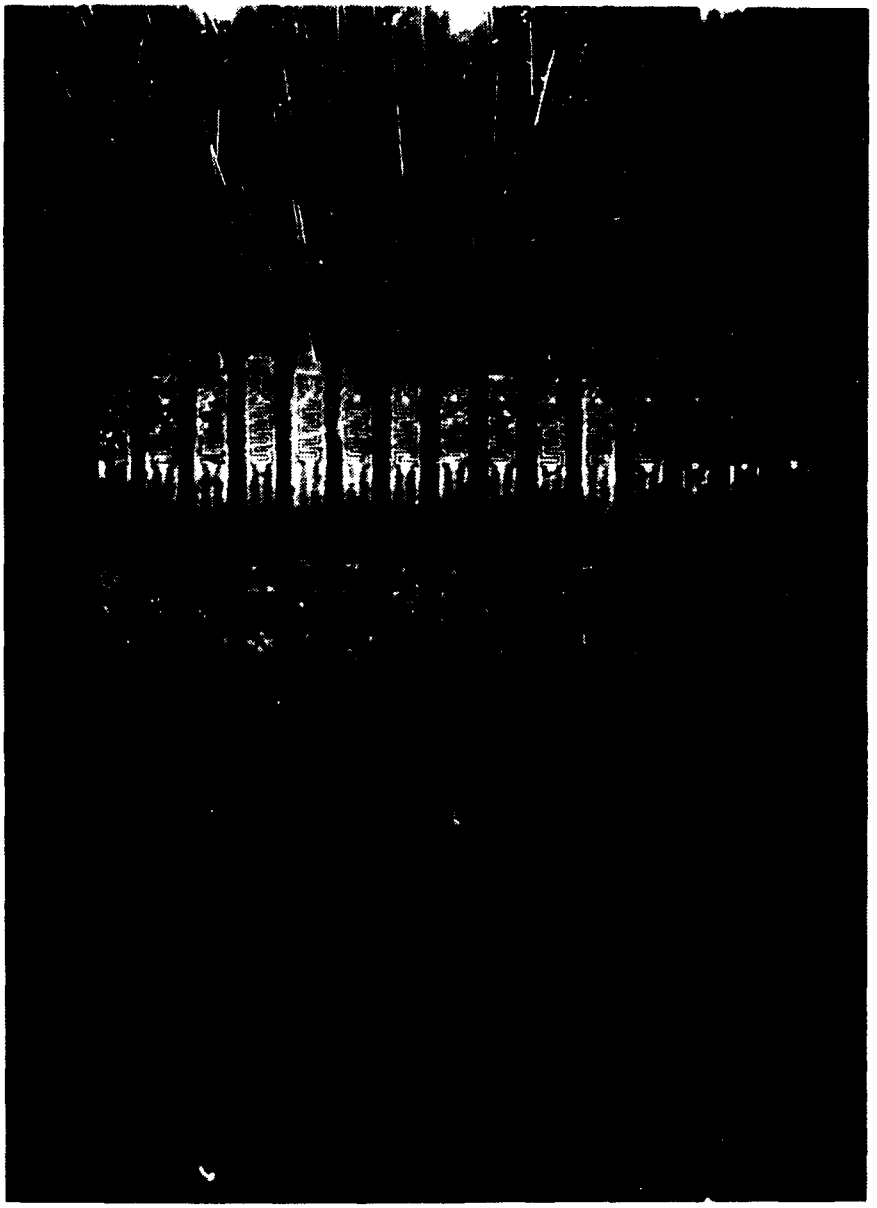

Figure 67. Steady Flow in the x-z Plane for 15 mm Shroud with 1 Watt Input Power

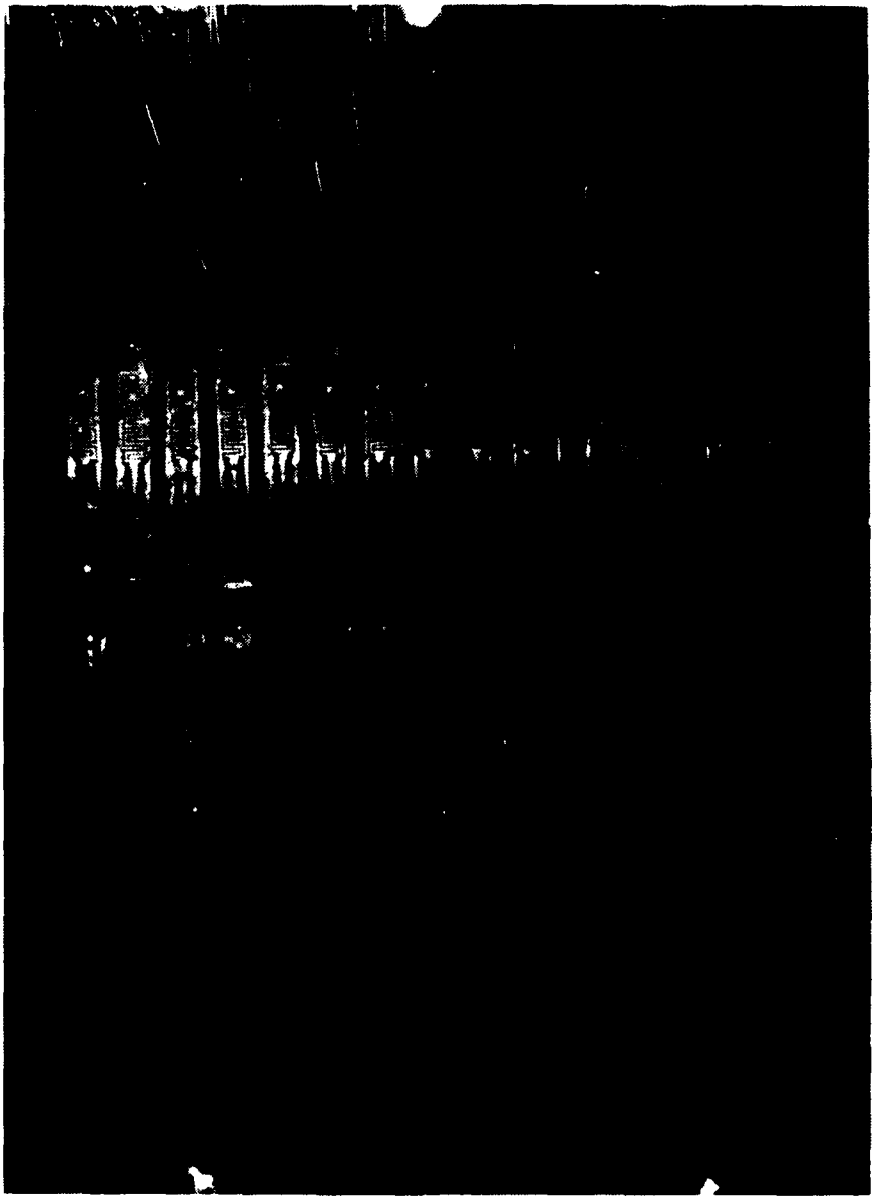

Figure 68. Steady Flow in the x-z Plane for 9 mm Shroud with .2 Watt Input Power

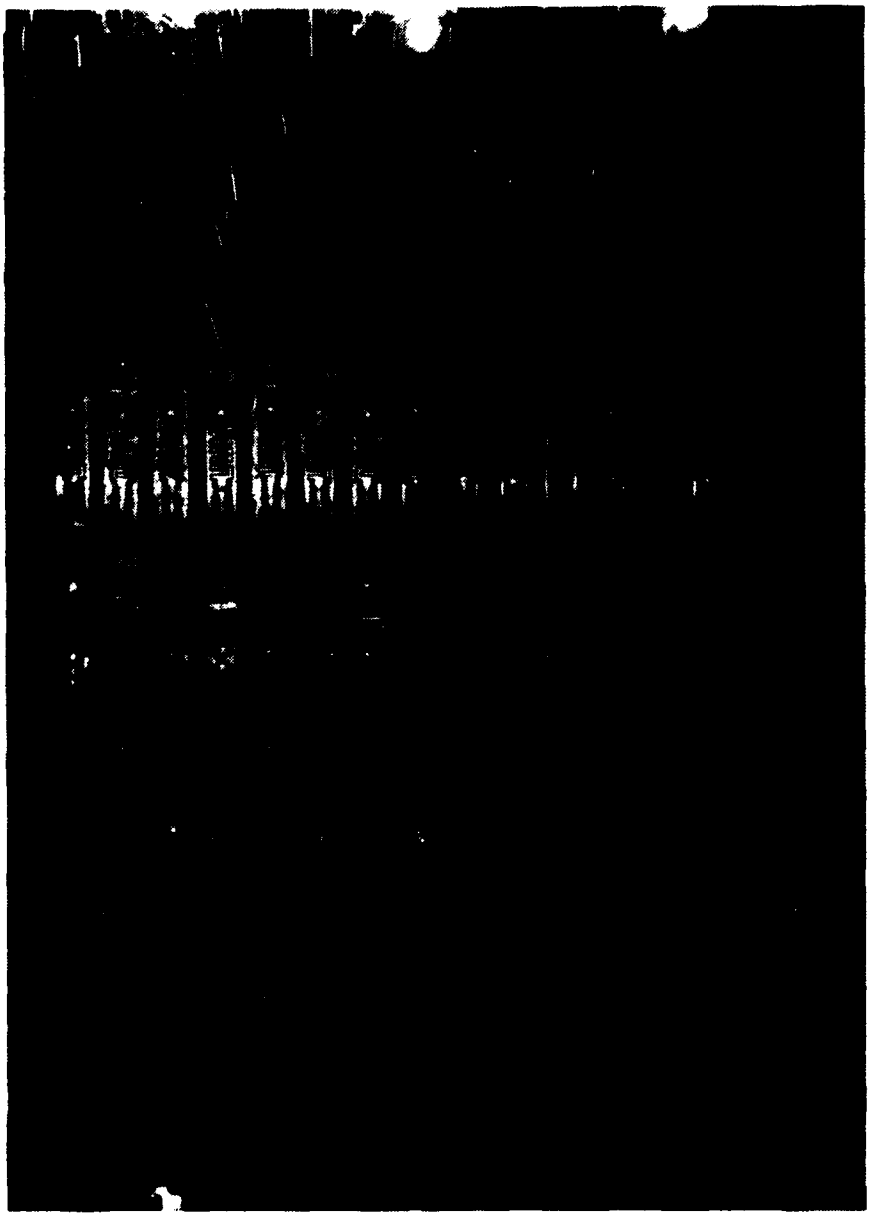

Figure 69. Steady Flow in the x-z Plane for 9 mm Shroud with 1 Watt Input Power

VI. CONCLUSIONS

During the course of this experimental study, several important conclusions were drawn about the transfer of heat from the vertical columns of discrete heat sources. The conductive transfer of energy from the heater surface to the substrate was primarily one dimensional in nature and was directed toward the back surface of the test board. This finding supports the use of a simple one dimensional model for evaluating the amount of conducted energy leaving the surface vise the use of more complicated three dimensional model. The conducted energy across the thickness of the substrate accounted for a little more than 3% of the total energy input and could be considered negligible.

The single column case study provided several interesting findings. It was first seen that the flow was laminar over the given range of power levels. The laminar flow of convected energy for the unshrouded condition was virtually two dimensional in nature near the central region of the elements, which allows for simple future modeling schemes. The boundary layer measurements indicated that the thermal layer is deeply imbedded within the momentum exchange region. The thermal layer and the momentum layer both decrease in thickness with increasing power. The momentum exchange region was thinnest for a given heater at the center. This indicates that the flow velocity in the downstream direction at the center of the column is greater than for the column edges. With the shroud in place the heat transfer characteristics agreed with those for the unshrouded condition as long as the shroud spacing was greater than 3 mm. The shroud increased the flow velocity which enhanced the heat transfer from the surface slightly. However, the correlation relating Nu* and Gr* developed for the unshrouded condition was found to provide reasonable results for the shrouded condition with shroud spacings greater than 3 mm.

The second part of the investigation examined the effects of having two flanking columns of heaters next to the central column. As for the single column, the flow remained laminar over the power ranges investigated. The main finding for the three column test case was that the flow of coolant over the central column involved fluid entrainment from the two flanking columns. For the unshrouded case, the entrainment of fluid from the flanking columns is weak and the flow over each column is virtually independent. This causes the thermal and momentum boundary layers to be of the same thickness as the unshrouded single column case for each of the three columns. Even though the flow from the flanking columns to the center is small as compared to the large rising buoyant flow in the x direction, the entrained flow still effects the heat transfer for both the central and flanking columns. It was seen that the entrained fluid will enhance the heat transfer for the flanking columns and at the same time hinders the flow of heat for the central column. Since the upward flow of coolant over each column for the unshrouded condition was found to be independent of the flow over the other two columns, the correlation developed for the single column case study will provide good results for the unshrouded three column arrangement. The results tend be conservative for the flanking columns and within acceptable range for the central column.

The results obtained for three columns powered with a shroud in position indicated that the entrainment of fluid from the flanking columns is enhanced with decreasing shroud spacings. This in turn caused the heater temperatures to decrease to even lower values for the flanking columns than what was seen for the unshrouded condition. The warm fluid entrained by the central column appeared to increase the upward buoyant flow. This increase in flow along the x axis for the central column kept the upper heater temperatures to within values that were seen for the unshrouded single and three column test conditions. These trends were observed for shroud spacings which were greater than 3 mm. Once the shroud spacing was reduced to 3 mm, the flow over the central column was restricted and

the heater temperatures increased dramatically. The heater temperatures for the flanking columns with a 3 mm shroud spacing continued to decrease. The correlation developed for the unshrouded single column does not apply for the shrouded three columns. In order for the data to match the correlation, the effects of entrained fluid must be added.

VII. RECOMMENDATIONS

In continuation of this study, it is suggested that the same configuration of three high density heater columns be used, however it is recommended that a follow on study :

- Increase the input power levels to the point where turbulent effects can be studied.
- Analyze transient conditions for the three column arrangement for both the shrouded and unshrouded arrangements.
- Analyze the effects of using non-steady power inputs on heat transfer.
- Incorporate the effects of shroud spacing on the correlation which relates the Nu* with Gr* in order to develop a more accurate and reliable expression.
- Utilize temperature sensitive liquid crystals within the flow field next to the test surface.

APPENDIX A
UNCERTAINTY ANALYSIS

In order to evaluate the accuracy of the values obtained from the reduction of data, an uncertainty analysis is required. The values measured during the experimental program are the power input, thermocouple temperature and the length used to determine heater dimensions. The accuracy in these variables, using the standard of 1/2 the smallest measurable unit, was ± 0.0001 Watt for the power, ± 0.050 ° C for temperatures and ± .5 mm for lengths. The estimates for the uncertainty in these measured variables were used for the calculation of uncertainty in the non-dimensional quantities of interest. Utilizing the technique provided by Kline and McClintock [Ref. 8] the uncertainty of a particular quantity R which is a function of several variables:

$$R = f\,(V_1,\ V2,\ V_3,\ldots..V_n)$$

can be determined through the use of a relation which is of the form:

$$\delta R = [((\partial R / \partial V_1)\,\delta V_1)^2 + ((\partial R / \partial V_2)\,\delta V_2)^2 + ...((\partial R / \partial V_n)\,\delta V_n)^2\,]^{1/2}$$

Defining δ Pwr, δ L and δ T as the uncertainty for input power, Length and temperature respectively, the above technique can be applied towards this experimental study in order to determine the uncertainty in the computed values of NDT, Nu and Gr*.

Recalling the equation for NDT from chapter 2, the uncertainty is given by the relation:

$$\delta NDT = [\ ((1 / \varnothing_0)\,\delta T)^2 + ((\varnothing / \varnothing_0^2)\,\delta \varnothing_0)^2\ ]^{1/2}$$

where $\delta \varnothing_0$ is given by:

$$\delta \varnothing_0 = [\ ((1 / P K_f)\,\delta Pwr)^2 + ((Q_{conv} / P^2 K_f)\,\delta L)^2\ ]^{1/2}$$

Using the above relations, the maximum uncertainty for NDT values is computed to be ± .004.

Using the same procedure followed for the uncertainty in NDT values, the uncertainty for the Gr* values are determined using the expression:

$$\delta Gr^* = g \beta / K_f Ç^2 [(L^4 \delta q'')^2 + (q'' 4 L^3 \delta L)^2]^{1/2}$$

where $\delta q''$ is given as:

$$\delta q'' = [((1 / A_s)\delta Pwr)^2 + ((Q_{conv} / A_s^2) \delta L)^2]^{1/2}$$

The above equations produce a maximum uncertainty for Gr* as ± 5.

This same procedure was once performed once again to determine the uncertainty for Nu values. Wtihout listing the equations, the maximum uncertainty for Nu was found to be ± .002.

APPENDIX B
DATA REDUCTION PROGRAM

```
10     REM PROGRAM DATADUC
20     !!!!!!!!!!!!!!!!!!!!!!!!!!!!!!!!!!!!!!!!!!!!!!!!!!!!!!!!!!!!!!!!!!!!!!!!!!
30     !!                                                                       !!
40     !!                        DATA REDUCING PROGRAM                          !!
50     !!                                                                       !!
60     !!!!!!!!!!!!!!!!!!!!!!!!!!!!!!!!!!!!!!!!!!!!!!!!!!!!!!!!!!!!!!!!!!!!!!!!!!
70     REAL T(48)
80     REAL Power,Tamb,G,Kpg,Delx,As,Per,Te,Qconv,Lbar
90     REAL Qflux,Delt,Tfilm,Beta,Spvol,Dynvisc,Qcond
100    REAL Kinvisc,Kf,Pr,Theta,Ndt,Hx,Grmod,Nux,Lnu,Lgr
110    PRINTER IS CRT
120    PRINT "INPUT DATA FILE NAME"
130    INPUT Filename$
140    PRINT
150    PRINT "INPUT POWER VALUE IN WATTS"
160    INPUT Power
170    PRINT
180    PRINT "INPUT SHROUD SPACING IN mm"
190    INPUT Space$
200    PRINT
210    PRINT "INPUT AMBIENT TEMPERATURE
220    INPUT Tamb
230    PRINTER IS 701
231    PRINT " "
232    PRINT DATE$(TIMEDATE)
233    PRINT "DATA REDUCTION OUTPUT"
234    PRINT " "
240    PRINT "POWER LEVEL (WATTS        :",Power
250    PRINT
260    PRINT "SHROUD POSITION (mm)      :",Space$
270    PRINT
280    PRINT "AMBIENT TEMPERATURE (C) :",Tamb
290    PRINT
300    PRINT
310    !
320    ASSIGN @Path TO Filename$
330    ENTER @Path;T(*)
340    !
350    G=9.81
360    Kpg=.1421
370    Delx=.006731
380    As=.0239*.0079
390    Per=2*.0239+2*.0075
```

```
400   Lbar=As/Per
401   A$="Qcond"
402   B$="X/L"
403   C$="NDT"
404   D$="LOG(Nux)"
405   E$="LOG(Grx*)"
406   F$="DELT"
407   G$="Hx"
408   H$="Nux"
409   I$="Grx*"
411   !!!!!!!!!!!!!!!!!!!!!!!!!!!!!!!!!!!!!!!!!!!!!!!!!!!!
420   !            ENTER CONDUCTION LOSSES                 !
431   !!!!!!!!!!!!!!!!!!!!!!!!!!!!!!!!!!!!!!!!!!!!!!!!!!!!
440   PRINT "INPUT CONDUCTION LOSSES AS COMPUTED FROM ELLPACK"
441   INPUT Qcond
491   !!!!!!!!!!!!!!!!!!!!!!!!!!!!!!!!!!!!!!!!!!!!!!!!!!!!
492   PRINTER IS 701
501   FOR I=16 TO 30
680   PRINT " "
690   PRINT " "
700   PRINT "                                        SURFACE #",I
710   PRINT " "
725   PRINT USING "2X,AAAAA,4X,AAA,4X,AAA,4X,AAAAAAAA,2X,AAAAAAAAA,3X,AAAA,5X,AA
,6X,AAA,4X,AAAA";A$,B$,C$,D$,E$,F$,G$,H$,I$
740   Qconv=Power-Qcond
750   Qflux=Qconv/As
760   Delt=T(I)-Tamb
770   Tfilm=273.15+(T(I)+Tamb)/2
780   Beta=(-7.9448598E-8*(Tfilm^2))+(5.7356479E-5*Tfilm)-.0097810563
790   Spvol=(4.59595E-9*(Tfilm^2))+(-2.537455E-6*Tfilm)+.001341803
800   Dynvisc=(3.2348511E-7*(Tfilm^2))+(-.00021474457*Tfilm)+.036165792
810   Kinvisc=Spvol*Dynvisc
820   Kf=(1.418181818E-3*Tfilm)+.1858
830   Pr=(4.557055E-3*(Tfilm^2))+(-2.922094*Tfilm)+453.3319
840   Theta=Qflux*Lbar/Kf
850   Ndt=Delt/Theta
860   Hx=Qflux/Delt
870   Grmod=(9*Beta*Qflux*(Lbar^4))/(Kf*Kinvisc^2)
880   Nux=Hx*Lbar/Kf
890   Lgr=LGT(Grmod)
891   Lnu=LGT(Nux)
901   Xtcl=(31.75-(6.985+(I-16)*1.270))/31.75
940   PRINT USING "1X,D.DDDD,2X,D.DDD,2X,D.DDD,4X,D.DDD,7X,D.DDD,4X,DD.DDD,2X,DD
DD.D,2X,DD.DDD,2X,DDDDD.D";Qcond,Xtcl,Ndt,Lnu,Lgr,Delt,Hx,Nux,Grmod
1700  NEXT I
1710  END
```

APPENDIX C
SAMPLE CALCULATIONS

The following calculations are based on the temperature data corresponding to a single unshrouded column at heater surface eight with 1.0 watt input power. The ambient fluid temperature and heater temperature were 17.60 ° C and 30.20 ° C respectively. The equations used to calculate the fluid properties are obtained from the data reduction program listed in Appendix B.

1. CHARACTERISTIC DIMENSIONS

$$P = 2(0.0078 + 0.0239)$$

$$= 0.063 \text{ m}$$

$$As = (0.0078)\ (0.0239)$$

$$= 1.864 \times 10^{-4} \text{ m}^2$$

$$L = 1.864 \times 10^{-4} / 0.0634$$

$$= 2.940 \times 10^{-3} \text{ m}$$

2. CONVECTED HEAT FLUX

$$Q_{CONV} = 1.0 - .0357$$

$$= 0.9643 \text{ W}$$

$$q'' = 0.9643 / 1.864 \times 10^{-4}$$

$$= 5173 \text{ W} / \text{m}^2$$

3. FLUID PROPERTIES

$$T_{film} = (30.20 + 17.61) / 2 + 273.15$$

$$= 297.06$$

β = $(-7.945 \times 10^{-8})(297.06)^2 + (5.736 \times 10^{-5})(297.06) - 9.781 \times 10^{-3}$

= 2.473×10^{-4} K^{-1}

v = $(4.697 \times 10^{-9})(297.06)^2 - (2.537 \times 10^{-6})(297.06) + 1.342 \times 10^{-3}$

= 1.003×10^{-3} m^3 / kg

μ = $(3.235 \times 10^{-7})(297.06)^2 - (2.147 \times 10^{-4})(297.06) + 0.0362$

= 9.684×10^{-4} $N\,s / m^2$

$Ç$ = $(1.003 \times 10^{-3})(9.684 \times 10^{-4})$

= 9.713×10^{-7} m^2 / s

K_f = $(1.418 \times 10^{-3})(297.06) + 0.1866$

= .607 W / m K

4. NON-DIMENSIONAL TEMPERATURE EXCESS

$\emptyset$ = 30.20 - 17.61 = 12.59 ° C

$\emptyset_O$ = $(5173)(2.940 \times 10^{-3}) / .607$ = 25.05 ° C

NDT = 12.59 / 25.05 = .503

5. HEAT TRANSFER COEFFICIENT

h_x = 5173 / (30.20 - 17.61) = 411.0 W / m^2 K

6. FLUX-BASED GRASHOF NUMBER

Gr*x = $((9.81)(2.473 \times 10^{-4})(5173)(2.940 \times 10^{-3})^4) / ((.607)(9.713 \times 10^{-7})^2)$

= 1804

7. NUSSELT NUMBER

Nu = $(411.0)(2.940 \times 10^{-3}) / .607$ = 1.988

APPENDIX D
ELLPACK PROGRAM

The following program is written using the data obtained for 1 watt input power.

```
*       ************************************************
*       *                                              *
*       *   3-D LAPLACIAN PROBLEM USING ELLPACK        *
*       *                                              *
*       *    THE FOLLOWING ELLPACK PROGRAM SOLVES A STEADY *
*       *    STATE CONDUCTION PROBLEM IN 3-D FOR A RECTAN- *
*       *    GULAR DOMAIN. NOTE THAT TWO  FACES HAVE ADIA- *
*       *    BATIC BOUNDARY  CONDITIONS,  WHILE THE  OTHER *
*       *    FACES ARE GIVEN AS FUNCTIONS OF TWO DEPENDENT *
*       *    VARIABLES OR CONSTANTS                    *
*       ************************************************
*
OPTION.       LEVEL=1   $   MEMORY   $   TIME
EQUATION.     UXX + UYY + UZZ = 0.
BOUNDARY.     U  = F1(Y)       ON X = 0.00
              UX = 0.0         ON X = 2.20
              U  = 18.6278     ON Y = 0.00
              U  = F2(X,Z)     ON Y = 1.10
              U  = F3(X,Y)     ON Z = 0.00
              UZ = 0.0         ON Z = 0.66
GRID.         21 X POINTS
              11 Y POINTS
               7 Z POINTS
DIS.          7 POINT 3D
INDEX.        AS IS
SOLUTION.     SOR
OUTPUT.       TABLE(U) $ TABLE(UZ) $ TABLE(UX) $ TABLE(UY)
SUBPROGRAMS.
          REAL FUNCTION F1(Y)
          F1 = 18.6278 + 1.3752*Y
          RETURN
          END

          REAL FUNCTION F2(X,Z)
          IF (X .GT. .44) GOTO 100
          F2 = 20.1405 + 0.0*X +0.0*Z
          GOTO 400
  100     IF (Z .GT. .22) GOTO 200
          F2 = 22.3584 + 0.0*X +0.0*Z
          GOTO 400
  200     F2 = 30.1998 + 0.0*X +0.0*Z
  400     RETURN
          END

          REAL FUNCTION F3(X,Y)
          IF (X .GT. .44) GOTO 100
          F3 = 18.6278 + 1.3752*Y + 0.0*X
          GOTO 400
  100     F3 = 18.6278 + 3.3915*Y + 0.0*X
  400     RETURN
          END
END.
```

LIST OF REFERENCES

1. Milanez, L. F. and Bergles, A. E., "Studies on Natural Convection Heat Transfer from Thermal Sources on a Vertical Surface," *Proceedings of the Eighth International Heat Transfer Conference*, Vol. 3, pp. 1347-1352, 1986.

2. Hannemann, R., Incropera, F. P., and Simons, R., "Single Phase Liquid Cooling," *Research Needs in Electronic Cooling*, PP. 6-25, December 1986.

3. Knight, D. L., "Natural Convection Liquid Immersion Cooling of a Column of Discrete Heat Sources in a Vertical Channel," M.S.M.E. Thesis, Naval Postgraduate School, Monterey, CA, September 1988.

4. Incropera, F. P., and DeWitt, D. P., *Fundamentals of Heat and Mass Transfer*, p. 774, John Wiley and Sons, 1981.

5. Rice, J. R., and Boisvert, R. F., *Solving Elliptic Problems Using ELLPACK*, pp. 16-59, Springer Verlag, 1985.

6. Burmeister, L. C., *Convective Heat Transfer*, pp. 530-533, John Wiley and Sons, 1983.

7. Gebhart, B., Jaluria, Y., Mahajan, R. L. and Sammakia, B., *Buoyancy Induced Flows and Transport*, Hemisphere Publishing , 1988.

8. Kline, S. J., and McClintock, F. A., "Describing Uncertainties in Single Sample Experiments," *Mechanical Engineering*, January, 1953.

INITIAL DISTRIBUTION LIST

	No. of Copies
1. Defense Technical Information Center Cameron Station Alexandria, VA 22304-6145	2
2. Library, Code 0142 Naval Postgraduate School Monterey, CA 93943-5002	2
3. Mr. Howard Stevens Head, Electrical Research Center David Taylor Research Center Annapolis, MD 21402	1
4. Superintendent Naval Postgraduate School Attn: Professor A. J. Healey, Code 69HY Department of Mechanical Engineering Monterey, CA 93943-5004	1
5. Superintendent Naval Postgraduate School Attn: Professor Y. Joshi, Code 69Ji Department of Mechanical Engineering Monterey, CA 93943-5004	3
6. Superintendent Naval Postgraduate School Attn: Professor M. D. Kelleher, Code 69Kk Department of Mechanical Engineering Monterey, CA 93943-5004	1
7. Superintendent Naval Postgraduate School Attn: Professor A. D. Kraus, Code 62Ks Department of Mechanical Engineering Monterey, CA 93943-5004	1

8. Mr. Duane Embree — 1
Naval Weapons Support Center
Code 6042
Crane, IN 47522

9. Mr. Alan Bosler — 1
Naval Weapons Support Center
Code 6042
Crane, IN 47522

10. Superintendent — 1
Naval Postgraduate School
Attn: Curricular Officer, Code 34
Monterey, CA 93943-5004

11. Mr. Joseph Cipriano — 1
Executive Director
Weapons and Combat Systems Directorate
Naval Sea Systems Command
Washington, D.C. 200362-5101

12. Lt. Alfred O. Gaiser — 2
2739 Eton Street
New Orleans, LA 70131

13. Lt. Larry O. Haukenes — 1
107 18th Street Apt B
Pacific Grove, CA 93950